ABSTRACT

FRANK, DENNIS ONYEKA. Acute Inflammatory Response to Endotoxin Challenge: Model Development, Parameter Estimation, and Treatment Control. (Under the direction of Hien T. Tran.)

Bacterial lipopolysaccharides (LPS; endotoxins) are the major outer surface membrane components present in almost all Gram-negative bacteria and act as extremely strong stimulators of innate or natural immunity in diverse eukaryotic species ranging from insects to humans. They also induce acute inflammatory response comparable to bacterial infection. Like most biological processes, modeling the inflammatory response involves using highly nonlinear dynamic systems of differential equations with a relatively large number of parameters. Several researchers have within the last seven years developed mathematical models of acute inflammatory response to infection; some of these models are low-order and are biologically irrelevant due to oversimplification of the real process. The high-order models on the contrary, are highly complex, computationally expensive and constitute challenges in calibrating the model to experimental data.

In the first phase of our work, we propose and validate a number of competing models of acute inflammatory response to compare with a recently developed model in the literature. Our desire to come up with models that can accurately predict the observed dynamics of the pro- and anti-inflammatory cytokines led us to conduct sensitivity analysis, subset selection and parameter estimation in order to obtain accurate parameter values from existing data. Next, we employ a model selection technique to aid with selecting the "best" model among all the potential candidates. In addition, we prove the existence and uniqueness of a solution to our "top choice" model as well as study the model's steady state and stability behavior.

At the next phase, we study the model under an open-loop optimal control based treatment strategy, this is the first step to achieving our goal of proposing treatment therapies to regulate inflammation. Since open-loop control problems do not have the ability to incorporate unexpected disturbances in the system as time progresses, we implement a feedback scheme known as Nonlinear Model Predictive Control (NMPC). In general, a better approach to implement NMPC is to combine it with Kalman filter. Hence, we demonstrate how this is done with an example where noise was added to our *in silico* simulated results to create an experimental data with noise. Unscented Kalman Filter (UKF) was then used to filter the noisy data and estimate the unobserved states at every recalculation step in the NMPC scheme.

Acute Inflammatory Response to Endotoxin Challenge: Model Development, Parameter Estimation, and Treatment Control

by
Dennis Onyeka Frank

A dissertation submitted to the Graduate Faculty of
North Carolina State University
in partial fulfillment of the
requirements for the Degree of
Doctor of Philosophy

Mathematics

Raleigh, North Carolina

2010

APPROVED BY:

Stephen L. Campbell	Negash G. Medhin
John E. Franke	Hien T. Tran Chair of Advisory Committee

DEDICATION

To my parents, Victor and Beatrice Ureh Frank, who had to sacrifice a lot to provide me with quality education, and to my second mom, Joyce Esuru Osoh, who helped shape my secondary education.

BIOGRAPHY

Dennis Onyeka Frank was born and raised in a city called Port Harcourt in southern Nigeria. He received his Bachelor of Science degree in Statistics from the University of Nigeria, Nsukka, Nigeria before moving to the United States of America for graduate school at Youngstown State University, Youngstown, Ohio, where he obtained a Master of Science degree in Mathematics. In 2005, he began his Ph.D. program in Operations Research (OR) at North Carolina State University, Raleigh, North Carolina before transferring to the Mathematics department. While he was in the OR program, he received a Master of Operations Research degree. Upon completion of his Ph.D. in Mathematics, he will begin a two year postdoctoral research position in the Department of Otolaryngology/Head and Neck Surgery at the University of North Carolina School of Medicine, Chapel Hill, North Carolina.

ACKNOWLEDGEMENTS

Only as I approached the tail end of this chapter of my life did I come to the realization that a Ph.D. is more about the journey than the end result. This entire journey has been one of mixed emotions, personal growth and maturation. In all of these, the most valuable lessons I learned are patience, perseverance and respect for people's accomplishments. In view of this, I would like to express my heartfelt gratitude to my advisor, Dr. Hien Tran. Thank you for your patience with me. Thank you for being very understanding. Thank you for your guidance and all the time you spent mentoring me.

To my committee members: Dr. Stephen L. Campbell, Dr. Negash G. Medhin and Dr. John E. Franke. Thank you for serving on my committee. I really do appreciate the conversations I had with each of you. Thank you for all your advice and encouraging words. More than anything else, thank you for your wisdom and how in a number of ways your words of wisdom were what made all the difference in my life. Thank you! Thank you!! Thank you!!!

I would also like to take this opportunity to thank the staff of the Mathematics department, especially Denise Seabrooks, Seyma Bennett-Shabbir, Nicole Dahlke, Carolyn Gunton and Charlene Wallace. I had a lot of personal interactions with all of you, and each of you is simply "awesome." You always provided "on the spot" help and assistance to me regardless of what you were doing. Thank you very much for your generous hearts.

To my parents, Victor and Beatrice U. Frank as well as Joyce O. Osoh, thank you for inspiring me, and thanks for all your prayers and encouragement. Thank you for believing in me more than I believed in myself, and thanks for giving me the gift of education when I was young. To my siblings, Eze, Odiri, Ike, Chima and Mary Ann, thanks for all your support.

Special thanks to my beloved wife, Ojochide, and the kids, Whanyichukwu, Elemchukwu and Ogochukwu. Thanks for tolerating me for these 5 years. I apologize for those times when I took my academic frustrations out on you guys. Thanks for giving me space and privacy to do my work. Thank you for sharing in my academic joys and sorrows.

Finally, my deepest gratitude goes to the Almighty Lord, without whom, I am nothing. Thanks for giving me the grace I needed all these years of studying. I have experienced your sustaining power as Paul did in 2nd Corinthians 12:9 - "My grace is sufficient for you, for my power is made perfect in weakness." So I too say, "Therefore I will boast all the more gladly of my weaknesses, so that the power of Christ may rest upon me."

TABLE OF CONTENTS

LIST OF TABLES

LIST OF FIGURES

Chapter 1

Introduction

The body responds to bacterial infection or tissue trauma by the activation of acute inflammatory response. This response, which is non-specific, is considered to be the body's first line of defense against danger [66]. Inflammation is vital for the removal/reduction of irritants to the organism and subsequent restoration of homeostasis. In an attempt to reestablish homeostasis, the inflammatory response is pivotal in clearing invading organisms and offending agents, enhancing wound healing, and promoting tissue repair [140]. This response is made up of a combination of local and systemic mobilization of immune, endocrine, and neurological mediators.

In an ideal situation, the inflammatory response becomes activated, clears the pathogen if there is any infection, begins a repair process and abates. However, inflammation itself can damage otherwise healthy cells which can then further stimulate inflammation. This process can become uncontrollable and lead to tissue damage, organ dysfunction, and ultimately death [24]. To curb the excessive inflammatory response, the body has some regulatory devices such as pro- and anti-inflammatory cytokines that assist with the initiation of tissue repair. The pro-inflammatory cytokines (e.g, interleukin-6 ($IL-6$)) and tumor necrosis factor-alpha ($TNF-\alpha$)) up-regulate inflammation and control infections, whereas anti-inflammatory mediators (e.g, interleukin-10 ($IL-10$)) down-regulate the inflammatory actions, ideally after infection control has been achieved [101].

Systemic inflammation followed by bacterial infection that is based on its clinical manifestations is known as sepsis [22]. Sepsis is a common and frequently fatal condition, with 750,000 cases annually in the United States alone in 1995 [9]. Given the complexity of inflammation, several studies have been conducted to understand the molecular and physiological pathways of the acute inflammatory response, but this has not resulted in many effective therapies against

sepsis. It is believed that the complex nature of the inflammatory response renders the effect of targeting isolated components of inflammation difficult to predict [76].

Bacterial lipopolysaccharides (LPS), also known as lipoglycans, are highly conserved, highly immunogenic, constituent molecules found in the outer membrane of Gram-negative bacteria, and act as endotoxins. When bacteria are lysed by immune effector cells and molecules, surges of endotoxin may be released into the host, intensifying the inflammatory response and causing further activation of immune effector cells [6]. The administration of antibiotics sometimes results in pulses of endotoxins release from Gram-negative bacteria as the antibiotics attempt to kill the invading bacteria, validating the clinical significance of this subject matter [45]. The fact that direct endotoxin administration in animals and humans is likely to trigger an acute inflammatory response that reproduces many of the features of an actual bacterial infection, such as fever, makes this a compelling reason to develop a valid mathematical model for investigating the inflammatory response [33, 98, 105]. Besides, elevated levels of endotoxin can be lethal.

To this end, the control of inflammatory response to endotoxin challenge has become imperative. Thus, we seek to construct a mathematical model that can provide important insights into the global dynamics of the inflammatory process from which therapies may be developed. The advent of the new millennium has brought considerable attention on the development of mathematical models of acute inflammatory response to infection. This includes the development of both low-order and high-order models of inflammatory response have been developed. For example, in [76] a system of 3 dimensional (3D) ordinary differential equations (ODEs) that consists of a response instigator (pathogen) and early and late pro-inflammatory mediators was proposed. This model was later modified and then extended to incorporate tissue damage as well as anti-inflammatory mediators in [120] to form a 4D model consisting of inflammatory stimulus (pathogen), pro-inflammatory mediators, tissue damage, and anti-inflammatory mediators. To examine repeated endotoxin administration in the context of acute inflammatory response, the pathogen equation in [120] was replaced with an endotoxin equation [38]. Although these models provided significant insight into key drivers of inflammatory response outcome, they were not calibrated to any experimental data. On the other end of the spectrum are high-complexity models of the acute inflammatory response cascade [29, 80, 112, 140] . For instance, in [80] the model consisted of 17 ODEs, while [112] had 15 ODEs and [140] contained 31 ODEs. It should be noted that all of these high-order models were calibrated to experimental data.

An 8-state ODE model (intermediate-scale) of the acute inflammatory response system to endotoxin challenge that was calibrated to experimental data (we shall call this model "8D")

was recently developed [126]. This model had a total of 46 parameters. Endotoxin challenges at $3mg/kg$, $6mg/kg$ and $12mg/kg$ were administered to rats and experimental data for pro-inflammatory cytokines such as interleukin-6 ($IL-6$) and tumor necrosis factor-alpha ($TNF-\alpha$) as well as anti-inflammatory cytokine such as interleukin-10 ($IL-10$) were obtained. Data on endotoxin challenges at $3mg/kg$ and $12mg/kg$ were used to calibrate the model, and model validation was performed at endotoxin level of $6mg/kg$. In view of the above, this research is motivated in part by:

- The need to come up with a moderate size model that is not as highly complex as that developed in [126], and can be calibrated to the same experimental data on inflammatory cytokines.
- The importance of designing an optimal treatment strategy that can control the effects of acute inflammatory response to endotoxins.

In accordance with our motivation, our contributions at the end of this study to the field of acute inflammatory response are as follows:

1) Development and validation of a reduced mathematical model that can accurately predict acute inflammatory response to endotoxin challenge.
2) Prove the existence and uniqueness of a solution to the reduced mathematical model.
3) Apply a Nonlinear Model Predictive Control (NMPC) scheme in conjunction with the Unscented Kalman Filter (UKF) to derive optimal therapeutic interventions for the control of acute inflammation triggered by endotoxins.

To the best of our knowledge, the only work that has been done regarding the control of inflammatory response using NMPC was in [39] (as at the time of writing this thesis, this paper though has been submitted for publication, is yet to be published). Besides, the work ([39]) used a low-order simulated model that was not calibrated to any experimental data.

This work is organized in two main parts. Part I which comprises Chapters 2 and 3 deals with the *derivation of mathematical models of acute inflammatory response to endotoxin challenge*. In Part II, we focus our attention on the *derivation of optimal treatment controls to modulate acute inflammation*; this part contains Chapters 4 through 6. For the remaining of this chapter, we will briefly describe the contents of the chapters in this thesis.

In Chapter 2 we discuss the materials and methods used in deriving the different models to be used in comparisons with the original model (8D) developed in [126]. This chapter begins with an overview of the 8D model, which is followed by the derivation of a reduced model.

We then present the reduced model equations describing the acute inflammatory response system to endotoxin challenge. We also presented a brief introductory background on Sensitivity analysis, Subset selection and Parameter estimation since they are the mathematical tools used to construct and calibrate our models with existing data. We conclude this chapter with a description of a model selection criterion called Akaike Information Criterion (AIC) [3].

We began Chapter 3 by displaying the relative sensitivity rankings at $3\,mg/kg$ and $12\,mg/kg$ endotoxin challenge levels for both 8D and the reduced model, respectively. With the aid of subset selection, the most linearly independent sensitive parameters are identified for all the models we proposed; this information is useful in the calibration of these models to the observed data on cytokines. Next, we present the model comparison and validation plots as well as AIC results. Following the construction of the reduced model in the previous chapter, we show a rigorous mathematical analysis of the existence and uniqueness proof for a solution of the reduced model as well as conduct steady state and stability analysis.

Optimal control methodolody is introduced in Chapter 4 to study our model under open-loop optimal control based treatment strategies. Two control inputs representing treatment therapies are added to the model and an open source solver known as GPOPS is used to solve the optimal control problem numerically. Lastly, we summarize the *in silico* simulation results of the optimal control solutions for each of the three endotoxin challenge levels ($3\,mg/kg$, $6\,mg/kg$ and $12\,mg/kg$).

In Chapter 5, we turn our attention to Model Predictive Control (MPC) and then present an introductory overview of MPC. Nonlinear Model Predictive Control (NMPC) which belongs to a family of MPC schemes that uses nonlinear models and/or considers a non-quadratic cost-functional is also reviewed. Some theoretical issues relating to stability and robustness are discussed as well. Chapter 6 contain the *in silico* simulation results from using NMPC in our optimal control problem. We also discuss a scenario on how a filter based on the Kalman Filter can be employed in conjunction with NMPC in the presence of noisy data. Finally, Chapter 7 summarize the significant contributions of this work and offer possible future directions of research.

Part I

Derivation of Mathematical Models

Chapter 2

Model Derivation

This chapter deals with the materials and methods for the derivation of a mathematical model of acute inflammatory response to endotoxin challenge. To this end, we discuss the formation of "modified 8D"[1] models from carrying out sensitivity and parameter identification analyses on the original 8D model. In addition, we elucidate our decision to construct a reduced model. We will wrap the chapter up by introducing a quantitative model selection technique use for model comparison. For completeness, we will begin with a summary of the 8D model developed in [126]. The interested reader should consult this reference for a comprehensive description of the 8D model development.

2.1 8D Model Overview

Experimental data on cytokines at $3\,mg/kg$ and $12\,mg/kg$ endotoxin challenge levels were used to calibrate the 8D model. The original experiments were conducted on three cohorts of Sprague-Dawley rats weighing approximately $200g$ and were performed according to an IACUC-approved protocol at the University of Pittsburgh, Department of Surgery, to study the acute inflammatory response to endotoxin insults at various concentration levels. The rats received endotoxin (*Escherichia Coli*) at levels of either $3mg/kg$, $6mg/kg$, or $12mg/kg$, intraperitoneally. Blood samples were collected at time points 0, 1, 2, 4, 8, 12 and 24 hours after endotoxin administration. Concentrations of pro- and anti-inflammatory cytokines such as interleukin-6 ($IL6$), interleukin-10 ($IL10$) and tumor necrosis factor-α (TNF) were measured in triplicate using commercially available ELISA kits (R & D Systems, Minneapolis, MN).

[1] "modified 8D" models are simplifications of the original 8D because only a smaller number of parameters will be estimated.

Table 2.1: Parameters of the 8D model

No.	Parameter	Value	Unit	No.	Parameter	Value	Unit
1†	d_P	3	hr^{-1}	24	$x_{IL6IL10}$	1.1818	$\frac{pg}{mL}$
2	k_N	5.5786e7	hr^{-1}	25	k_{IL6IL6}	122.92	–
3	x_N	14.177	$N-unit$	26	x_{IL6IL6}	1.987e5	$\frac{pg}{mL}$
4	d_N	0.1599	hr^{-1}	27‡	x_{IL6CA}	4.2352	$\frac{pg}{mL}$
5	k_{NP}	41.267	$\frac{N-unit \cdot kg}{mg}$	28	k_{TNF}	3.9e-8	$\frac{pg}{mL \cdot N-unit^{1.5}}$
6	k_{ND}	0.013259	$\frac{N-unit}{D-unit}$	29	d_{TNF}	2.035	hr^{-1}
7	x_{NTNF}	1693.9509	$\frac{pg}{mL}$	30	$x_{TNFIL10}$	2.2198e7	$\frac{pg}{mL}$
8	x_{NIL6}	58080.742	$\frac{pg}{mL}$	31‡	x_{TNFCA}	0.19342	$\frac{pg}{mL}$
9‡	x_{NCA}	0.07212	$\frac{pg}{mL}$	32	k_{TNFTNF}	1.0e-10	–
10	x_{NIL10}	147.68	$\frac{pg}{mL}$	33	x_{TNFTNF}	9.2969e6	$\frac{pg}{mL}$
11	k_{NTNF}	12.94907	–	34	x_{TNFIL6}	55610	$\frac{pg}{mL}$
12	k_{NIL6}	2.71246	–	35	$k_{IL10TNF}$	2.9951e-5	–
13	k_D	2.5247	$\frac{D-unit}{hr}$	36	$x_{IL10TNF}$	1.1964e6	$\frac{pg}{mL}$
14	d_D	0.37871	hr^{-1}	37	$k_{IL10IL6}$	4.1829	–
15	x_D	1.8996e7	$N-unit$	38	$x_{IL10IL6}$	26851	$\frac{pg}{mL}$
16‡	k_{CA}	0.154625e-8	$\frac{pg}{mL \cdot hr \cdot N-unit}$	39	k_{IL10}	1.3374e5	$\frac{pg}{mL \cdot hr}$
17‡	d_{CA}	0.31777e-1	hr^{-1}	40	d_{IL10}	98.932	hr^{-1}
18‡†	s_{CA}	0.004	$\frac{pg}{mL \cdot hr}$	41	x_{IL10}	8.0506e7	$N-unit$
19	k_{IL6TNF}	4.4651	–	42†	s_{IL10}	1187.2	$\frac{pg}{mL \cdot hr}$
20	x_{IL6TNF}	1211.3	$\frac{pg}{mL}$	43	x_{IL10d}	791.27	$\frac{pg}{mL}$
21	k_{IL6}	9.0425e7	$\frac{pg}{mL \cdot hr}$	44	k_{IL102}	1.3964e7	$\frac{Y_{IL10}-Unit}{hr}$
22	d_{IL6}	0.43605	hr^{-1}	45	d_{IL102}	0.0224	hr^{-1}
23	x_{IL6}	1.7856e8	$N-unit$	46	x_{IL102}	37.454	$D-unit$

‡ Parameter not part of reduced model

† Parameter not estimated in both reduced and 8D models

The 8D model comprised of eight ordinary differential equations with the following states: Endotoxin concentration ($P(t)$); total number of activated phagocytic cells ($N(t)$), which includes all activated immune response cells, such as neutrophils, monocytes, etc.; a non-accessible tissue damage marker ($D(t)$); concentrations of pro-inflammatory cytokines interleukin-6 ($IL6(t)$) and tumor necrosis factor-α ($TNF(t)$); concentration of the anti-inflammatory cytokine interleukin-10 ($IL10(t)$); a tissue damage driven non-accessible IL-10 promoter ($Y_{IL10}(t)$); and a non-accessible state representing slow acting anti-inflammatory mediators ($CA(t)$). 8D had a total

of 46 parameters of which 43 were estimated. These parameters and their nominal values are displayed in Table 2.1. The actual representation of the 8D ODE system described in [126] is given in Appendix A.

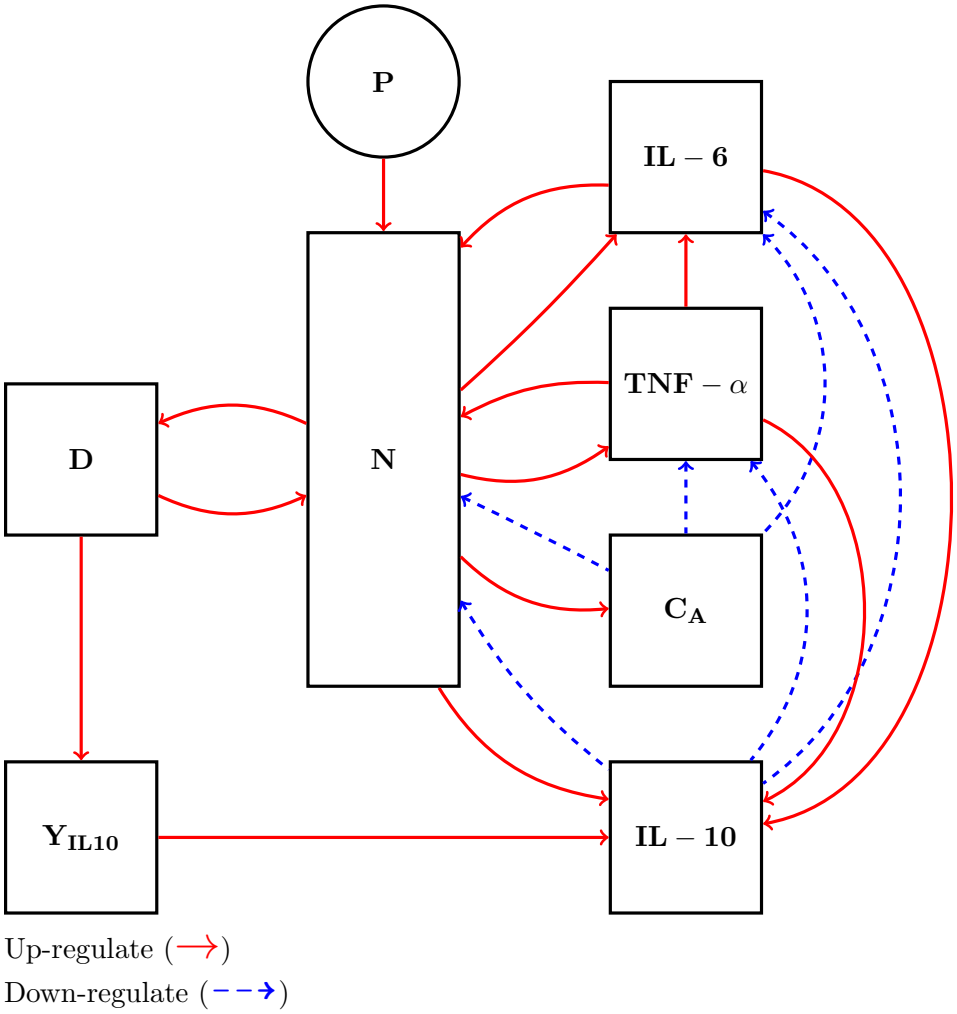

Figure 2.1: Schematic diagram of the inflammatory response system challenged by endotoxin [36, 126]

Figure 2.1 shows the 8D schematic diagram capturing all major interactions among the state variables. The administration of endotoxin $P(t)$ into the system activates $N(t)$. Once activated, $N(t)$ up-regulates production/release of all inflammatory mediators ($TNF(t)$, $IL6(t)$, $IL10(t)$

and $C_A(t)$) [53]. The pro-inflammatory cytokines exert positive feedback on the system; hence, further activate $N(t)$ and up-regulate other cytokines [14, 53]. The anti-inflammatory mediators exert negative feedback on the system; hence, $IL10(t)$ and $C_A(t)$ inhibit the activation of $N(t)$ and down-regulate other cytokines [107, 110]. The model also incorporates tissue damage due to activated phagocytic cells, represented by a damage marker, $D(t)$. Tissue damage further up-regulates activation of $N(t)$ [93] and also contributes to up-regulation of $IL10(t)$ [55, 72].

2.2 Derivation of Model

In this section, the various mathematical tools used in creating "modified 8D" and the reduced models are discussed. First, we justify our rational for building adequate reduced models capable of predicting the observed dynamics of pro- and anti-inflammatory cytokines.

2.2.1 Derivation of Reduced Model

In order to derive a reduced model, we used information in [38, 39, 120, 126] to categorize the state variables in the 8D model into five groups:

- Endotoxin concentration: $P(t)$
- Inflammation : Total number of activated phagocytic cells ($N(t)$)
- Collection of pro-inflammatory cytokines: $IL6(t)$ and $TNF(t)$
- Collection of anti-inflammatory mediators: $IL10(t)$ and $C_A(t)$
- Tissue damage: $D(t)$ and $Y_{IL10}(t)$.

As evidenced in Figure 2.1, the concentration of $C_A(t)$, which is a combination of slow acting anti-inflammatory mediators, appears to have the least interactions of all the other inflammatory mediators. Furthermore, $C_A(t)$ was the only inflammatory mediator not measured in the experiment done on rats [126]. Perhaps it cannot be measured since it is a combination of slow acting anti-inflammatory mediators. Lastly, a subtle fact to consider will be the order of magnitude for $C_A(t)$, which is -1; the inflammatory mediator with the next smallest order of magnitude is $IL10(t)$ with a value of 2 (these information can be obtained from the plots in [126]). Hence, we can deduce that $C_A(t)$ is relatively less significant in the overall contribution to acute inflammatory response triggered by endotoxin. To this end, $C_A(t)$ will be eliminated from the 8D model to form a reduced model called 7D. This decision will also result in a reduction of the number of parameters from 46 to 40.

As part of our model building cycle, we intend to calibrate our models to the experimental data on inflammatory cytokine. Since we do not have access to the original experimental observations, *Engauge digitizer* version 4.1 [46] was used to digitize the data in [126]. Plots of the digitized data were compared visually with the reported data. *Engauge digitizer* is an open source digitizing software that converts an image file of a graph or map into numerics [46]. Finally, we will adopt the same approach used in the 8D model building cycle by calibrating the 7D and "modified 8D" models at endotoxin levels $3\,mg/kg$ and $12\,mg/kg$, respectively. Endotoxin challenge level $6mg/kg$ will then be used for model prediction.

2.2.2 7D ODE Model

The reduced 7D mathematical model of acute inflammatory response to endotoxin challenge is described in this section, the model consist of 7 ordinary differential equations and 40 parameters.

$$\frac{dP(t)}{dt} = -d_p \cdot P(t) \tag{2.1}$$

$$\frac{dN(t)}{dt} = k_N \cdot \frac{\mathbf{\Gamma(t)}}{x_N + \mathbf{\Gamma(t)}} - d_N \cdot N(t) \tag{2.2}$$

$$\frac{dD(t)}{dt} = k_D \cdot \frac{N(t)^6}{x_D^6 + N(t)^6} - d_D \cdot D(t) \tag{2.3}$$

$$\frac{dIL6(t)}{dt} = k_{IL6} \cdot \frac{N(t)^4}{x_{IL6}^4 + N(t)^4} \cdot \mathbf{\Omega(t)} - d_{IL6} \cdot IL6(t) \tag{2.4}$$

$$\frac{dTNF(t)}{dt} = k_{TNF} \cdot N(t)^{1.5} \mathbf{\Phi(t)} - d_{TNF} \cdot TNF(t) \tag{2.5}$$

$$\frac{dIL10(t)}{dt} = k_{IL10} \cdot \frac{N(t)^3}{x_{IL10}^3 + N(t)^3} \cdot \mathbf{\Psi(t)} - \mathbf{\Theta(t)} + Y_{IL10}(t) + s_{IL10} \tag{2.6}$$

$$\frac{dY_{IL10}(t)}{dt} = k_{IL102} \cdot \frac{D(t)^4}{x_{IL102}^4 + D(t)^4} - d_{IL102} \cdot Y_{IL10}(t), \tag{2.7}$$

with the initial condition

$$\begin{aligned} &P(0) = 3,\ 6,\ or\ 12; \quad N(0) = 0; \quad D(0) = 0; \quad IL6(0) = 0 \\ &TNF(0) = 0; \quad IL10(0) = \frac{s_{IL10} \cdot x_{IL10d}}{d_{IL10} \cdot x_{IL10d} - s_{IL10}}; \quad Y_{IL10}(0) = 0. \end{aligned} \tag{2.8}$$

In addition, from Equation (2.2)

$$\begin{aligned}
\mathbf{\Gamma(t)} &= [k_{NP} \cdot P(t) + k_{ND} \cdot D(t)] \cdot fDN_{NIL10}(t) \cdot \gamma(t) \\
\gamma(t) &= (1 + k_{NTNF} \cdot fUP_{NTNF}(t)) \cdot (1 + k_{NIL6} \cdot fUP_{NIL6}(t)) \\
fDN_{NIL10}(t) &= \frac{x_{NIL10}}{x_{NIL10} + IL10(t)} \\
fUP_{NTNF}(t) &= \frac{TNF(t)}{x_{NTNF} + TNF(t)} \\
fUP_{NIL6}(t) &= \frac{IL6(t)}{x_{NIL6} + IL6(t)},
\end{aligned} \tag{2.9}$$

from Equation (2.4)

$$\begin{aligned}
\mathbf{\Omega(t)} &= (1 + k_{IL6TNF} \cdot fUP_{IL6TNF}(t) + k_{IL6IL6} \cdot fUP_{IL6IL6}(t)) \cdot fDN_{IL6IL10}(t) \\
fDN_{IL6IL10}(t) &= \frac{x_{IL6IL10}}{x_{IL6IL10} + IL10(t)} \\
fUP_{IL6TNF}(t) &= \frac{TNF(t)}{x_{IL6TNF} + TNF(t)} \\
fUP_{IL6IL6}(t) &= \frac{IL6(t)}{x_{IL6IL6} + IL6(t)},
\end{aligned} \tag{2.10}$$

from Equation (2.5)

$$\begin{aligned}
\mathbf{\Phi(t)} &= [1 + k_{TNFTNF} \cdot fUP_{TNFTNF}(t)] \cdot fDN_{TNFIL10}(t) \cdot fDN_{TNFIL6}(t) \\
fDN_{TNFIL10}(t) &= \frac{x_{TNFIL10}}{x_{TNFIL10} + IL10(t)} \\
fDN_{TNFIL6}(t) &= \frac{x_{TNFIL6}}{x_{TNFIL6} + IL6(t)} \\
fUP_{TNFTNF}(t) &= \frac{TNF(t)}{x_{TNFTNF} + TNF(t)},
\end{aligned} \tag{2.11}$$

and from Equation (2.6)

$$
\begin{aligned}
\mathbf{\Psi(t)} &= 1 + k_{IL10IL6} \cdot fUP_{IL10IL6}(t) + k_{IL10TNF} \cdot fUP_{IL10TNF} \\
\mathbf{\Theta(t)} &= d_{IL10} \cdot fDN_{IL10d}(t) \cdot IL10(t) \\
fDN_{IL10d}(t) &= \frac{x_{IL10d}}{x_{IL10d} + IL10(t)} \\
fUP_{IL10IL6}(t) &= \frac{IL6(t)^4}{x_{IL10IL6}^4 + IL6(t)^4} \\
fUP_{IL10TNF} &= \frac{TNF(t)}{x_{IL10TNF} + TNF(t)}.
\end{aligned}
\tag{2.12}
$$

We will mimic the description of the original 8D model [126] in describing the 7D model. The dynamics of $P(t)$ are described in Equation (2.1); $P(t)$ decays exponentially with a decay rate of d_P. We used the same value for the decay rate as in [126], which is fixed at $3\,hr^{-1}$. This value is also in accordance with published results [38, 79, 142].

Equations (2.2) and (2.9) denote the total number of activated phagocytic cells $N(t)$. Resting phagocytic cells are activated by the presence of endotoxin, k_N is the rate of activation of $N(t)$ and d_N is the elimination rate. $N(t)$ is activated by $P(t)$ and $D(t)$ via $\mathbf{\Gamma(t)}$ as described in Equation (2.9). Functions with nomenclature $fUP_{ij}(t)$ and $fDN_{ij}(t)$ represent up-regulating (UP) and down-regulating (DN) effects of inflammatory cytokine j on cytokine i. These functions are bounded between 0 and 1 and are dimensionless. The up-regulating functions, $fUP_{NTNF}(t)$ and $fUP_{NIL6}(t)$, in Equation (2.9) are Michaelis-Menten type equations; as the concentrations increase, the values of these functions approach 1 asymptotically. Gain parameters k_{NTNF} and k_{NIL6} scale the up-regulating functions to get the real effect of $N(t)$. The inhibitory effects of $IL10(t)$ are represented by the down-regulating function fDN_{NIL10}; as the level of $IL10(t)$ raises, fDN_{NIL10} approaches 0 asymptotically. x_N, x_{NTNF}, x_{NIL6} and x_{NIL10} are the half-saturation parameters that determine the concentration levels of the states so that the corresponding $fUP_{NTNF}(t)$, $fUP_{NIL6}(t)$, and fDN_{NIL10} functions will attain half of its saturation point.

Equation (2.3) corresponds to the tissue damage instigated by the inflammatory response to endotoxin challenge. k_D is the rate of production of $D(t)$, d_D is the corresponding rate of elimination, and x_D is the half-saturation parameter. Increased levels of $D(t)$ further activates $N(t)$ and thus produced $IL10(t)$. A 6^{th} order Hill function was used to accurately capture the data [126].

The concentration of $IL6(t)$ is described in Equations (2.4) and (2.10). $IL6(t)$ is up-regulated by the activation of $N(t)$, the presence of elevated levels of $TNF(t)$, and $IL6(t)$ itself. This behav-

ior is captured by the up-regulating functions, $fUP_{IL6TNF}(t)$ and $fUP_{IL6IL6}(t)$, respectively, in Equation (2.10); the down-regulating function, $fDN_{IL6IL10}(t)$, is the inhibitory effect and d_{IL6} is the clearance rate of $IL6(t)$. A 4^{th} order Hill function was used to accurately capture the data [126], and x_{IL6}, x_{IL6TNF}, x_{IL6IL6} and $x_{IL6IL10}$ are the half-saturation parameters.

The pro-inflammatory cytokine $TNF(t)$ is described in Equations (2.5) and (2.11), respectively. $TNF(t)$ is produced by the activation of $N(t)$; k_{TNF} is the rate production of $TNF(t)$ and d_{TNF} is the clearance rate. An exponent of 1.5 was assigned to $N(t)$ to accurately represent the rapid production and elimination of $TNF(t)$; the justification for this choice is discussed in [126]. The $fUP_{TNFTNF}(t)$ function in Equation (2.11) is the up-regulating effect of $TNF(t)$ on its own production; whereas $fDN_{TNFIL10}(t)$ and $fDN_{TNFIL6}(t)$ are the inhibitory effects. x_{TNFTNF}, $x_{TNFIL10}$ and x_{TNFIL6} are the half-saturation parameters.

The concentration of the anti-inflammatory cytokine $IL10(t)$ is represented in Equations (2.6) and (2.12), respectively. $IL10(t)$ is up-regulated by the $fUP_{IL10IL6}(t)$ and $fUP_{IL10TNF}$, respectively. This is described in Equation (2.12); the production of $IL10(t)$ in the basal state is given by s_{IL10}, which can be obtained from the experimental data. It was shown in [125] that the rate of elimination of $IL10(t)$ is inversely proportional to the circulating concentration of $IL10(t)$, this is depicted by the down-regulating function $fDN_{IL10d}(t)$ in Equation (2.12) alongside the parameter d_{IL10}. x_{IL10}, x_{IL102}, $x_{IL10IL6}$, $x_{IL10TNF}$ and x_{IL10d} are the half-saturation parameters.

The dynamics of $Y_{IL10}(t)$ are described by Equation (2.7). k_{IL102} is the rate of production of $Y_{IL10}(t)$ and d_{IL102} is the rate of elimination. A 4^{th} order Hill function, which is driven by $D(t)$, is used to model $Y_{IL10}(t)$,

2.2.3 Sensitivity Analysis

Sensitivity analysis is an important concept in model building since it is used to determine how sensitive a given measured output is as the parameters of the model are perturbed. Parameters that are found to be sensitive to a given measured output are considered to have strong influence in affecting the trajectory of the output when varied slightly and those that are insensitive have little or no effect on the output regardless of the magnitude of perturbation made on them. Sensitivity analysis is particularly useful in mathematical modeling because models can contain large number of parameters and estimating the values of these parameters accurately is usually difficult. Parameter sensitivity helps in narrowing the focal point on those that are identified as sensitive; this is achieved by examining the influence each parameter has on the variability of a particular measured output.

To formally introduce this concept, we consider a nonlinear system of the form:

$$\frac{d\mathbf{y}(t)}{dt} = f(t, \mathbf{y}; \mathbf{q}), \qquad \mathbf{y} \in \mathbb{R}^n, \quad \mathbf{q} \in \mathbb{R}^m \tag{2.13}$$

$$\mathbf{z}(t) = h(t, \mathbf{y}, \mathbf{q}), \qquad \mathbf{z} \in \mathbb{R}^r, \tag{2.14}$$

with the initial condition

$$\mathbf{y}(0) = \mathbf{y_0}, \tag{2.15}$$

where $\mathbf{y}$, $\mathbf{z}$ and $\mathbf{q}$ denote state, output and parameter vectors, respectively. We are interested in how $\mathbf{z}$ changes with respect to $\mathbf{q}$ (sensitivity), i.e., $\frac{\partial \mathbf{z}(t)}{\partial \mathbf{q}}$. To determine the sensitivity of the outputs $\mathbf{z}$ with respect to the parameters $\mathbf{q}$, we take the partial derivative of Equation (2.14)

$$\frac{\partial \mathbf{z}}{\partial \mathbf{q}} = \frac{\partial \mathbf{h}}{\partial \mathbf{y}} \frac{\partial \mathbf{y}}{\partial \mathbf{q}} + \frac{\partial \mathbf{h}}{\partial \mathbf{q}}. \tag{2.16}$$

In order to obtain $\frac{\partial \mathbf{y}}{\partial \mathbf{q}}$ we need to derive a system of differential equations for the sensitivities by differentiating both sides of (2.13) with respect to $\mathbf{q}$ and switching the order of differentiation to yield the sensitivity equations

$$\frac{d}{dt} \frac{\partial \mathbf{y}}{\partial \mathbf{q}} = \frac{\partial \mathbf{f}}{\partial \mathbf{y}} \frac{\partial \mathbf{y}}{\partial \mathbf{q}} + \frac{\partial \mathbf{f}}{\partial \mathbf{q}}. \tag{2.17}$$

We assume that the initial conditions of the sensitivities are zero (that is, $\frac{\partial \mathbf{y}(0)}{\partial \mathbf{q}} = 0$) since the initial conditions of the model would not be considered to be dependent on the model parameters. By coupling equations (2.13) and (2.17), we have an $n + nm$ dimensional system of differential equations for both the model and the sensitivities. Coupling ensures that the solution for $\mathbf{y}(t)$ is sufficiently accurate to solve the sensitivity system to the desired accuracy. On the other hand, if the equations are not coupled, some interpolating scheme will be required when the differential equations are solved numerically using adaptive mesh methodologies.

The partial derivatives $\frac{\partial z_i(t)}{\partial q_j}$, for $i = 1 \ldots r, j = 1 \ldots m$, are known as first-order sensitivities [30, 64]. The second-order sensitivities, $\frac{\partial^2 z_i(t)}{\partial q_j \partial q_k}$, for $i = 1 \ldots r, j, k = 1 \ldots m$ can also be calculated and they ascertain the sensitivity of the the first-order sensitivity $\frac{\partial z_i(t)}{\partial q_j}$ with respect to changes in q_k. Besides, they contain information about the quadratic dependence of the measured states on changes in the parameters [64]. In [30] the second-order sensitivity values were applied in the presentation of a new parameter subset selection procedure because it plays an important role in the uncertainty analysis of the selection procedure. Finally, the sensitivity analysis technique we are using in this work is widely embraced in the literature [1, 37, 44, 108].

In this work, we only consider the first-order sensitivity of the experimental data ($IL6(t)$, $TNF(t)$ and $IL10(t)$). In addition, our output equations (Equation (2.14)) are linear functions of the state

$$\mathbf{z}(t) = \mathbf{C}\mathbf{y}(t), \tag{2.18}$$

where $\mathbf{C}$ is given by

$$\mathbf{C} = \begin{pmatrix} 0 & 0 & 0 & 1 & 0 & 0 & 0 \\ 0 & 0 & 0 & 0 & 1 & 0 & 0 \\ 0 & 0 & 0 & 0 & 0 & 1 & 0 \end{pmatrix}. \tag{2.19}$$

From the experiment carried out in [126], three parameters were specified in the 8D model; the clearance rate of endotoxin concentration $P(t)$ captured by d_p was obtained from the literature [79, 142], while s_{CA} and s_{IL10} were extracted from the experimental data. This implies that in the construction of "modified 8D" $\mathbf{z} \in \mathbb{R}^3_+$ and $\mathbf{q} \in \mathbb{R}^{43}_+$; where $\mathbb{R}^r_+$ is the space of r-tuple nonnegative real numbers, $\mathbf{z} \in \mathbb{R}^3_+$ denote the 3 outputs (measured cytokines) and $\mathbf{q} \in \mathbb{R}^{43}_+$ indicate the 43 parameters we wish to investigate their sensitivity levels for each output. Similarly, in building the reduced 7D model, $\mathbf{z} \in \mathbb{R}^3_+$ and $\mathbf{q} \in \mathbb{R}^{38}_+$ because we excluded d_p and s_{IL10} in the 7D model sensitivity analysis; s_{CA} is not in the reduced model since it is linked with $C_A(t)$ which was removed to form 7D.

The matrix $\mathbf{S}(t) = \frac{\partial z_i(t)}{\partial q_j}$ for $i = 1 \dots 3, j = 1 \dots m$ is known as the sensitivity matrix (or the Jacobian matrix or the Fréchet derivative [64]) at time t, where $m = 43$ for 8D and $m = 38$ for 7D depending on the model we wish to analyze. $\mathbf{S}(t)$ can be normalized by $\mathbf{RS}(t) = \frac{\partial z_i(t)}{\partial q_j}\frac{q_j}{z_i(t)}$, which is known in the literature as relative sensitivity matrix at time t (here $t = 1$, 2, 4, 8, 12 and 24. These represent the time points blood samples were taken in the experiment). Let $\bar{\mathbf{RS}}$ be the relative sensitivity matrix across all time period; this matrix can be constructed by stacking the time dependent relative sensitivity matrices $\mathbf{RS}(t)$ for $t = 1$, 2, 4, 8, 12 and 24 as follows

$$\bar{\mathbf{RS}} = \begin{bmatrix} \mathbf{RS}(t=1) \\ \mathbf{RS}(t=2) \\ \mathbf{RS}(t=4) \\ \mathbf{RS}(t=8) \\ \mathbf{RS}(t=12) \\ \mathbf{RS}(t=24) \end{bmatrix}_{18\times m}. \tag{2.20}$$

Note that $\bar{\mathbf{RS}}$ will be constructed for endotoxin dose levels $3\,mg/kg$ and $12\,mg/kg$, respectively. Sensitivity computations were carried out using a relative and generalized sensitivity analysis solver called "tssolve" [11]. This "tssolve" solver uses Automatic Differentiation (AD) [49] to compute the partial derivatives in Equations (2.16) and (2.17), respectively. The computations were performed using MATLAB version "R2009a" (©2009 The Mathworks Inc., Natick, MA).

Finite difference methods can also be utilized in the approximation of the partial derivatives contained in the sensitivity equations (Equations (2.16) and (2.17)). For example, [1, 36, 64, 108] used finite differences in their respective computations, while [37, 50] made use of AD and [44] employed both methods. Whenever numerical approximation methods such as finite difference is utilized, it is always important to consider the relationship between the difference increment used in the computation of the derivative and the accuracy of the solution obtained from the integrator. However, AD does not have such considerations since it is a "machine precision exact" method that breaks down a function into small component operations before taking derivatives by applying chain rule.

The relative sensitivity matrix computed in Equation (2.20) yields sensitivity information as a function of time. In any case, our priority in this work is to distinguish those model dynamic parameters that significantly influence the outputs of our process over time. To achieve this goal, we compute the *relative sensitivity ranking* using a modified $\mathcal{L}_2$ norm,

$$\left\| \frac{\partial z_i}{\partial q_j} \right\|_2 \cdot \left(\frac{q_j}{\max\, z_i} \right) = \left[\frac{1}{t_f - t_0} \int_{t_0}^{t_f} \left(\frac{\partial z_i}{\partial q_j} \right)^2 dt \right]^{\frac{1}{2}} \cdot \left(\frac{q_j}{\max\, z_i} \right). \tag{2.21}$$

In general, the *relative sensitivity ranking* contain information regarding the number of parameters that are most sensitive to each output since it ranks the model parameters according to their respective sensitive levels. Finally, it is noted that there are other norms adapted in the literature to compute the sensitivity value. For example,
in [1], an $\mathcal{L}_2$ norm of the form was used

$$\sqrt{\frac{1}{N^j} \sum_{i=1}^{N^j} \left| \frac{\partial z}{\partial q_k}(t^{ij}; q^j) q_k \right|^2},$$

whereas another $\mathcal{L}_2$ norm of the form was used in [37]

$$\|f(t)\|_2^2 = \int f^2(t) dt,$$

and [44] employed an unspecified norm of the form

$$\|S_{jk}(t, q_0)\| = \left\| \frac{dy_j(t_i, q_0)}{dq_k} \frac{q_k}{y_j(t_i, q_0)} \right\|.$$

2.2.4 Subset Selection

We will begin this section by introducing the concept of *identifiability* with two simple illustrations.

Problem 2.2.1 *This problem is taken from [32], which was first discussed in [16]. Consider the first-order model:*

$$\frac{dx(t)}{dt} = -p_1 x(t) + p_2 u(t), \qquad x(0) = 0 \tag{2.22}$$

$$y(t) = p_3 x(t). \tag{2.23}$$

In this problem, $x(t)$ represents the concentration of a drug introduced into a biological system, $u(t)$ is a test-input injection of the drug of known wave form and in mass units, and $y(t)$ is a temporal measurement of the drug concentration in the system, say by bioassay. There are three parameters in the model: p_1, the fractional rate constant for the drug; p_2 is the inverse of its distribution volume and p_3, the unknown proportionality constant for the bioassay measure of drug concentration. For any known u, the explicit solution of Equations (2.22) *and* (2.23) *is given by*

$$y(t) = p_2 p_3 \int_0^t e^{-p_1(t-\tau)} u(\tau) d\tau. \tag{2.24}$$

If the drug is introduced rapidly as a brief pulse of unit magnitude, i.e., an approximation impulse $u(t) = \delta(t)$, one obtains the more familiar solution

$$y(t) = p_2 p_3 e^{-p_1 t}. \tag{2.25}$$

Semi-logarithmic plot of the data represented as $y(t)$ for this model yields the coefficient $A \equiv p_2 p_3$ and exponent $\lambda \equiv p_1$. Thus only p_1 and the product $p_2 p_3$ can be determined and not p_2 or p_3. When this happens, the model is said to be ***unidentifiable****. If p_2 or p_3 were known, or related in a known way, all parameters could be uniquely determined from $y(t)$. In this case, we say the model (or model parameters) is (are)* ***uniquely identifiable****.*

Problem 2.2.2 *In [42], the notion of* ***sensitivity identifiability*** *was discussed, although it was originally introduced in [119].*

Consider an m by P output sensitivity function matrix with respect to the parameters, $S(t, \mathbf{p}) \equiv [\frac{\partial y(t,\mathbf{p})}{\partial p_j}]$, *evaluated at a nominal* $\mathbf{p}^0$. *To define this inherently local concept, let* $\triangle\mathbf{p}$ *denote a local perturbation about a nominal* $\mathbf{p}^0$, *i.e.,* $\triangle\mathbf{p} \equiv \mathbf{p} - \mathbf{p}^0$, *which gives rise to a local perturbation* $\triangle\mathbf{y}$ *in the output, i.e.,* $\triangle\mathbf{y} \equiv y(t, \mathbf{p}) - y(t, \mathbf{p}^0)$. *Then*

$$\triangle\mathbf{y} \cong S\triangle\mathbf{p}. \tag{2.26}$$

A structure is ***sensitivity identifiability*** *if* (2.26) *can be solved uniquely (in the local sense) for* $\triangle\mathbf{p}$. *This is the case if and only if the column rank of the matrix S is equal to P, the number of unknown parameters, or*

$$\det(S^T S) \neq 0. \tag{2.27}$$

One of the drawbacks of sensitivity analysis is that it identifies "sensitive" parameters that are both *unidentifiable* (linearly dependent) as well as *identifiable* (linearly independent). In such situation, subset selection can be employed to separate the most linearly independent sensitive parameter from the rest. These become the identifiable parameters and the less identifiable set will be fixed to some nominal values during the optimization process. Subset selection methodologies for partitioning the parameter space into well-conditioned and ill-conditioned subsets were described in [50]. Similarly, the following subset selection methods were discussed in [108];

i. QR Factorization with column pivoting

ii. SVD followed by QR with column pivoting

iii. Gu-Eisenstat's strong rank revealing QR

iv. SVD followed by Gu-Eisenstat's SRRQR.

Methods (i) and (ii) were earlier described by [58, 59], respectively. The last two methods were proposed in [62] and are considered to be very efficient and more theoretically sound but are quite complicated to implement [108]. The *QR Factorization with column pivoting* algorithm is widely recognized to be computationally efficient and has been implemented in many applications, including the rank-deficient least squares problems. However, it has been shown that this algorithm fails for some examples [62]. Analyses on the performance of these four subset selection methods were also carried out in [108]; the results obtained revealed that the *SVD followed by QR with column pivoting* performed just as well as the more theoretically sound methods (*Gu-Eisenstat's strong rank revealing QR* and *Gu-Eisenstat's strong rank revealing QR*). For this reason, we will use the *SVD followed by QR with column pivoting* algorithm

on the relative sensitivity matrix $\bar{\mathbf{RS}}$ in (2.20) to obtain the most identifiable parameters at endotoxin levels $3\,mg/kg$ and $12\,mg/kg$, respectively. In addition, we favored this algorithm because it is relatively easy to implement.

The *SVD followed by QR with column pivoting* algorithm is outlined below.

- Compute the SVD of $\bar{\mathbf{RS}} = U\Sigma V^T$ and determine the numerical rank $\hat{r}$ of $\bar{\mathbf{RS}}$.
  Hence, we employed the technique described in [50] to determine $\hat{r}$ as follows

$$\hat{r} = \max\left\{ i \,\middle|\, \frac{|\sigma_i|}{|\sigma_1|} > \epsilon \, \|\bar{\mathbf{RS}}\| \, m \right\},$$

  where σ_i represent the sorted singular values of $\bar{\mathbf{RS}}$ such that $\sigma_1 = \max\{\sigma_i\}$, m is the number of parameters, which corresponds with the number of columns in $\bar{\mathbf{RS}}$ and the tolerance ϵ is a problem dependent constant. Usually ϵ is the machine precision tolerance; for this work ϵ=3.55e-15. The MATLAB code for computing the numerical rank is as follows:

Code:
```
[row col]=size(RS);
sigma=svd(RS);
ratio=abs(sigma)/abs(sigma(1));
NumRank=find(ratio > eps(norm(RS))*norm(RS)*col,1,'last');
```

- Let $V = [V_{\hat{r}} \quad V_{N-\hat{r}}]$ where $V_{\hat{r}}$ is the first $\hat{r}$ columns of V.
- Perform a QR factorization with pivoting on $V_{\hat{r}}^T$ to obtain $V_{\hat{r}}^T P = QR$.
  QR with column pivoting will align the linearly independent columns of $\bar{\mathbf{RS}}$ to the left and the permutation matrix P contains the information on how the columns of $\bar{\mathbf{RS}}$ were repositioned.
- Choose as the subset of components of x the first $\hat{r}$ components of $P^T x$, where $x = [1,\, 2,\, 3, \ldots,\, 43]^T$ for 8D and $x = [1,\, 2,\, 3, \ldots,\, 38]^T$ for 7D.

An extension of the *SVD followed by QR with column pivoting* algorithm that applies its eigenvalue decomposition on the Hessian matrix was proposed in [138]. This algorithm is claimed to be more appropriate for nonlinear least squares estimation; the interested reader is referred to [64] for an application of this method.

We conclude this section with some additional remarks. An alternative approach to compute the numerical rank $\hat{r}$ was described in [58]. Define a tolerance $\delta > 0$ for the computed singular

values $\hat{\sigma}_i$. $\bar{\mathbf{RS}}$ has a numerical rank $\hat{r}$ if the $\hat{\sigma}_i$ satisfy

$$\hat{\sigma}_1 \geq \ \ldots \geq \hat{\sigma}_{\hat{r}} > \delta \geq \hat{\sigma}_{\hat{r}+1} \geq \ \ldots \geq \hat{\sigma}_n.$$

Usually, the tolerance δ is chosen to be consistent with the machine precision, for example, $\delta = \mathbf{u}\|\bar{\mathbf{RS}}\|_\infty$. If the relative error in the data is larger than $\mathbf{u}$, then δ should be bigger, for instance, if the entries in $\bar{\mathbf{RS}}$ are correct to two digits then $\delta = 10^{-2}\|\bar{\mathbf{RS}}\|_\infty$. [44] applied this approach with the 2-norm rather than the ∞-norm. Lastly, subset selection can also be applied on the generalized sensitivity matrix $\bar{\mathbf{S}}$, which can be constructed by stacking the time dependent matrices $\mathbf{S}(t = i)$ for each i time point, or the Fisher Information Matrix (FIM), $\bar{\mathbf{S}}^T\mathbf{Q}^{-1}\bar{\mathbf{S}}$ where $\mathbf{Q}$ is the measurement covariance matrix. The choice of matrix to use is dependent on how well-conditioned /ill-conditioned the problem is; we used the relative sensitivity matrix $\bar{\mathbf{RS}}$ because of the large variation in the order of magnitude of the experimental data.

2.2.5 Parameter Estimation

The goal of parameter estimation (also known as inverse problem or model calibration) is to obtain parameter values of a model that give the best fit to a set of experimental data. To carry out parameter estimation the free parameters must be assigned nominal values that serve as an "initial guess" before commencing the optimization process [85]. The most convenient approach to estimate unknown parameters is from available data; this is usually achieved by calibrating the model to reproduce the experimental results in the best possible way. This calibration is carried out by minimizing a given cost function that measures the goodness of fit [124]. The cost functions, which are represented by bayesian estimator, maximum likelihood estimator, and (weighted) least squares estimator, have been shown to perform relatively well in practice. The bayesian estimation, which happens to be the most complicated, requires the parameter probability distribution and the conditional probability distribution of the measurements for the specified parameters to be parameterized. The least squares estimation, considered to be the least complicated, can be carried out effectively with the availability of observed data, or *in silico* simulated data [87, 124].

The following potential pitfalls and difficulties when conducting parameter estimation for dynamic systems were outlined in [130]:

- Lack of convergence to local solutions. This arises when only bad starting values for the parameters are used.
- The model functions are poorly scaled.

- The cost function appears very flat in the neighborhood of the solution.
- Some of the terms in the system's dynamics are non-differentiable.

In addition, Schittkowski [130] classified the existing methods for parameter estimation for dynamic systems into two main groups (the excerpt is from [124]):

1) Initial value methods (also known as single shooting): The parameter estimation problem is solved as a nonlinear optimization (NLO) problem which requires the solution of an inner initial values problem (IVP) for each function evaluation. The outer NLO is usually solved using Levenberg-Marquardt or Gauss-Newton methods. These methods are very efficient and converge globally to the correct solution when a good initial guess for the parameters is specified, otherwise, they converge to local solutions. As these NLOs are frequently multimodal, a lack of fit could be due to convergence to one of such local solutions, even if the model can represent the data perfectly well.

2) Multiple shooting ([21, 136]): Here the dynamic state variables are discretized in some way, leading to larger NLOs (i.e., more degrees of freedom) but avoiding the need of solving an inner IVP. Also, it has been shown that this method does not introduce as much multimodality as single shooting methods. However, since the resulting large NLO is usually solved using Gauss-Newton methods, which are of local nature, it can still converge to a local solution, especially when only a poor initial guess is available.

In this work, a nonlinear least-squares method with a normalized residual was formulated to use as the cost function describing the error between the computed model output and the experimental data. Similar method was applied in [36]. To this end, we defined

$$\mathbf{J_{IL6_3}}(\mathbf{q}) = \frac{1}{\max_j(y^{IL6_3}_{j(j=1,\ldots,7)})} \sum_{i=1}^{7} [y_i^{IL6_3} - y(t_i,\mathbf{q})^{IL6_3}]^2, \quad IL6(t) \text{ at } 3mg/kg, \tag{2.28}$$

$$\mathbf{J_{TNF_3}}(\mathbf{q}) = \frac{1}{\max_j(y^{TNF_3}_{j(j=1,\ldots,7)})} \sum_{i=1}^{7} [y_i^{TNF_3} - y(t_i,\mathbf{q})^{TNF_3}]^2, \quad TNF(t) \text{ at } 3mg/kg, \tag{2.29}$$

$$\mathbf{J_{IL10_3}}(\mathbf{q}) = \frac{1}{\max_j(y^{IL10_3}_{j(j=1,\ldots,7)})} \sum_{i=1}^{7} [y_i^{IL10_3} - y(t_i,\mathbf{q})^{IL10_3}]^2, \quad IL10(t) \text{ at } 3mg/kg, \tag{2.30}$$

$$\mathbf{J_{IL6_{12}}}(\mathbf{q}) = \frac{1}{\max_j(y^{IL6_{12}}_{j(j=1,\ldots,7)})} \sum_{i=1}^{7} [y_i^{IL6_{12}} - y(t_i,\mathbf{q})^{IL6_{12}}]^2, \quad IL6(t) \text{ at } 12mg/kg, \tag{2.31}$$

$$\mathbf{J_{TNF_{12}}}(\mathbf{q}) = \frac{1}{\max_j(y^{TNF_{12}}_{j(j=1,\ldots,7)})} \sum_{i=1}^{7} [y_i^{TNF_{12}} - y(t_i,\mathbf{q})^{TNF_{12}}]^2, \; TNF(t) \text{ at } 12mg/kg, \tag{2.32}$$

$$\mathbf{J_{IL10_{12}}}(\mathbf{q}) = \frac{1}{\max_j(y^{IL10_{12}}_{j(j=1,\ldots,7)})} \sum_{i=1}^{7} [y_i^{IL10_{12}} - y(t_i,\mathbf{q})^{IL10_{12}}]^2, \; IL10(t) \text{ at } 12mg/kg, \tag{2.33}$$

where y_i^k is the experimental data at time $t = i$ for state variable k, $y(t_i,\mathbf{q})^k$ is the model prediction at time t_i for $\mathbf{q}$ model parameters and state variable k and $\max_j(y_j^k)$ is the maximum value of the experimental data over all time points for state variable k.

Combine (2.28) to (2.33) to form the desired cost function that we aim to minimize:

$$\mathcal{K}(\mathbf{q}) = \mathbf{J_{IL6_3}}(\mathbf{q}) + \mathbf{J_{TNF_3}}(\mathbf{q}) + \mathbf{J_{IL10_3}}(\mathbf{q}) + \mathbf{J_{IL6_{12}}}(\mathbf{q}) + \mathbf{J_{TNF_{12}}}(\mathbf{q}) + \mathbf{J_{IL10_{12}}}(\mathbf{q}), \tag{2.34}$$

where $\mathbf{q}$ is a vector of model parameters. As proposed in [12], the cost (in Equation (2.34)) will be minimized using an optimization function in MATLAB known as *fminsearch* to search for the parameter estimated values that yield the best fit of the model to the experimental data. Note that *fminsearch* is a multidimensional unconstrained minimizer that uses the Nelder-Mead algorithm. Nelder-Mead is a derivative-free algorithm that is widely used for nonlinear optimization problems. Nelder-Mead evaluates the cost function at the vertices of a simplex of parameters, orders the function values, replaces the worst value with a better one based on a set of rules, and repeats until a user-prescribed error tolerance or number of functions evaluations allowed has been reached.

2.3 Akaike Information Criterion (AIC)

AIC [3] is a *model selection tool* commonly used to compare different models quantitatively. It was developed by a Japanese statistician called Hirotsugu Akaike in 1971 to measure a model's goodness of fit. AIC measures the amount of information lost when a given model is used to describe the behavior of a real system. When two or more models having different number of parameters are compared, the model with the lowest AIC value is preferred. The formula for calculating AIC is given by

$$AIC = k \ln\left(\frac{\mathbf{J}}{k}\right) + 2p, \tag{2.35}$$

$$\mathbf{J} = \frac{1}{\max_j(y_j)} \sum_{i=1}^{n} [y_i - y(t_i, \mathbf{q})]^2, \tag{2.36}$$

where k is the total number of data points, p is the total number of model parameters, $\mathbf{J}$ is a nonlinear least-squares method with a normalized residual, $y(t_i, \mathbf{q})$ is the model prediction at time t_i for $\mathbf{q}$ parameters, y_i is the experimental data, and $\max_j(y_j)$ is the maximum value of the experimental data over all time points.

It is a known fact that the goodness of fit improves with the addition of more free parameters to be estimated irrespective of the number of free parameters in the data generating process. One outstanding characteristic of AIC is that it not only rewards goodness of fit but it contains a penalty term ("$2p$" in Equation (2.35)) that helps to restrain overfitting. The role of AIC is to discover the model that best explains the data set with the fewest number of free parameters.

Chapter 3

Model Analysis

3.1 8D Relative Sensitivity Ranking

We examine the relative sensitivity ranking results of the parameters for $IL6$, TNF and $IL10$ at $3\,mg/kg$ and $12\,mg/kg$ endotoxin challenge levels, respectively. These results are obtained from the 8D model with the primary goal of identifying the most sensitive parameters that will be used to construct "modified 8D" models.

3.1.1 8D Relative Sensitivity Ranking at 3 mg/kg endotoxin challenge level

Figure 3.1 shows the relative sensitivity ranking plots of the parameters for each inflammatory cytokine.

These plots give a general idea of the number of parameters that are sensitive to each inflammatory cytokine at $3\,mg/kg$ endotoxin challenge level. Also, a close examination of the relative sensitivity levels of the parameters indicate a strong correlation with their respective outputs. For example, the parameters are more sensitive to $IL10$ than the other inflammatory cytokines. A cutoff point can usually be determined to separate the most sensitive parameters from the less sensitive ones for each output. A "back of the envelope" technique for assigning a cutoff is often where the largest break in magnitude occurs. However, this is a crude method to use in making an important decision regarding parameter sensitivity; rather a more analytical approach is to find the smallest parameter rank such that an $\alpha\%$ perturbation in the original value results in a significant change in the output trajectory. The smallest rank position that satisfies this criterion becomes the cutoff point, where α can be 10, 20, or 30. The main disad-

vantage with this approach is that it is very cumbersome to implement. We implemented the second technique in this work with a 20% perturbation for the case of the reduced 7D relative sensitivity ranking plots in Figures 3.9 and 3.10.

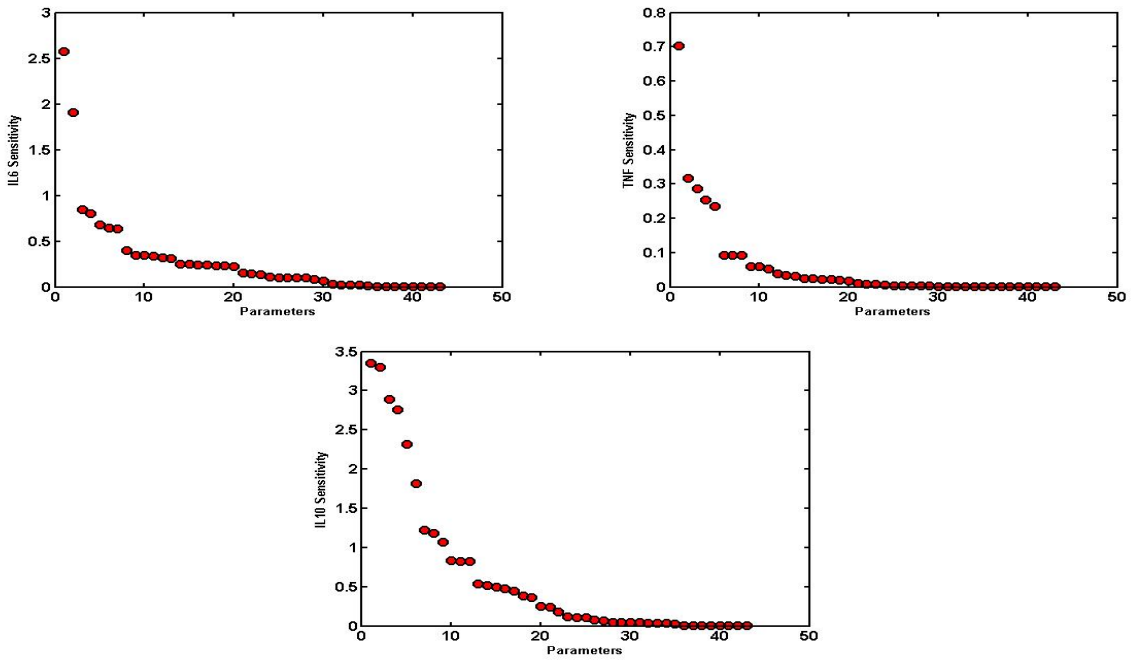

Figure 3.1: 8D relative sensitivity ranking plots at $3\,mg/kg$ endotoxin level for $IL6$, TNF and $IL10$

Table 3.1 contains essentially the same information with Figure 3.1. However, this table identifies each parameter, the corresponding rank, and the computed modified $\mathcal{L}_2$ norm value using Equation (2.21). It is easy to observe from the table that the ranks of some parameters vary widely across the different inflammatory cytokines, for instance, k_D is ranked 15^{th} for $IL6$, 29^{th} for TNF and 1^{st} for $IL10$. Other parameters with similar characterization are d_D, x_D and d_{IL6}. Meanwhile, there was no variability in the ranks of the least sensitive parameters: $x_{TNFIL10}$, $k_{IL10TNF}$, $x_{IL10TNF}$, k_{TNFTNF} and x_{TNFTNF} with respective ranks 39^{th} , 40^{th} , 41^{st} , 42^{nd} and 43^{rd} across the outputs. Perhaps a more interesting observation is that these parameters are all associated with TNF and $IL10$.

Table 3.1: 8D relative sensitivity ranking at $3\,mg/kg$. Number in parenthesis is the computed $\mathcal{L}_2$ norm; the prior number is the rank: 1 implies most sensitive and 43 is least sensitive.

Parameter	$IL6$ **Rank**	TNF **Rank**	$IL10$ **Rank**
k_N	4 (0.7985)	5 (0.2360)	4 (2.7549)
x_N	10 (0.3435)	7 (0.0915)	7 (1.2260)
d_N	16 (0.2455)	14 (0.0326)	6 (1.8123)
k_{NP}	11 (0.3381)	8 (0.0913)	8 (1.1816)
k_{ND}	37 (0.0058)	36 (0.0005)	29 (0.0451)
x_{NTNF}	23 (0.1401)	12 (0.0376)	15 (0.4974)
x_{NIL6}	35 (0.0169)	27 (0.0038)	27 (0.0710)
x_{NCA}	19 (0.2303)	9 (0.0606)	11 (0.8280)
x_{NIL10}	28 (0.0992)	15 (0.0247)	19 (0.3663)
k_{NTNF}	18 (0.2335)	10 (0.0603)	10 (0.8361)
k_{NIL6}	34 (0.0180)	26 (0.0039)	26 (0.0765)
k_D	15 (0.2458)	29 (0.0026)	1 (3.3498)
d_D	25 (0.1025)	34 (0.0009)	5 (2.3215)
x_D	27 (0.1006)	32 (0.0010)	3 (2.8923)
k_{CA}	22 (0.1473)	4 (0.2533)	20 (0.2519)
d_{CA}	33 (0.0206)	13 (0.0331)	33 (0.0377)
k_{IL6TNF}	20 (0.2275)	21 (0.0109)	28 (0.0485)
x_{IL6TNF}	26 (0.1014)	25 (0.0046)	35 (0.0222)
k_{IL6}	6 (0.6435)	17 (0.0231)	24 (0.1105)
d_{IL6}	8 (0.3980)	24 (0.0061)	32 (0.0396)
x_{IL6}	1 (2.5711)	6 (0.0921)	17 (0.4415)
$x_{IL6IL10}$	7 (0.6368)	18 (0.0228)	25 (0.1091)
k_{IL6IL6}	12 (0.3226)	22 (0.0080)	30 (0.0436)
x_{IL6IL6}	13 (0.3099)	23 (0.0078)	31 (0.0420)
x_{IL6CA}	31 (0.0309)	33 (0.0009)	38 (0.0048)
k_{TNF}	17 (0.2411)	2 (0.3173)	14 (0.5170)
d_{TNF}	21 (0.1510)	3 (0.2875)	21 (0.2449)
$x_{TNFIL10}$	39 (8.15e-7)	39 (1.67e-6)	39 (1.41e-06)
x_{TNFCA}	9 (0.3473)	1 (0.7039)	13 (0.5400)
k_{TNFTNF}	42 (2.806e-15)	42 (6.02e-15)	42 (4.921e-15)
x_{TNFTNF}	43 (2.8055e-15)	43 (6.01e-15)	43 (4.920e-15)
x_{TNFIL6}	36 (0.0079)	19 (0.0193)	36 (0.0097)
$k_{IL10TNF}$	40 (2.63e-8)	40 (7.02e-10)	40 (1.7695e-08)
$x_{IL10TNF}$	41 (2.62e-8)	41 (7.01e-10)	41 (1.7666e-08)
$k_{IL10IL6}$	32 (0.0218)	37 (0.0003)	37 (0.0095)
$x_{IL10IL6}$	29 (0.0853)	31 (0.0013)	34 (0.0370)
k_{IL10}	5 (0.6800)	20 (0.0184)	18 (0.3819)
d_{IL10}	3 (0.8422)	16 (0.0237)	16 (0.4803)
x_{IL10}	2 (1.9094)	11 (0.0518)	9 (1.0688)
x_{IL10d}	24 (0.1102)	28 (0.0027)	23 (0.1163)
k_{IL102}	30 (0.0629)	35 (0.0006)	12 (0.8263)
d_{IL102}	38 (0.0012)	38 (6.88e-6)	22 (0.1775)
x_{IL102}	14 (0.2514)	30 (0.0023)	2 (3.3047)

3.1.2 8D Relative Sensitivity Ranking at 12 mg/kg endotoxin challenge level

The relative sensitivity results at $12\,mg/kg$ endotoxin challenge level summarized in this section are similar to those in Section 3.1.1. Analogous to Figure 3.1, in Figure 3.2 we see that the magnitude of the relative sensitivity level is largest in $IL10$, followed by $IL6$ and TNF, repectively. The plot of $IL10$ displays a more evenly distributed parameter spread than the pro-inflammatory cytokines where there exists large break in magnitude between the most sensitive parameter(s) and other significantly sensitive parameters. With such disparity between the sensitive parameters it is unwise to use where the largest break in magnitude occurred as cutoff. Figures 3.1 and 3.2 revealed an interesting feature about the sensitivity levels of the inflammatory cytokines since the parameter with the largest sensitivity level for $IL6$ is higher in at $3\,mg/kg$ (Figure 3.1). This is the complete reverse for TNF and $IL10$ where their respective highest sensitivity levels occurred at $12\,mg/kg$ (Figure 3.2). This indicates that increase endotoxin challenge levels do not lead to higher sensitivity levels across the inflammatory cytokines.

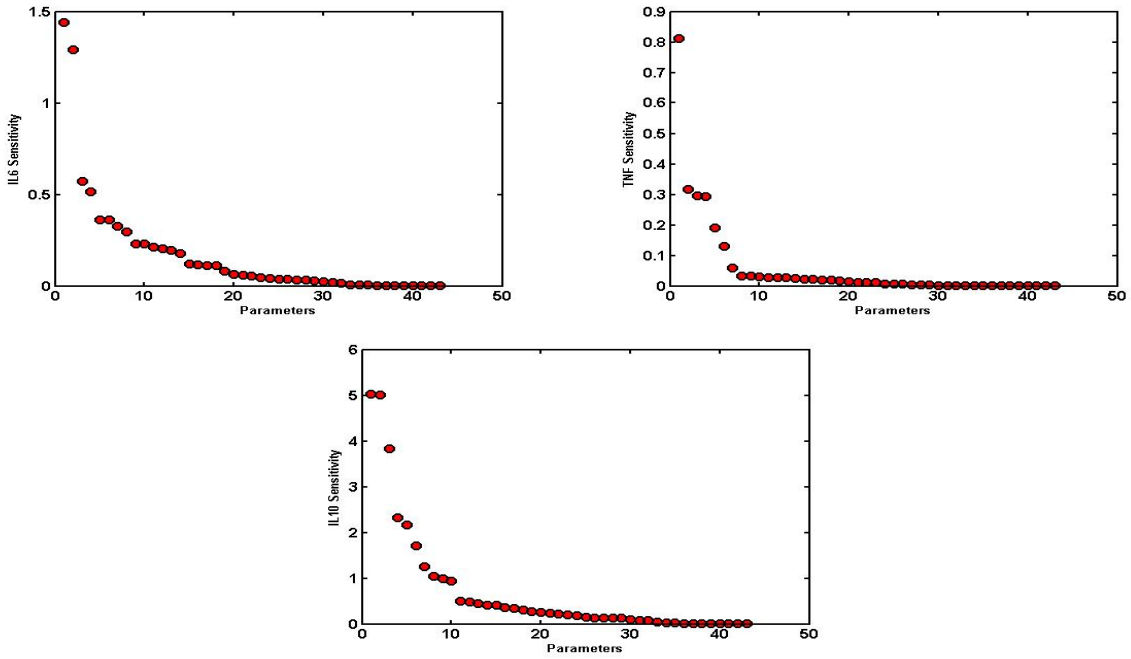

Figure 3.2: 8D relative sensitivity ranking plots at $12\,mg/kg$ endotoxin level for $IL6$, TNF and $IL10$

Table 3.2: 8D relative sensitivity ranking at $12\,mg/kg$. Number in parenthesis is the computed $\mathcal{L}_2$ norm; the prior number is the rank: 1 implies most sensitive and 43 is least sensitive.

Parameter	$IL6$ **Rank**	TNF **Rank**	$IL10$ **Rank**
k_N	14 (0.1775)	5 (0.1905)	6 (1.7024)
x_N	25 (0.0390)	11 (0.0278)	11 (0.5023)
d_N	18 (0.1107)	17 (0.0192)	5 (2.1712)
k_{NP}	26 (0.0384)	12 (0.0277)	12 (0.4887)
k_{ND}	38 (0.0008)	37 (8.59e-5)	36 (0.0144)
x_{NTNF}	32 (0.0144)	23 (0.0107)	24 (0.1807)
x_{NIL6}	35 (0.0050)	29 (0.0034)	32 (0.0711)
x_{NCA}	29 (0.0274)	18 (0.0191)	16 (0.3582)
x_{NIL10}	30 (0.0230)	19 (0.0164)	18 (0.3154)
k_{NTNF}	28 (0.0314)	16 (0.0226)	14 (0.4117)
k_{NIL6}	34 (0.0056)	27 (0.0037)	31 (0.0801)
k_D	10 (0.2305)	32 (0.0007)	1 (5.0274)
d_D	15 (0.1213)	34 (2.38e-4)	3 (3.8323)
x_D	27 (0.0327)	36 (1.23e-4)	4 (2.3309)
k_{CA}	20 (0.0621)	2 (0.3177)	22 (0.2129)
d_{CA}	33 (0.0066)	10 (0.0311)	35 (0.0227)
k_{IL6TNF}	16 (0.1170)	20 (0.0158)	30 (0.0963)
x_{IL6TNF}	24 (0.0438)	26 (0.0058)	33 (0.0357)
k_{IL6}	5 (0.3613)	8 (0.0328)	19 (0.2632)
d_{IL6}	7 (0.3264)	25 (0.0059)	29 (0.1243)
x_{IL6}	1 (1.4388)	6 (0.1305)	8 (1.0477)
$x_{IL6IL10}$	6 (0.3599)	9 (0.0326)	20 (0.2621)
k_{IL6IL6}	11 (0.2149)	21 (0.0112)	25 (0.1405)
x_{IL6IL6}	12 (0.2021)	22 (0.0109)	26 (0.1326)
x_{IL6CA}	31 (0.0206)	30 (0.0013)	37 (0.0136)
k_{TNF}	22 (0.0563)	3 (0.2959)	23 (0.2011)
d_{TNF}	23 (0.0463)	4 (0.2939)	27 (0.1311)
$x_{TNFIL10}$	39 (6.48e-7)	38 (5.07e-6)	39 (2.11e-6)
x_{TNFCA}	17 (0.1139)	1 (0.8116)	17 (0.3393)
k_{TNFTNF}	42 (1.0331e-15)	42 (7.812e-15)	42 (3.831e-15)
x_{TNFTNF}	43 (1.0329e-15)	43 (7.810e-15)	43 (3.830e-15)
x_{TNFIL6}	36 (0.0036)	13 (0.0265)	38 (0.0095)
$k_{IL10TNF}$	40 (2.49e-8)	40 (1.234e-9)	40 (2.96e-8)
$x_{IL10TNF}$	41 (2.48e-8)	41 (1.231e-9)	41 (2.95e-8)
$k_{IL10IL6}$	19 (0.0822)	31 (0.0009)	34 (0.0333)
$x_{IL10IL6}$	8 (0.2960)	28 (0.0034)	28 (0.1252)
k_{IL10}	4 (0.5135)	15 (0.0228)	15 (0.4057)
d_{IL10}	3 (0.5718)	14 (0.0248)	10 (0.9374)
x_{IL10}	2 (1.2895)	7 (0.0585)	9 (0.9882)
x_{IL10d}	13 (0.1971)	24 (0.0065)	13 (0.4415)
k_{IL102}	21 (0.0578)	35 (1.59e-2)	7 (1.2539)
d_{IL102}	37 (0.0016)	39 (2.21e-6)	21 (0.2299)
x_{IL102}	9 (0.2313)	33 (0.0006)	2 (5.0134)

Table 3.2 captures basically the same information as in Table 3.1. The relative sensitivity

ranking information displayed in both tables will be used together with subset selection to determine a subset of parameters that are most identifiable from the experimental data.

3.2 8D Parameter Identifiability Analysis

The *SVD followed by QR with column pivoting* subset selection method discussed in Section 2.2.4 was used to determine the parameters that are most identifiable at both $3\,mg/kg$ and $12\,mg/kg$ endotoxin challenge levels across the different inflammatory cytokines. The following parameters were selected as most identifiable:

- At endotoxin challenge level $3\,mg/kg$, the numerical rank $\hat{r} = 18$. This means that subset selection identifies 18 most identifiable parameters. They are:

$$k_N,\ d_N,\ k_{NTNF},\ k_D,\ d_D,\ x_D,\ k_{CA},\ d_{CA},\ k_{IL6TNF},\ x_{IL6TNF},$$
$$d_{IL6},\ x_{IL6},\ k_{IL6IL6},\ d_{TNF},\ x_{TNFCA},\ x_{IL10IL6},\ x_{IL10},\ d_{IL102}.$$

- At challenge level $12\,mg/kg$, with a numerical rank $\hat{r} = 18$. The most identifiable parameters are:

$$k_N,\ d_N,\ k_{NP},\ k_D,\ d_D,\ x_D,\ k_{CA},\ d_{CA},\ d_{IL6},\ x_{IL6},\ k_{IL6IL6}$$
$$d_{TNF},\ x_{TNFCA},\ x_{TNFIL6},\ x_{IL10IL6},\ x_{IL10},\ x_{IL10d},\ d_{IL102}.$$

Further investigation on the most identifiable parameters from both endotoxin challenge levels showed that 15 parameters were commonly identified by both levels and each challenge level identified 3 parameters that were unique to that level. Those parameters that were uniquely identified by each challenge level are given below:

- Parameter identified by only $3\,mg/kg$ endotoxin challenge level:

$$k_{NTNF},\ k_{IL6TNF},\ x_{IL6TNF}$$

- Parameter identified by only $12\,mg/kg$ endotoxin challenge level:

$$k_{NP},\ x_{TNFIL6},\ x_{IL10d}$$

These results were useful in constructing the two "modified 8D" models outlined below:

8D-15: This model will be known as **8D-15** because it is described by the 15 parameters that were identified by **both** endotoxin challenge levels.

8D-21: This model will be described by the 21 parameters identified by **either** challenge levels and it shall be referred to as **8D-21**.

3.3 8D Parameter Estimation and Model Validation

In this section, we present parameter estimation results on both **8D-15** and **8D-21** models. This is accomplished via the method presented in Section 2.2.5. Both models are calibrated to the existing experimental data on inflammatory cytokines in order to determine the best parameter estimates for the free parameters in the "modified 8D" models. In addition, we present the curve fitting plots comparing the original **8D** model in [126] and each "modified 8D" model.

3.3.1 8D-15 Parameter Estimation and Model Validation

Table 3.3 shows the nominal and optimized (estimated) values of the 15 parameters that defined **8D-15**. The nominal values are the assigned values from [126] used in the **8D** model. In addition to this table, we also present curve fitting plots showing the predictions of $IL6$, TNF and $IL10$ for **8D-15** (*red dashed line* (- -)) and **8D** (*blue solid line* (—)). The experimental data *black circle* (mean±SD) represent each inflammatory cytokine at endotoxin challenge levels $3\,mg/kg$ and $12\,mg/kg$, respectively. Based on the amount of information contained in these plots, we can evaluate the performance of the models by analyzing how well they predict the observed data.

The $IL6(t)$ plots in Figure 3.3 illustrate a very good fit for **8D-15**. At those time instance when **8D-15** missed the target, it was well within the error bar. The plot at $12\,mg/kg$ endotoxin challenge level (right) shows a better fit for **8D-15**. Comparing the plots of **8D-15** and **8D** at both endotoxin levels reveals **8D-15** as having a slight edge.

Table 3.3: 8D-15 Model Parameter Estimation

Parameter	**Nominal Value**	**Estimated Value**
k_N	5.5786e7	4.169362e7
d_N	0.1599	0.47063257
k_D	2.5247	3.57420325
d_D	0.37871	0.28300584
x_D	1.8996e7	1.563785e7
k_{CA}	0.154625e-8	1.47234e-9
d_{CA}	0.31777e-1	0.25099371
d_{IL6}	0.43605	0.31829930
x_{IL6}	1.7856e8	1.889077e8
k_{IL6IL6}	122.92	175.583580
d_{TNF}	2.035	1.75628386
x_{TNFCA}	0.19342	0.07727691
$x_{IL10IL6}$	26851	1.812930e4
x_{IL10}	8.0506e7	5.940355e7
d_{IL102}	0.0224	0.00923201

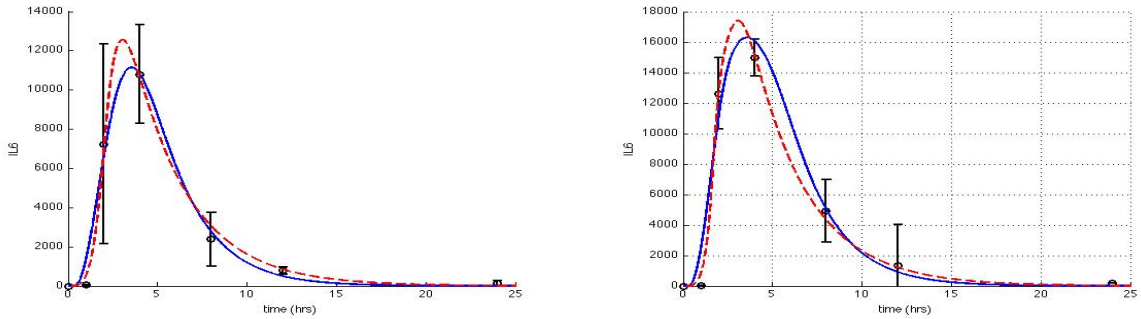

Figure 3.3: $IL6(t)$ curve fitting plots comparing 8D-15 (- -) and 8D (—) against experimental data in *black circle* (mean±SD) at $3\,mg/kg$ and $12\,mg/kg$ endotoxin challenge levels; the plot on the left represents $3\,mg/kg$ and the right plot denote $12\,mg/kg$.

It is obvious from the plots of $TNF(t)$ in Figure 3.4 that **8D-15** had a better prediction at

$12\,mg/kg$ endotoxin levels (right plot) than at $3\,mg/kg$ endotoxin level (left plot). Unlike the plot at $12\,mg/kg$, **8D-15** was completely off target while attempting to capture the 4^{th} data point at $3\,mg/kg$. However, as evidenced from Figure 3.4, **8D-15** and **8D** accurately captured the concentration of TNF at both endotoxin levels.

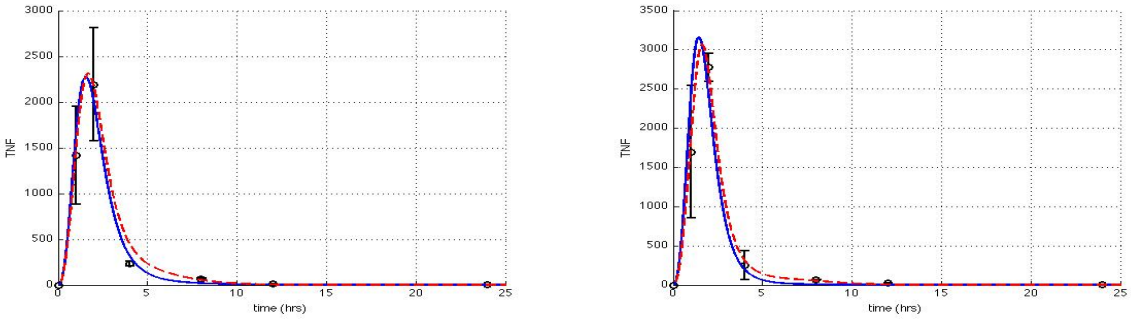

Figure 3.4: $TNF(t)$ curve fitting plots comparing 8D-15 (- -) and 8D (—) against experimental data in *black circle* (mean±SD) at $3\,mg/kg$ and $12\,mg/kg$ endotoxin challenge levels; the plot on the left represents $3\,mg/kg$ and the right plot denote $12\,mg/kg$.

It is apparent from Figure 3.5 that the predictions made by **8D-15** for each inflammatory cytokine at $12\,mg/kg$ endotoxin level were more consistent than at $3\,mg/kg$ endotoxin level. Albeit **8D-15** performed poorly capturing the concentration of $IL10$ at both endotoxin challenge levels, it is clear that the prediction at $12\,mg/kg$ is preferable to $3\,mg/kg$. Despite the mediocre predictions of $IL10$ at both endotoxin levels, **8D-15** was within one standard deviation of the mean for the majority of the data points.

A complete analysis of the plots of **8D-15** and **8D** across all the inflammatory cytokines indicate that one cannot draw any precise conclusion about the model with a superior performance, though it is understandably clear that **8D** had better predictions of $IL10(t)$.

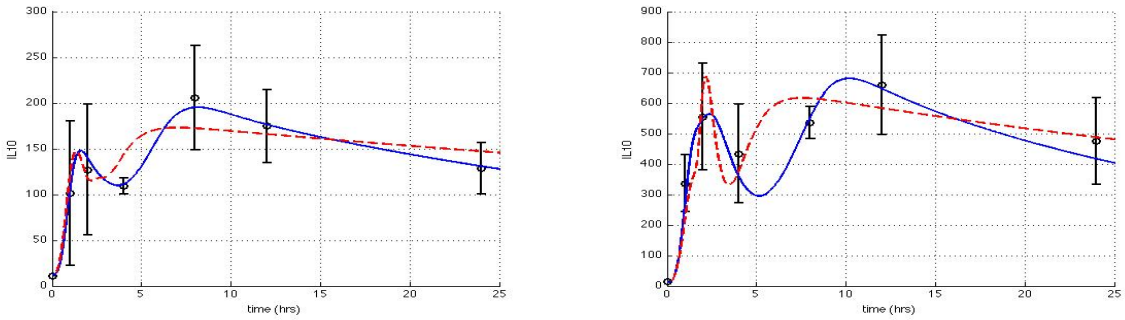

Figure 3.5: $IL10(t)$ curve fitting plots comparing 8D-15 (- -) and 8D (—) against experimental data in *black circle* (mean±SD) at $3\,mg/kg$ and $12\,mg/kg$ endotoxin challenge levels; the plot on the left represents $3\,mg/kg$ and the right plot denote $12\,mg/kg$.

3.3.2 8D-21 Parameter Estimation and Model Validation

The optimized (estimated) values of the 21 parameters that defined **8D-21** are displayed in Table 3.4. The table shows that some of the free parameters optimized values were significantly different from their nominal values including k_{NP}, k_{IL6TNF}, x_{IL6TNF}, k_{IL6IL6} and x_{IL10d}. In addition, curve fitting plots of $IL6(t)$, $TNF(t)$ and $IL10(t)$ for **8D-21** (*red dashed line* (- -)) and **8D** (*blue solid line* (—)) are presented. The experimental data are represented by *black circle* (mean±SD) for the respective inflammatory cytokines.

From the plots of $IL6(t)$ in Figure 3.6, the predictions of **8D-21** are consistent with the experimental data at both $3\,mg/kg$ (left plot) and $12\,mg/kg$ (right plot) endotoxin challenge levels. **8D-21** was within one standard deviation of the mean measurement at those points it missed the target. The quality of fit for **8D-21** was quite impressive in capturing the data. Recall that both "modified 8D" and the **8D** models performed equally well is describing the dynamics of $IL6(t)$.

Table 3.4: 8D-21 Model Parameter Estimation

Parameter	**Nominal Value**	**Estimated Value**
k_N	5.5786e7	4.465195e7
d_N	0.1599	0.54915952
$k_{NP}{}^{\ddagger}$	41.267	184.871881
$k_{NTNF}{}^{\dagger}$	12.94907	22.7269753
k_D	2.5247	4.63254241
d_D	0.37871	0.15237897
x_D	1.8996e7	2.620924e7
k_{CA}	0.154625e-8	9.26423e-9
d_{CA}	0.31777e-1	0.12553346
$k_{IL6TNF}{}^{\dagger}$	4.4651	103.803383
$x_{IL6TNF}{}^{\dagger}$	1211.3	1.504963e5
d_{IL6}	0.43605	0.31720533
x_{IL6}	1.7856e8	2.417754e8
k_{IL6IL6}	122.92	2693.10339
d_{TNF}	2.035	3.13284175
x_{TNFCA}	0.19342	0.64397278
$x_{TNFIL6}{}^{\ddagger}$	55610	2.200224e6
$x_{IL10IL6}$	26851	1.509456e4
x_{IL10}	8.0506e7	6.900804e7
$x_{IL10d}{}^{\ddagger}$	791.27	5957.89231
d_{IL102}	0.0224	0.01665673

† Most identifiable only at dose level $3mg/kg$

‡ Most identifiable only at dose level $12mg/kg$

Figure 3.7 also depicted an excellent curve fitting plots for **8D-21** and **8D** at $3\,mg/kg$ (left plot) and $12\,mg/kg$ (right plot) endotoxin challenge levels, respectively. Both models (**8D-21** and **8D**) followed identical trajectories in predicting the experimental data on $TNF(t)$ at $3\,mg/kg$ endotoxin level.

Unlike in Figures 3.6 and 3.7 that demonstrated near perfect curve fitting plots for **8D-21**, in Figure 3.8 the model showed inconsistencies in capturing the trajectories of the data points at both endotoxin challenge levels for $IL10(t)$. Nonetheless, **8D-21** was within the error bar for majority of the data points.

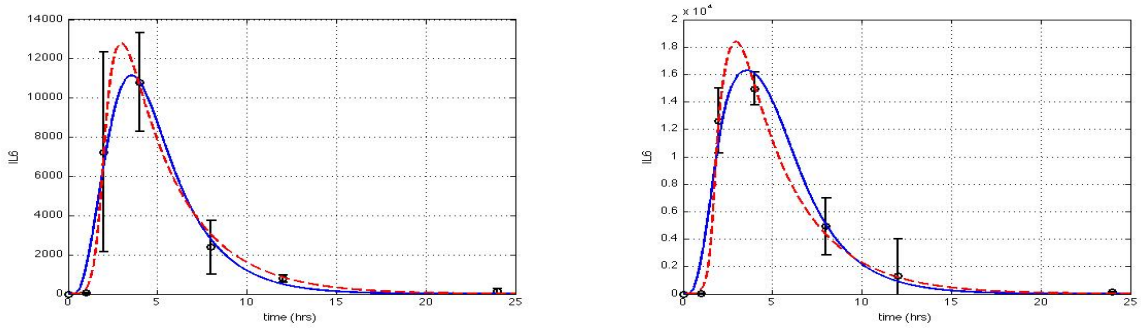

Figure 3.6: $IL6(t)$ curve fitting plots comparing 8D-21 (- -) and 8D (—) against experimental data in *black circle* (mean±SD) at $3\,mg/kg$ and $12\,mg/kg$ endotoxin challenge levels; the plot on the left represents $3\,mg/kg$ and the right plot denote $12\,mg/kg$.

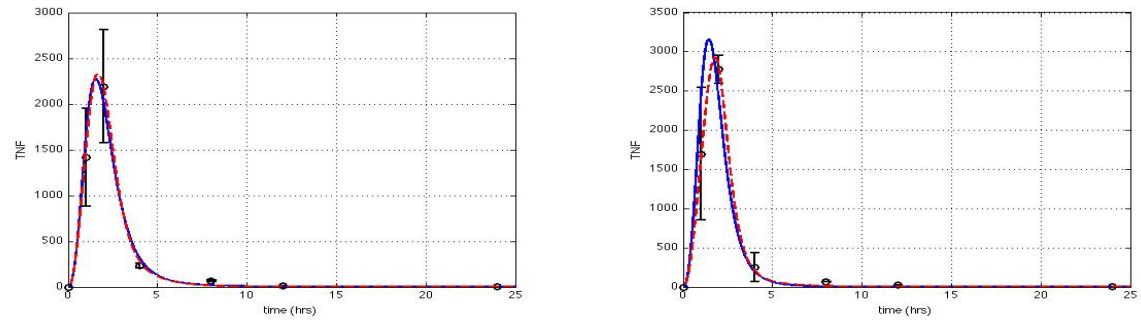

Figure 3.7: $TNF(t)$ curve fitting plots comparing 8D-21 (- -) and 8D (—) against experimental data in *black circle* (mean±SD) at $3\,mg/kg$ and $12\,mg/kg$ endotoxin challenge levels; the plot on the left represents $3\,mg/kg$ and the right plot denote $12\,mg/kg$.

The quality of curve fitting plots for **8D-15**, **8D-21** and **8D** while predicting the behavior of the experimental data on pro-inflammatory cytokines ($IL6$ and TNF) were very good. A thorough scrutiny of all the models disclosed that **8D-21** had a slight edge in consistently reproducing the data behavior of the inflammatory cytokines than the others. On the flipside, these models were unable to capture the dynamics of the experimental data on anti-inflammatory cytokine ($IL10$); **8D** had the best prediction. For this reason, we cannot make any determination about which model best represented the behavior of the different inflammatory cytokines based on curve fitting plots alone. Next, we will discuss the results of the reduced 7D models; this should

increase the pool of models to compare.

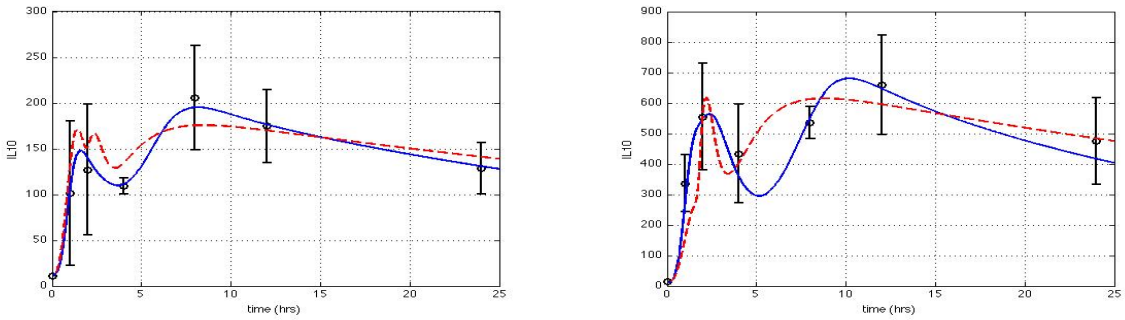

Figure 3.8: $IL10(t)$ curve fitting plots comparing 8D-21 (- -) and 8D (—) against experimental data in *black circle* (mean±SD) at $3\,mg/kg$ and $12\,mg/kg$ endotoxin challenge levels; the plot on the left represents $3\,mg/kg$ and the right plot denote $12\,mg/kg$.

3.4 7D Relative Sensitivity Ranking

In this section, we will redo the analysis that was carried out with the "modified 8D" models for the reduced 7D model.

3.4.1 7D Relative Sensitivity Ranking at 3 mg/kg endotoxin challenge level

The relative sensitivity ranking plots for $IL6$, TNF and $IL10$ are shown in Figure 3.9.

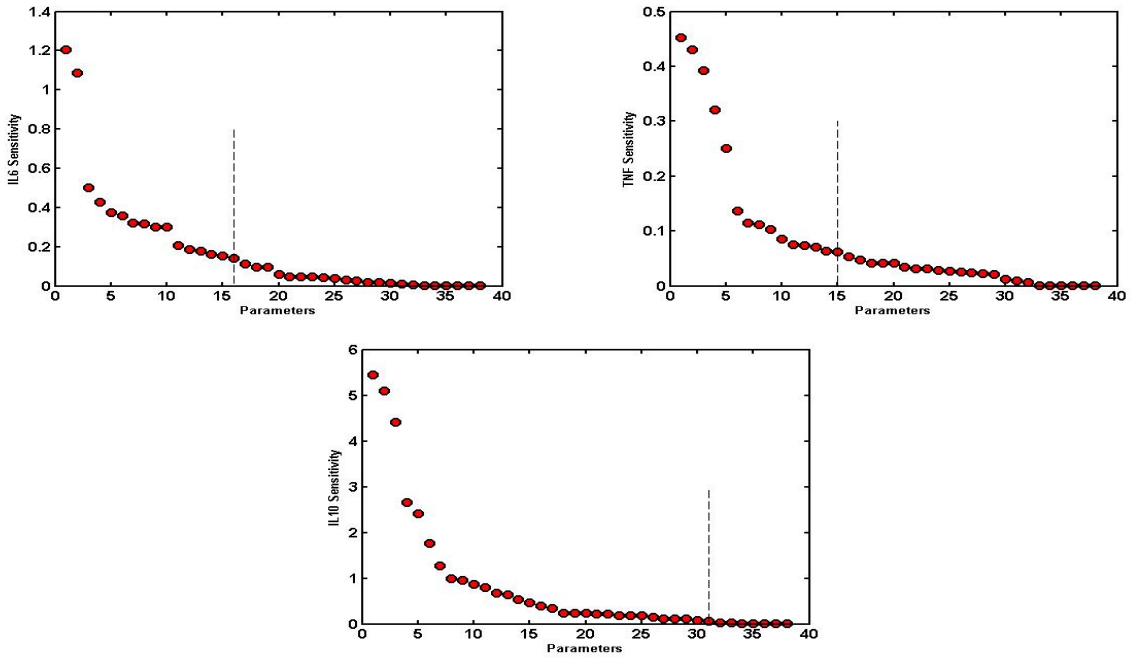

Figure 3.9: 7D relative sensitivity ranking plots at $3\,mg/kg$ endotoxin level for $IL6$, TNF, $IL10$. The vertical dashed line in each plot indicate the cutoff point for the respective inflammatory response using the method discussed in Section 3.1.1.

The plots displayed in this section (Figure 3.9) appear to be consistent with those in Sections 3.1.1 and 3.1.2 in that parameter sensitivity levels are output dependent. The plots in Figure 3.9 show that the parameters are most sensitive to the anti-inflammatory cytokine $IL10$. A notable feature from Figure 3.9 is the near even formation in the spread of the parameters in the plots of TNF and $IL10$. Usually such pattern makes it quite difficult to determine an unambiguous cutoff point that clearly separates the most sensitive parameters from the rest by using the location where the "largest break in magnitude" occurred.

Table 3.5: 7D relative sensitivity ranking at $3\,mg/kg$. Number in parenthesis is the computed $\mathcal{L}_2$ norm; the prior number is the rank: 1 implies most sensitive and 38 is least sensitive.

Parameter	$IL6$ **Rank**	TNF **Rank**	$IL10$ **Rank**
k_N	12 (0.1849)	3 (0.3927)	6 (1.7710)
x_N	20 (0.0585)	6 (0.1363)	11 (0.7907)
d_N	16 (0.1428)	4 (0.3210)	5 (2.4101)
k_{NP}	24 (0.0427)	8 (0.1112)	15 (0.4563)
k_{ND}	28 (0.0194)	20 (0.0416)	17 (0.3473)
x_{NTNF}	29 (0.0181)	19 (0.0421)	19 (0.2430)
x_{NIL6}	31 (0.0107)	28 (0.0225)	26 (0.1550)
x_{NIL10}	25 (0.0369)	10 (0.0858)	14 (0.5275)
k_{NTNF}	21 (0.0490)	7 (0.1142)	12 (0.6720)
k_{NIL6}	30 (0.0129)	25 (0.0265)	24 (0.1866)
k_D	6 (0.3574)	12 (0.0732)	1 (5.4455)
d_D	11 (0.2059)	17 (0.0472)	3 (4.4099)
x_D	22 (0.0485)	30 (0.0120)	4 (2.6571)
k_{IL6TNF}	17 (0.1128)	27 (0.0235)	30 (0.0822)
x_{IL6TNF}	26 (0.0308)	32 (0.0062)	33 (0.0220)
k_{IL6}	9 (0.3022)	14 (0.0629)	21 (0.2183)
d_{IL6}	8 (0.3170)	18 (0.0422)	28 (0.1111)
x_{IL6}	1 (1.2038)	5 (0.2504)	10 (0.8692)
$x_{IL6IL10}$	10 (0.3010)	15 (0.0627)	22 (0.2175)
k_{IL6IL6}	14 (0.1622)	21 (0.0337)	27 (0.1164)
x_{IL6IL6}	15 (0.1520)	22 (0.0317)	29 (0.1091)
k_{TNF}	23 (0.0463)	1 (0.4518)	18 (0.2434)
d_{TNF}	27 (0.0283)	2 (0.4304)	25 (0.1796)
$x_{TNFIL10}$	34 (5.44e-07)	34 (1.09e-05)	34 (3.57e-06)
k_{TNFTNF}	37 (1.2231e-15)	37 (1.92e-14)	37 (6.889e-15)
x_{TNFTNF}	38 (1.2226e-15)	38 (1.91e-14)	38 (6.886e-15)
x_{TNFIL6}	32 (0.0042)	11 (0.0748)	32 (0.0270)
$k_{IL10TNF}$	35 (3.80e-08)	35 (2.66e-09)	35 (3.42e-08)
$x_{IL10TNF}$	36 (3.79e-08)	36 (2.65e-09)	36 (3.40e-08)
$k_{IL10IL6}$	18 (0.0947)	31 (0.0090)	31 (0.0530)
$x_{IL10IL6}$	7 (0.3232)	23 (0.0307)	23 (0.1885)
k_{IL10}	4 (0.4289)	24 (0.0280)	16 (0.3885)
d_{IL10}	3 (0.4996)	16 (0.0539)	9 (0.9496)
x_{IL10}	2 (1.0883)	13 (0.0714)	8 (0.9940)
x_{IL10d}	13 (0.1792)	29 (0.0207)	13 (0.6386)
k_{IL102}	19 (0.0942)	26 (0.0259)	7 (1.2766)
d_{IL102}	33 (0.0031)	33 (0.0014)	20 (0.2386)
x_{IL102}	5 (0.3765)	9 (0.1035)	2 (5.1043)

Table 3.5 contains information about the parameters, their corresponding ranks, and their relative sensitivities computed values using the modified $\mathcal{L}_2$ norm in Equation (2.21). From the table, x_{IL6} ranked 1$^{\text{st}}$ in $IL6$, and k_{TNF} ranked 1$^{\text{st}}$ in TNF; this seems logical since these constants are affiliated with $IL6$ and TNF, respectively. The situation is different with $IL10$

where k_D ranked 1st but k_D is associated with tissue damage (D); however, the second elevation in the concentration of $IL10$ is attributed to tissue damage [126] . Lastly, those parameters that appear most sensitive for each inflammatory cytokine are inherently intertwined with that cytokine.

3.4.2 7D Relative Sensitivity Ranking at 12 mg/kg endotoxin challenge level

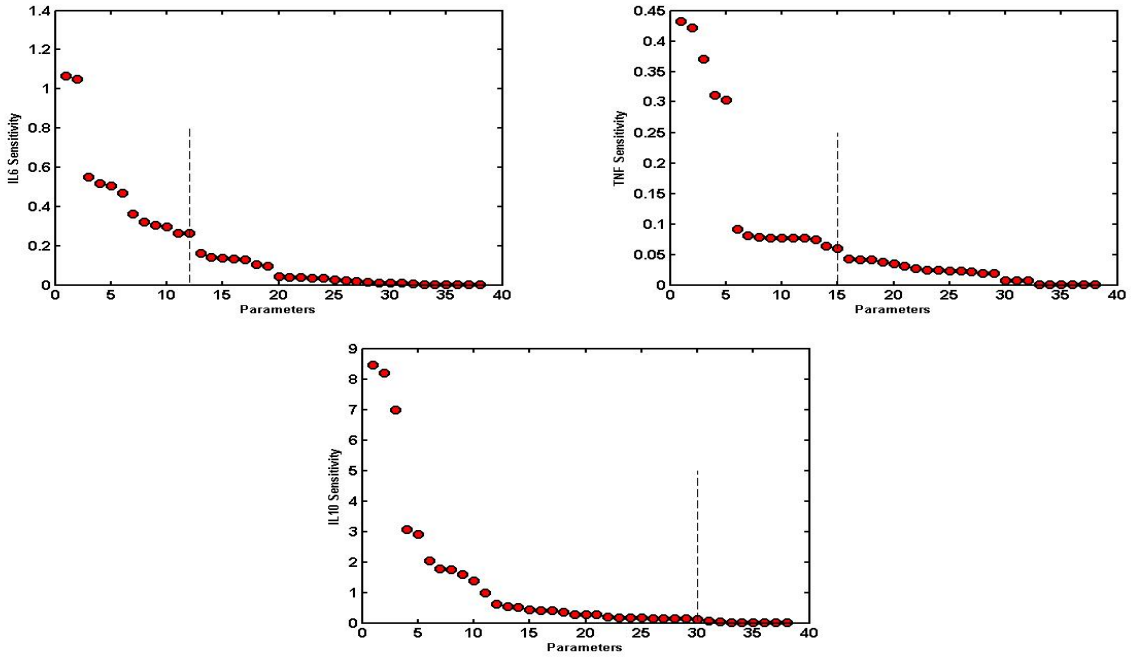

Figure 3.10: 7D relative sensitivity ranking plots at $12\,mg/kg$ endotoxin level for $IL6$, TNF, $IL10$. The vertical dashed line in each plot indicate the cutoff point for the respective inflammatory response using the method discussed in Section 3.1.1.

Table 3.6: 7D relative sensitivity ranking at $12\,mg/kg$. Number in parenthesis is the computed $\mathcal{L}_2$ norm; the prior number is the rank: 1 implies most sensitive and 38 is least sensitive.

Parameter	$IL6$ **Rank**	TNF **Rank**	$IL10$ **Rank**
k_N	15 (0.1358)	3 (0.3710)	8 (1.7543)
x_N	20 (0.0432)	6 (0.0909)	12 (0.6169)
d_N	13 (0.1610)	4 (0.3116)	4 (3.0707)
k_{NP}	24 (0.0338)	9 (0.0774)	18 (0.3534)
k_{ND}	28 (0.0128)	24 (0.0244)	21 (0.2798)
x_{NTNF}	31 (0.0098)	27 (0.0216)	26 (0.1557)
x_{NIL6}	30 (0.0100)	29 (0.0193)	29 (0.1424)
x_{NIL10}	23 (0.0364)	13 (0.0744)	14 (0.5115)
k_{NTNF}	21 (0.0390)	7 (0.0808)	13 (0.5489)
k_{NIL6}	29 (0.0120)	26 (0.0228)	24 (0.1714)
k_D	5 (0.5070)	14 (0.0641)	1 (8.4687)
d_D	9 (0.3053)	16 (0.0434)	3 (6.9928)
x_D	22 (0.0388)	32 (0.0068)	5 (2.9191)
k_{IL6TNF}	19 (0.0980)	21 (0.0309)	25 (0.1676)
x_{IL6TNF}	26 (0.0243)	30 (0.0077)	32 (0.0416)
k_{IL6}	11 (0.2644)	11 (0.0765)	16 (0.4009)
d_{IL6}	8 (0.3226)	17 (0.0417)	28 (0.1438)
x_{IL6}	2 (1.0490)	5 (0.3033)	9 (1.5868)
$x_{IL6IL10}$	12 (0.2637)	12 (0.0763)	17 (0.3997)
k_{IL6IL6}	14 (0.1432)	19 (0.0369)	22 (0.1851)
x_{IL6IL6}	16 (0.1345)	20 (0.0349)	23 (0.1761)
k_{TNF}	25 (0.0266)	1 (0.4328)	27 (0.1514)
d_{TNF}	27(0.0186)	2 (0.4219)	30 (0.1255)
$x_{TNFIL10}$	34 (6.72e-07)	34 (2.48e-05)	34 (5.10e-06)
k_{TNFTNF}	37 (9.242e-16)	37 (2.605e-14)	37 (6.221e-15)
x_{TNFTNF}	38 (9.238e-16)	38 (2.603e-14)	38 (6.219e-15)
x_{TNFIL6}	33 (0.0031)	10 (0.0769)	33 (0.0203)
$k_{IL10TNF}$	35 (5.44e-08)	35 (3.76e-09)	35 (5.19e-08)
$x_{IL10TNF}$	36 (5.41e-08)	36 (3.74e-09)	36 (5.17e-08)
$k_{IL10IL6}$	18 (0.1026)	31 (0.0072)	31 (0.0782)
$x_{IL10IL6}$	7 (0.3612)	23 (0.0245)	19 (0.2892)
k_{IL10}	6 (0.4693)	22 (0.0264)	15 (0.4332)
d_{IL10}	3 (0.5504)	18 (0.0417)	7 (1.7765)
x_{IL10}	1 (1.0658)	15 (0.0603)	11 (0.9881)
x_{IL10d}	10 (0.2958)	25 (0.0233)	10 (1.3924)
k_{IL102}	17 (0.1299)	28 (0.0196)	6 (2.0486)
d_{IL102}	32 (0.0045)	33 (0.0011)	20 (0.2891)
x_{IL102}	4 (0.5195)	8 (0.0784)	2 (8.1899)

Figure 3.10 displays the relative sensitivity plots for $IL6, TNF$ and $IL10$ at $12\,mg/kg$ endotoxin challenge level. Contrary to the 7D relative sensitivity ranking plots at $3\,mg/kg$ in Figure 3.9, the plots here do not demonstrate any even parameter spread formation among the inflammatory cytokines. Rather there exists a number of parameters clustered together

with relatively small and large gaps separating each cluster. With such formation it easy to determine a cutoff point that separates sensitive parameters from less sensitive ones using the "largest break in magnitude" method.

Table 3.6 contains no parameters with wide variability in rank across the inflammatory cytokines. Rather it is common to find a parameter with ranks within three positions apart for two of the three cytokines including x_{NTNF}, x_{NIL10}, d_N, k_{TNF} and x_{IL102}. Another information revealing in this table that is dramatically different from the previous tables is the fact that x_{IL10} ranked 1^{st} in $IL6$ but this parameter is not in any way linked with $IL6$. However, Table 3.6 has a common information consistent with the other tables regarding the set of parameters that are least sensitive, namely, $k_{IL10TNF}$, $x_{IL10TNF}$, k_{TNFTNF} and x_{TNFTNF}.

3.5 7D Parameter Identifiability Analysis

The reduced model parameter identifiability analysis is conducted in a similar manner as in Section 3.2. The *SVD followed by QR with column pivoting* subset selection method presented in Section 2.2.4 produced the following results at endotoxin challenge levels $3\,mg/kg$ and $12\,mg/kg$, respectively:

- At challenge level $3\,mg/kg$, the numerical rank $\hat{r} = 18$. This implies that subset selection identifies the following as the 18 most linearly independent parameters:

$$k_N,\ d_N,\ k_{NP},\ x_{NIL10},\ k_{NTNF},\ k_D,\ d_D,\ x_D,\ x_{IL6TNF},\ d_{IL6},$$
$$x_{IL6},\ k_{IL6IL6},\ d_{TNF},\ x_{TNFIL6},\ x_{IL10IL6},\ x_{IL10},\ x_{IL10d},\ d_{IL102}.$$

- At level $12\,mg/kg$, $\hat{r} = 18$. The 18 most identifiable parameters are:

$$k_N,\ d_N,\ k_{NP},\ k_{ND},\ d_D,\ x_D,\ x_{IL6TNF},\ d_{IL6},\ x_{IL6},\ k_{IL6IL6},$$
$$d_{TNF},\ x_{TNFIL6},\ x_{IL10IL6},\ d_{IL10},\ x_{IL10},\ x_{IL10d},\ d_{IL102},\ x_{IL102}.$$

15 parameters were commonly identified by both endotoxin challenge levels, 3 parameters were uniquely identified by each level.

- These are the parameters uniquely identified at $3\,mg/kg$ endotoxin challenge level:

$$x_{NIL10},\ k_{NTNF}\ k_D$$

- Parameters that are uniquely identified at $12\,mg/kg$ endotoxin challenge level include:

$$k_{ND},\ d_{IL10}\ x_{IL102}$$

From the above parameter identifiability analysis, we constructed two 7D models. These models are known as

7D-15: This model is defined by the 15 parameters identified by **both** dose levels, we will referred to is as **7D-15**.

7D-21: This model is defined by the 21 parameters identified by **either** dose level, it shall be known as **7D-21**.

3.6 7D Parameter Estimation and Model Validation

Parameter estimation is carried out using similar technique as in Section 3.3. The reduced models will be calibrated to the existing experimental data on inflammatory cytokine to determine best parameter estimates that can produce the most consistent representations of the data. We also present curve fitting plots comparing the original **8D** model in [126] with **7D-15** and **7D-21**.

3.6.1 7D-15 Parameter Estimation and Model Validation

The parameter estimation results on the 15 free parameters in **7D-15** are displayed in Table 3.7. The table contains the nominal and optimized (estimated) values of the free parameters, the nominal values corresponds with those used in the **8D** model [126]. Together with the table we also present curve fitting plots comparing **7D-15** (*red dashed line* (- -)), and **8D** (*blue solid line* (—)). The experimental data in *black circle* (mean±SD) denote the observed inflammatory cytokines.

Table 3.7: 7D-15 Model Parameter Estimation

Parameter	**Nominal Value**	**Estimated Value**
k_N	5.5786e7	4.6297682e7
d_N	0.1599	1.004344813
k_{NP}	41.267	54.14849008
d_D	0.37871	0.099359171
x_D	1.8996e7	1.1646809e7
x_{IL6TNF}	1211.3	1.5125569e8
d_{IL6}	0.43605	0.308883173
x_{IL6}	1.7856e8	2.3833727e8
k_{IL6IL6}	122.92	1.1191631e4
d_{TNF}	2.035	1.651880958
x_{TNFIL6}	55610	1.9446269e4
$x_{IL10IL6}$	26851	1.6942234e4
x_{IL10}	8.0506e7	5.6323712e7
x_{IL10d}	791.27	488.5519610
d_{IL102}	0.0224	0.016876136

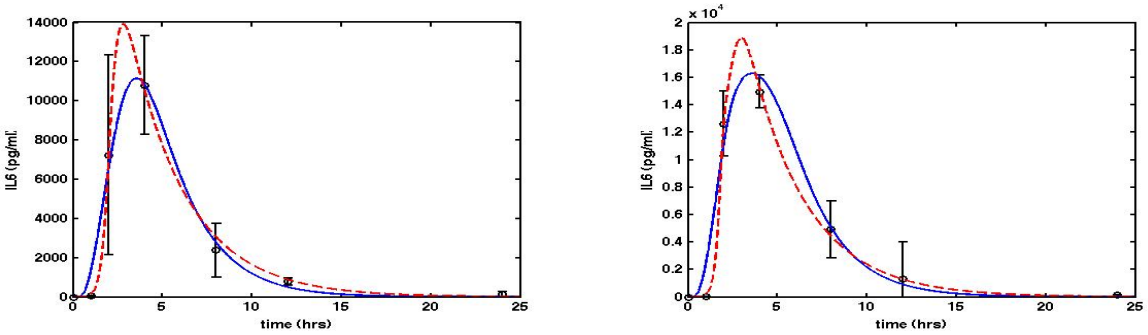

Figure 3.11: $IL6(t)$ curve fitting plots comparing 7D-15 (- -) and 8D (—) against experimental data in *black circle* (mean±SD) at $3\,mg/kg$ and $12\,mg/kg$ endotoxin challenge levels; the plot on the left represents $3\,mg/kg$ and the right plot at $12\,mg/kg$.

The plots of $IL6(t)$ for **7D-15** in Figure 3.11 appeared almost identical to those of **8D-**

15 and **8D-21** in Figures 3.3 and 3.6, respectively. The plots from Figure 3.11 showed that **7D-15** successfully captured the dynamics of the experimental data on pro-inflammatory cytokine $IL6$ at $3\,mg/kg$ (left plot) and $12\,mg/kg$ (right plot) endotoxin challenge levels, repectively. A visual comparison of **7D-15** and **8D** for $IL6(t)$ indicate superior predictions in favor of **7D-15**.

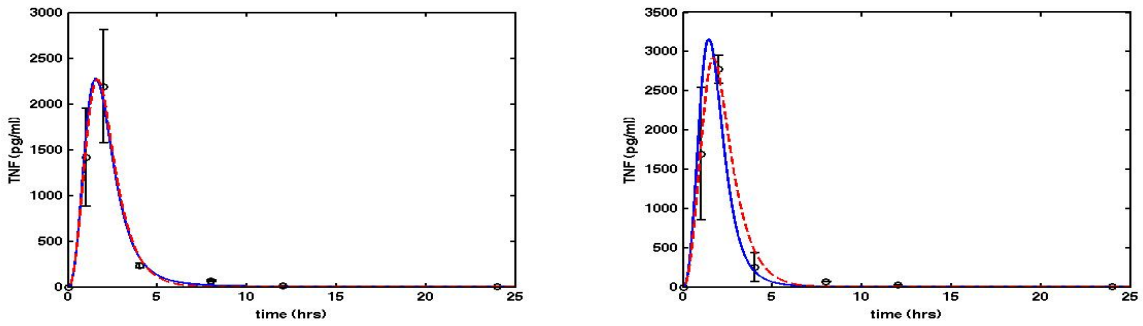

Figure 3.12: $TNF(t)$ curve fitting plots comparing 7D-15 (- -) and 8D (—) against experimental data in *black circle* (mean±SD) at $3\,mg/kg$ and $12\,mg/kg$ endotoxin challenge levels; the plot on the left represents $3\,mg/kg$ and the right plot at $12\,mg/kg$.

Figure 3.12 shows the plots of pro-inflammatory cytokine TNF for **7D-15** and **8D** at $3\,mg/kg$ and $12\,mg/kg$ endotoxin challenge levels. The curve fitting of both models illustrate an overall better quality predictions for **8D**, this is attributed to **7D-15** poor quality of fit at $12\,mg/kg$ endotoxin level. Thus far **8D-21** appears to have the best predictions of TNF at both endotoxin challenge levels.

The concentrations of interleukin-10 ($IL10$) are displayed in Figure 3.13. The predictions of **7D-15** captured the dynamics of $IL10$ much better than both **8D-15** and **8D-21**. Although it is obvious that **7D-15** quality of fit for $IL10$ is worse when compared with those of $IL6$ and TNF.

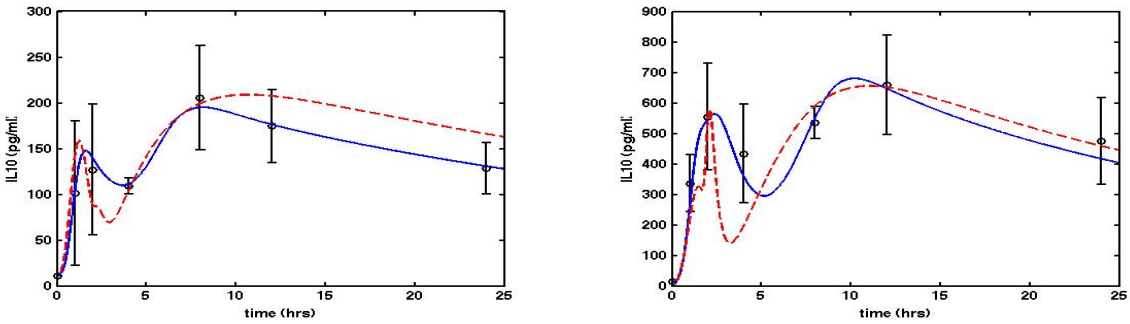

Figure 3.13: $IL10(t)$ curve fitting plots comparing 7D-15 (- -) and 8D (—) against experimental data in *black circle* (mean±SD) at $3\,mg/kg$ and $12\,mg/kg$ endotoxin challenge levels; the plot on the left represents $3\,mg/kg$ and the right plot at $12\,mg/kg$.

3.6.2 7D-21 Parameter Estimation and Model Validation

Parameter estimation on the 21 parameters that defined **7D-21** are shown in Table 3.8. The optimized (estimated) values of the free parameters in this model are displayed in the table.

Figure 3.14 shows **7D-21** model prediction of $IL6$. All the competing models accurately predicted the data on the concentrations of $IL6$. Also, these models captured $IL6$ better than **8D**.

The plot of TNF at $12\,mg/kg$ endotoxin challenge level (right plot) in Figure 3.15 shows a less refined fit for **7D-21** than at $3\,mg/kg$ endotoxin level (left plot). The quality of fit for the reduced models, **7D-15** and **7D-21** at $12\,mg/kg$ endotoxin level were not as good as **8D-15** and **8D-21**.

Table 3.8: 7D-21 Model Parameter Estimation

Parameter	**Nominal Value**	**Estimated Value**
k_N	5.5786e7	4.4091207e7
d_N	0.1599	0.972982028
k_{NP}	41.267	146.6611987
$k_{ND}{}^{\ddagger}$	0.013259	0.036994368
$x_{NIL10}{}^{\dagger}$	147.68	197.6274307
$k_{NTNF}{}^{\dagger}$	12.94907	11.43917219
$k_D{}^{\dagger}$	2.5247	0.905100790
d_D	0.37871	0.172933699
x_D	1.8996e7	2.0523098e7
x_{IL6TNF}	1211.3	6.5236077e4
d_{IL6}	0.43605	0.311674004
x_{IL6}	1.7856e8	1.6006218e8
k_{IL6IL6}	122.92	1.6011498e3
d_{TNF}	2.035	2.005164169
x_{TNFIL6}	55610	2.3509087e4
$x_{IL10IL6}$	26851	2.1336983e4
$d_{IL10}{}^{\ddagger}$	98.932	23.52073290
x_{IL10}	8.0506e7	1.0203669e8
x_{IL10d}	791.27	481.3224356
d_{IL102}	0.0224	0.010827097
$x_{IL102}{}^{\ddagger}$	37.454	12.30982416

† Most identifiable only at dose level $3mg/kg$

‡ Most identifiable only at dose level $12mg/kg$

From Figure 3.16, it is evident that the competing models were unable to accurately predict the dynamics of $IL10$, where **7D-15** and **7D-21** were not as off target as **8D-15** and **8D-21**. However, it is noted that **8D** and **7D-15** are the only models with trajectories that closely captured the experimental data on interleukin-10 at both endotoxin levels.

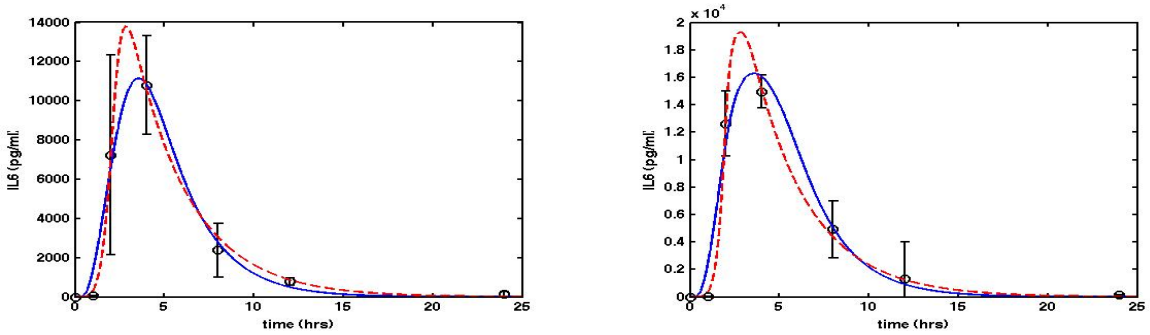

Figure 3.14: $IL6(t)$ curve fitting plots comparing 7D-21 (- -) and 8D (—) against experimental data in *black circle* (mean±SD) at $3\,mg/kg$ and $12\,mg/kg$ endotoxin challenge levels; the plot on the left represents $3\,mg/kg$ and the right plot at $12\,mg/kg$.

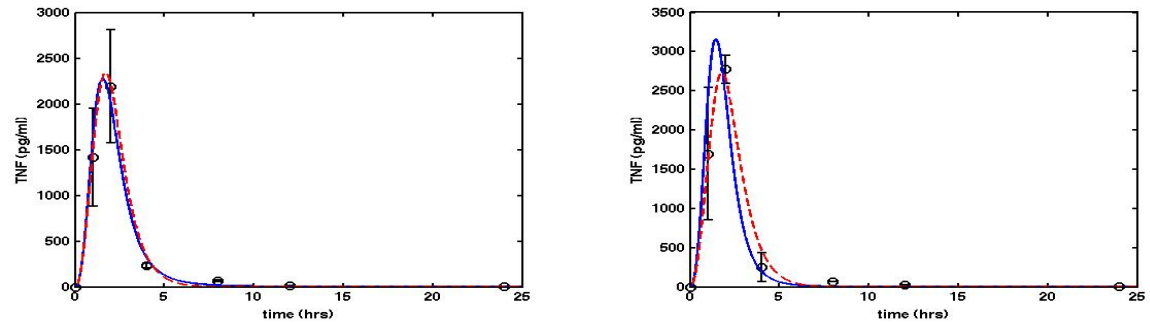

Figure 3.15: $TNF(t)$ curve fitting plots comparing 7D-21 (- -) and 8D (—) against experimental data in *black circle* (mean±SD) at $3\,mg/kg$ and $12\,mg/kg$ endotoxin challenge levels; the plot on the left represents $3\,mg/kg$ and the right plot at $12\,mg/kg$.

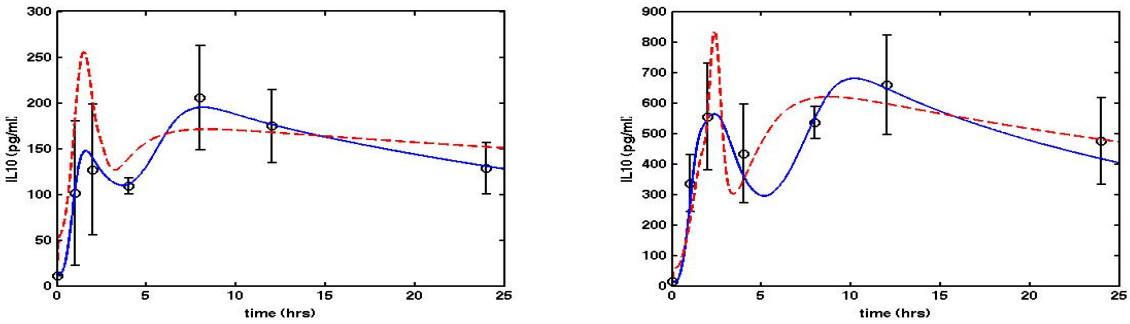

Figure 3.16: $IL10(t)$ curve fitting plots comparing 7D-21 (- -) and 8D (—) against experimental data in *black circle* (mean±SD) at $3\,mg/kg$ and $12\,mg/kg$ endotoxin challenge levels; the plot on the left represents $3\,mg/kg$ and the right plot at $12\,mg/kg$.

3.7 Model Prediction

Model prediction was carried out using the existing experimental data at $6\,mg/kg$ endotoxin challenge level. Recall that all the models were calibrated to experimental data at $3\,mg/kg$ and $12\,mg/kg$ endotoxin challenge levels. In this section, the proposed models (**8D-15**, **8D-21**, **7D-15**, and **7D-21**) alongside **8D** will be validated by examining the quality of their predictions of the experimental data at $6\,mg/kg$ endotoxin challenge level for each of the inflammatory cytokines.

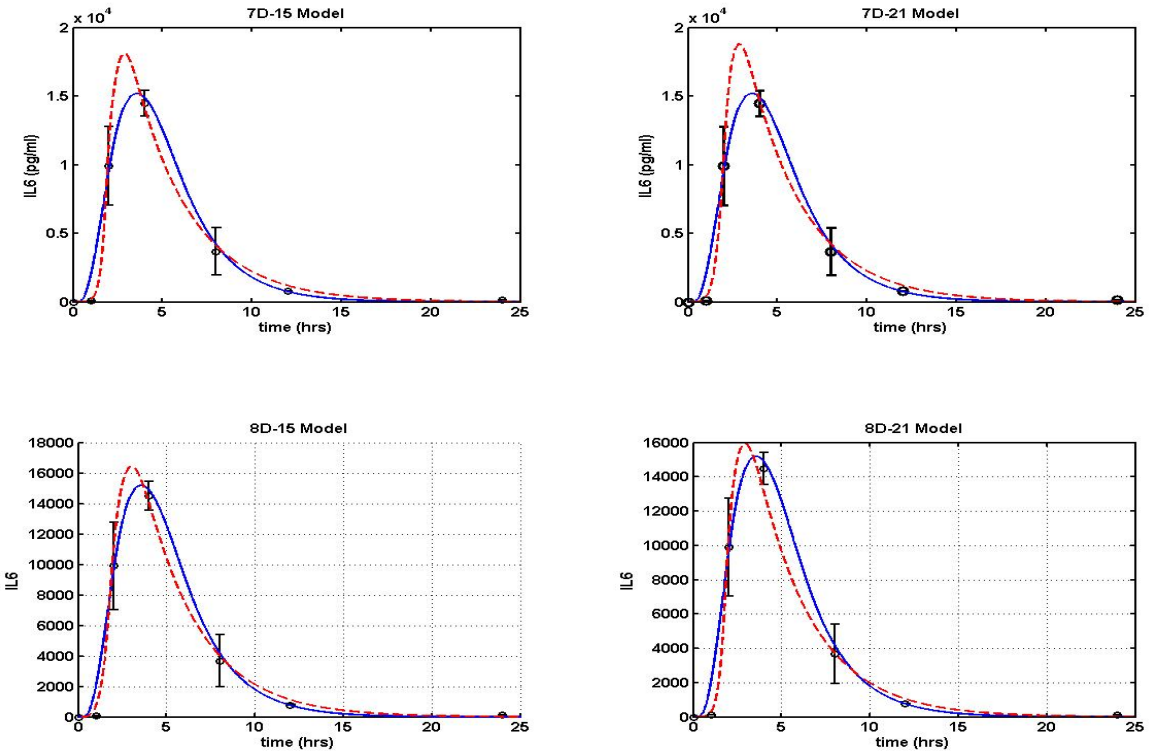

Figure 3.17: $IL6(t)$ model validation plots at $6\,mg/kg$ endotoxin challenge level comparing the quality of predictability for the following models:

Top Left: 7D-15 (- -); 8D (—) , and experimental data in *black circle* (mean±SD),
Top Right: 7D-21 (- -); 8D (—), and experimental data in *black circle* (mean±SD),
Bottom Left: 8D-15 (- -); 8D (—), and experimental data in *black circle* (mean±SD),
Bottom Right: 8D-21 (- -); 8D (—), and experimental data in *black circle* (mean±SD).

As depicted in Figure 3.17, all the models predictions of interleukin-6 ($IL6$) at $6\,mg/kg$ endotoxin challenge level are consistent and they captured the true representation of the experimental data.

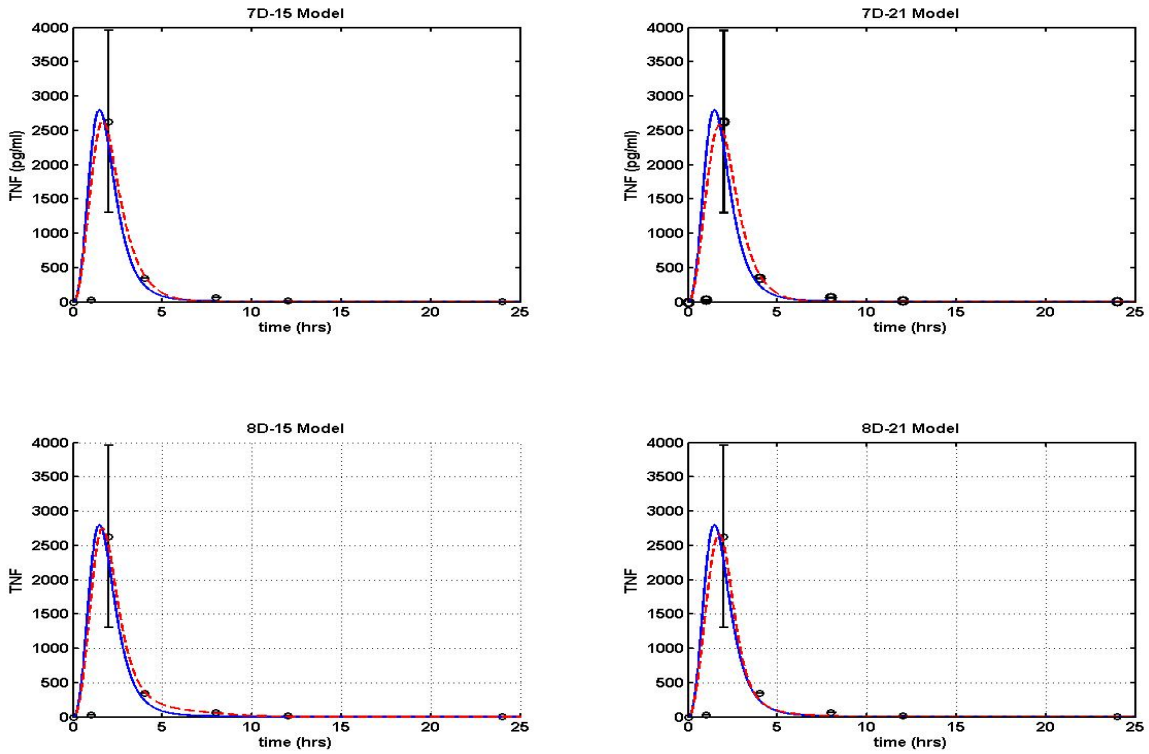

Figure 3.18: $TNF(t)$ model validation plots at $6\,mg/kg$ endotoxin challenge level comparing the quality of predictability for the following models:

Top Left: 7D-15 (- -); 8D (—) , and experimental data in *black circle* (mean±SD),
Top Right: 7D-21 (- -); 8D (—), and experimental data in *black circle* (mean±SD),
Bottom Left: 8D-15 (- -); 8D (—), and experimental data in *black circle* (mean±SD),
Bottom Right: 8D-21 (- -); 8D (—), and experimental data in *black circle* (mean±SD).

The models' predictability of TNF at $6\,mg/kg$ endotoxin challenge level in Figure 3.18 shows a high level of consistency even though they were off target at the 2^{nd} data point. The reason for this could be due to the fact that endotoxin challenge levels $3\,mg/kg$ and $12\,mg/kg$ used to calibrate the models did not exhibit such behavior at time point 2.

Figure 3.19 revealed another poor quality predictions of $IL10$ at $6\,mg/kg$ endotoxin challenge level for all the models. However, **8D** and **7D-15** appeared to have the best predictions of $IL10$.

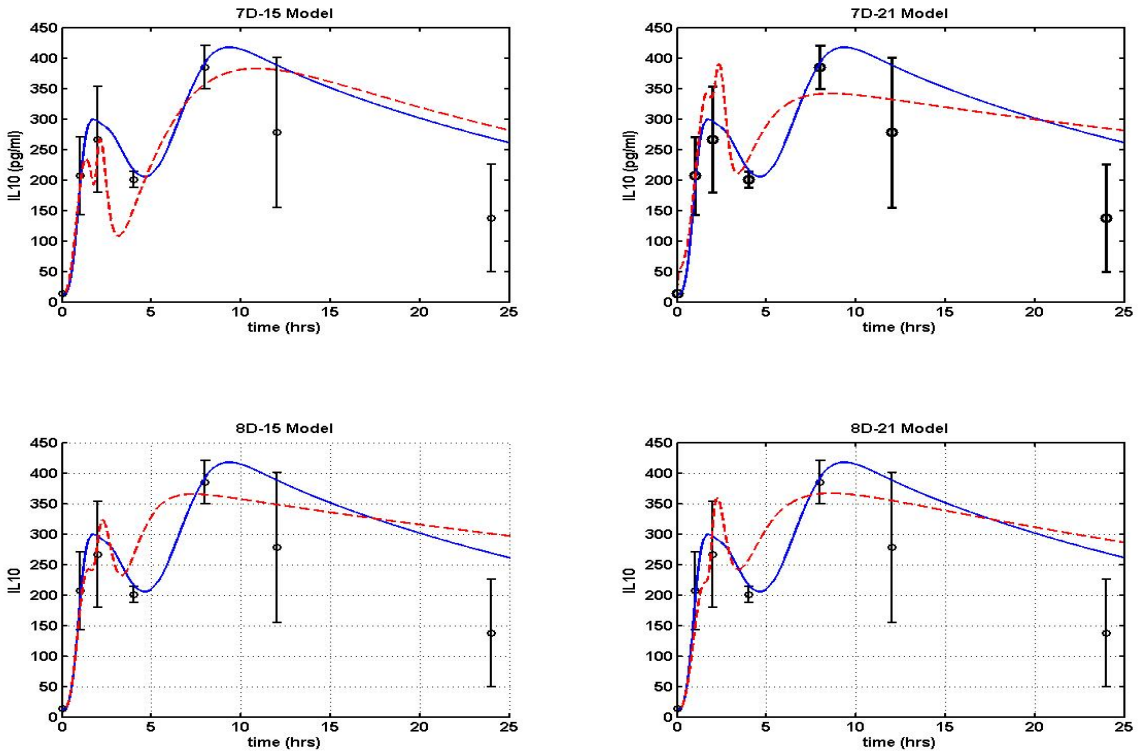

Figure 3.19: $IL10(t)$ model validation plots at $6\,mg/kg$ endotoxin challenge level comparing the quality of predictability for the following models:

Top Left: 7D-15 (- -); 8D (—) , and experimental data in *black circle* (mean±SD),
Top Right: 7D-21 (- -); 8D (—), and experimental data in *black circle* (mean±SD),
Bottom Left: 8D-15 (- -); 8D (—), and experimental data in *black circle* (mean±SD),
Bottom Right: 8D-21 (- -); 8D (—), and experimental data in *black circle* (mean±SD).

Results from the models curve fitting plots and the validation plots demonstrate that all the models performed comparatively well with the only exception at predicting the concentration of the anti-inflammatory cytokine, interleukin-10 ($IL10$). No model can be distinguished from the others as having superior representations of the experimental data on inflammatory cytokines. However, **8D**, **8D-21** and **7D-15** showed a slight advantage over the others. Next, the Akaike information criterion (AIC) discussed in Section 2.3 will be employed to compare the models quantitatively. Finally, a decision will be made on the "best" model based on their AIC results and the quality of their plots.

3.8 AIC Result

Table 3.9 contains the calculated AIC values for all five models (**8D**, **8D-15**, **8D-21**, **7D-15** and **7D-21**). Recall that AIC selects the model that best explains the data set with the fewest number of free parameters.

Table 3.9: Calculated AIC values

Variable	Model	3mg/kg dose	12mg/kg dose
IL6	8D	116.0984	123.4298
	8D-15	109.0618	108.4062
	8D-21	105.7331	103.3354
	7D-15	**94.2663**	**88.6931**
	7D-21	94.5823	91.3639
TNF	8D	105.3654	116.9512
	8D-15	100.4195	97.8565
	8D-21	91.3872	88.2548
	7D-15	86.6118	**87.8016**
	7D-21	**81.8431**	90.0322
IL10	8D	**80.9505**	99.9839
	8D-15	97.5898	106.7768
	8D-21	97.5208	107.9757
	7D-15	89.6408	99.3188
	7D-21	96.0837	**93.9691**

Number in **bold** indicate lowest value in each combination of state and challenge level.

Results from the table indicate that **7D-15** had lowest AIC value in 3 combinations of inflammatory cytokines and endotoxin dose levels ($IL6(t)$ at levels $3\,mg/kg$ and $12\,mg/kg$, and $TNF(t)$ at level $12\,mg/kg$), followed by **7D-21** with lowest AIC value in 2 combinations ($TNF(t)$ at level $3\,mg/kg$ and $IL10(t)$ at level $12\,mg/kg$), **8D** came in third place with lowest AIC value in 1 combination ($IL10(t)$ at level $3\,mg/kg$).

AIC head-to-head comparison between **7D-15** and the other models are given below:

- **7D-15** and **8D** is 5 to 1 in favor of **7D-15**.
- **7D-15** and **8D-15** is 6-0 in favor of **7D-15**.
- **7D-15** and **8D-21** is 6-0 in favor of **7D-15**.
- **7D-15** and **7D-21** is 4 to 2 in favor of **7D-15**.

Based on the AIC values, the quality of their respective least squares fit, and the accuracy of their model prediction at 6mg/kg, **7D-15** emerged to be the most consistent model that can successfully predict the acute inflammatory response that is triggered by endotoxin. To this end, **7D-15** is the model of choice that will be used for the remainder of this work, for brevity this model shall be referred to as 7D.

3.9 Mathematical Analysis of 7D

In this section, we give a rigorous mathematical proof of the existence and uniqueness for a solution to the 7D model. In addition, we will carry out a steady state and stability analysis.

3.9.1 Existence and Uniqueness

Consider the initial value problem

$$\dot{y} = f(t, y(t)), \tag{3.1}$$

with initial condition

$$y(t_0) = y_0, \tag{3.2}$$

where $y(t) = [P(t), N(t), D(t), IL6(t), TNF(t), IL10(t), Y_{IL10}(t)]$. Equations (3.1) and (3.2) denote the compact form of the reduce 7D model described in Section 2.2.2. The theory of existence and uniqueness of a solution to Equations (3.1) and (3.2) usually appeals to Lipschitz continuity in y of the function f in Equation (3.1). In particular,

Theorem 3.9.1 *(Theorem 3.10 from [96]).*
Suppose that for $x_0 \in \mathbb{R}^n$, there is a constant b such that $f : B_b(x_0)$[1] $\to \mathbb{R}^n$ is Lipschitz with constant K. Then, the initial value problem (3.1) *and* (3.2) *has a unique solution, $x(t)$ for $t \in J = [t_0 - a, t_0 + a]$, provided*

$$a = \frac{b}{M} \quad \textit{where } M = \max_{x \in B_b(x_0)} |f(x)|.$$

[1] $B_b(x_0) \equiv \{x \in \mathbb{R}^n \mid |x - x_0| < b\}$

We proceed with the determination of a global Lipschitz bound by separating the model into source, linear and nonlinear terms, respectively [1, 23, 37]. Hence,

$$\dot{y} = f(t, y) = S + L(t)y + g(t, y), \tag{3.3}$$

where S is the source term, $L(t)$ is the linear term, and $g(t, x)$ the nonlinear term. Some nonlinear terms in $g(t, y)$ do not satisfy Lipschitz condition in $y(t)$ since they can become unbounded. This problem can be resolved by replacing these terms with standard saturated nonlinear piecewise differentiable terms.

From Equation (2.2),

$$g_2(t, y) = k_N \cdot \frac{\mathbf{\Gamma(t)}}{x_N + \mathbf{\Gamma(t)}} \leq k_N,$$

and

$$\frac{\partial g_2(t,y)}{\partial P(t)} \leq k_N, \quad \frac{\partial g_2(t,y)}{\partial D(t)} \leq k_N, \quad \frac{\partial g_2(t,y)}{\partial IL6(t)} \leq k_N, \quad \frac{\partial g_2(t,y)}{\partial TNF(t)} \leq k_N.$$

Hence, $\frac{\partial g_2(t,y)}{\partial y} \leq k_N$.

From Equation (2.3),

$$g_3(t, y) = k_D \cdot \frac{N(t)^6}{x_D^6 + N(t)^6} \leq k_D$$

and

$$\frac{\partial g_3(t,y)}{\partial N(t)} \leq 6 \cdot k_D.$$

Hence, $\frac{\partial g_3(t,y)}{\partial y} \leq 6 \cdot k_D$.

From Equation (2.4),

$$g_4(t, y) = k_{IL6} \cdot \frac{N(t)^4}{x_{IL6}^4 + N(t)^4} \cdot \mathbf{\Omega(t)} \leq k_{IL6} \cdot (1 + k_{IL6TNF} + k_{IL6IL6}),$$

and

$$\frac{\partial g_4(t,y)}{\partial N(t)} \leq 4{\cdot}k_{IL6}{\cdot}(1{+}k_{IL6TNF}{+}k_{IL6IL6}),\ \frac{\partial g_4(t,y)}{\partial IL6(t)} \leq k_{IL6}{\cdot}k_{IL6IL6},\ \frac{\partial g_4(t,y)}{\partial TNF(t)} \leq k_{IL6}{\cdot}k_{IL6TNF}$$

Hence, $\frac{\partial g_4(t,y)}{\partial y} \leq 4 \cdot k_{IL6} \cdot (1 + k_{IL6TNF} + k_{IL6IL6})$.

From Equation (2.5)

$$g_5(t, y) = k_{TNF} \cdot N(t)^{1.5} \mathbf{\Phi(t)}$$

Notice that $N(t)^{1.5}$ has the potential to become unbounded. Therefore, we will replace it with the saturated term $\check{N(t)}^{1.5}$, where

$$\check{N(t)} = \begin{cases} 0 & N(t) < 0 \\ N(t) & 0 \leq N(t) \leq \bar{N(t)} \\ \bar{N(t)} & \bar{N(t)} < N(t). \end{cases}$$

Observe that $g_5^s(t,y) \leq k_{TNF}(1 + k_{TNFTNF}) \cdot \bar{N(t)}^{1.5}$, ($g_5^s$ is the saturated nonlinear term in Equation (2.5)),
and

$$\frac{\partial g_5^s(t,y)}{\partial N(t)} \leq 1.5 \cdot k_{TNF} \cdot \sqrt{\bar{N(t)}}(1 + k_{TNFTNF}),\ \frac{\partial g_5^s(t,y)}{\partial TNF(t)} \leq k_{TNF} \cdot k_{TNFTNF} \cdot \bar{N(t)}^{1.5}.$$

Hence, $\frac{\partial g_5(t,y)}{\partial y} \leq \max\{1.5 \cdot k_{TNF} \cdot \sqrt{\bar{N(t)}}(1 + k_{TNFTNF}), k_{TNF} \cdot k_{TNFTNF} \cdot \bar{N(t)}^{1.5}\}$.
Note that the new rate function defined by $g_5^s(t,y)$ is globally bounded and piecewise differentiable. Also, the rates in the form of a rational function are bounded with bounded derivatives.

From Equation (2.6)

$$g_6(t,y) = k_{IL10} \cdot \frac{N(t)^3}{x_{IL10}^3 + N(t)^3} \cdot \mathbf{\Psi(t)} - \beta(\mathbf{t}) \leq k_{IL10}(1 + k_{IL10IL6} + k_{IL10TNF}),$$

and

$$\frac{\partial g_6(t,y)}{\partial N(t)} \leq 3 \cdot k_{IL10}(1 + k_{IL10IL6} + k_{IL10TNF}),\ \frac{\partial g_6(t,y)}{\partial IL6(t)} \leq 4 \cdot k_{IL10} \cdot k_{IL10IL6},$$

$$\frac{\partial g_6(t,y)}{\partial TNF(t)} \leq k_{IL10} \cdot k_{IL10TNF},\ \frac{\partial g_6(t,y)}{\partial IL10(t)} \leq |-d_{IL10}|.$$

Hence, $\frac{\partial g_6(t,y)}{\partial y} \leq \max\{3 \cdot k_{IL10}(1 + k_{IL10IL6} + k_{IL10TNF}), 4 \cdot k_{IL10} \cdot k_{IL10IL6}, |-d_{IL10}|\}$.

From Equation (2.7),

$$g_7(t,y) = k_{IL102} \cdot \frac{D(t)^4}{x_{IL102}^4 + D(t)^4} \leq k_{IL102},$$

and

$$\frac{\partial g_7(t,y)}{\partial D(t)} \leq k_{IL102}.$$

Hence, $\frac{\partial g_7(t,y)}{\partial y} \leq k_{IL102}$.

The only notable difference between the nonlinear term $g(t,y)$ and the saturated nonlinear term $g^s(t,y)$ is in Equation (2.5), where $g_5(t,y)$ is replaced by $g_5^s(t,y)$. Whenever the model states drop below the saturated limits, the saturated model equals the original model since $g^s(t,y) = g(t,y)$, otherwise the rate in Equation (2.5) saturates. Notice that the saturated model only affects $g(t,y)$.

These bounds show that the derivative of the saturated nonlinear term is bounded above, i.e.,

$$\|\mathcal{D}_y g^s(t,y)\|_\infty < \infty.$$

We are now in a position to prove global existence and uniqueness of a solution to the saturated model; $f^s(t,y) = S + L(t)y + g^s(t,y)$. The Lipschitz continuity of the saturated model is:

$$|f^s(t,x) - f^s(t,y)| = |L(t)(x-y) + g^s(t,x) - g^s(t,y)| \tag{3.4}$$

As shown in [23], the multidimensional Mean Value Theorem implies that for $x, y \in \mathbb{R}^7$

$$g^s(t,x) - g^s(t,y) = \int_0^1 \mathcal{D}_x g^s(t, y + z(x-y))(x-y)dz.$$

Hence,

$$\begin{aligned} |f^s(t,x) - f^s(t,y)| &= |L(t)(x-y) + \int_0^1 \mathcal{D}_x g^s(t, y + z(x-y))(x-y)dz| && (3.5)\\ &\leq |L(t)||x-y| + \|\mathcal{D}_x g^s(t,x)\|_\infty |x-y| && (3.6)\\ &= \mathcal{K}_L |x-y|, && (3.7) \end{aligned}$$

when $t \in J$. Consequently, f^s is a contraction and has a unique fixed point that is a solution to Equation (3.1) provided that

$$a \leq \frac{b}{M} \quad \text{and } a < \frac{1}{\mathcal{K}_L}.$$

Hence, from Theorem 3.9.1, we have shown that the solution to the saturated model exists and is unique over the interval J.

3.9.2 Steady State and Stability Analysis

We begin this section with the following definitions:

Definition 3.9.1 Equilibrium [26].
$y = a$ is an equilibrium or steady state solution of Equation (3.1) *precisely when* $f(a) = 0$.

Definition 3.9.2 Stability [96].
A linear system is spectrally stable if none of its eigenvalues has a positive real part.

A general analytical analysis of the steady states and local stability of the 7D model in Section 2.2.2 would be nontrivial due to the complexity of the mathematical model. However, we can use the numerical values of the parameters and specifying initial values of the state variables to compute the steady states and also carry out a standard linearization to obtain the eigenvalues of the linearized model. This was done using the Matlab function *fsolve*. From Definition 3.9.2, we know that a system is stable if the eigenvalues of the jacobian matrix have negative real parts at the steady state.

To compute the steady state (equilibrium) of the reduced 7D system in Section 2.2.2, we specify the following initial conditions. These conditions represent the three different concentrations of endotoxin insults that the rats received:

$$y_0 = [3, 0, 0, 0, 0, 12.302, 0],$$
$$y_0 = [6, 0, 0, 0, 0, 12.302, 0],$$
$$y_0 = [12, 0, 0, 0, 0, 12.302, 0].$$

Using "fsolve" in Matlab to solve $f(t, y, q) = 0$ at the respective initial conditions, the solutions obtained all converge to the same basal state:

$$y^e \approx [0,\ 0,\ 0,\ 0,\ 0,\ 12.302,\ 0]$$

This implies that in the long run the body will settle at a position with basically no endotoxin concentration, zero number of activated phagocytic cells, no tissue damaged, the concentrations of pro-inflammatory cytokins will have vanished, and a small amount of interleukin-10 (anti-inflammatory cytokine).

To proceed with the steady state stability analysis, we obtained the jacobian matrix evaluated at y^e:

$$\mathbf{JM} \approx \begin{bmatrix} -3 & 0 & 0 & 0 & 0 & 0 & 0 \\ 1.6323e8 & -1.0043 & 3.9970e4 & 0 & 0 & 0 & 0 \\ 0 & 0 & -0.099359 & 0 & 0 & 0 & 0 \\ 0 & 0 & 0 & -0.3089 & 0 & 0 & 0 \\ 0 & 0 & 0 & 0 & -1.6519 & 0 & 0 \\ 0 & 0 & 0 & 0 & 0 & -94.132 & 1 \\ 0 & 0 & 0 & 0 & 0 & 0 & -0.01688 \end{bmatrix}, \quad (3.8)$$

with eigenvalues of **JM**:

$$EIG_{JM} \approx \begin{bmatrix} -0.30888 \\ -1.6519 \\ -94.132 \\ -0.016876 \\ -1.0043 \\ -0.099359 \\ -3 \end{bmatrix}. \quad (3.9)$$

Hence, we have demonstrated that the 7D system exhibits a stable steady state.

Part II

Derivation of Optimal Treatment Control

Chapter 4

Optimal Control Methodolody

4.1 Introduction

Optimal control deals with finding a control law that will cause a system to satisfy some physical or design constraints and at the same time minimize (or maximize) a chosen cost function. The history of optimal control theory as justified by [134] dates back to 1696 in the Netherlands, when Johann Bernoulli challenged his contemporaries with the *brachistochrone* problem. Given two points A and B in a vertical plane, find the orbit AMB of the movable point M which, starting from A and under the influence of its own weight, arrives at B in the shortest possible time. Indeed, this problem was a true minimum-time problem, and the first to deal with a dynamical behavior and explicitly ask for the optimal selection of the path. However, the era of modern optimal control theory began in the 1950s with the formulation of two main optimization approaches:

1) *Pontryagin Maximum Principle*: The maximum principle is a generalization of the Euler-Lagrange equations that stems from calculus of variations. In this approach, the optimal control is located in a manner that makes sure the neighboring controls cannot lead to smaller costs, thus ensuring that the derivative of the cost function about the optimal control will be zero.

2) *Dynamic Programming*: This technique is considered to have originated from the Hamilton-Jacobi approach. Here the optimal control remains optimal at intermediate points in time.

In the ensuing two sections, we give a detailed description of these approaches. The materials in these sections are due to [111].

4.1.1 Calculus of Variation: Euler-Lagrange equations

Consider a nonlinear time invariant dynamical system given by

$$\min_{u(\cdot)} J = \psi(x(t_f)) + \int_0^{t_f} (q(x) + u^T u)dt \tag{4.1}$$

subject to

$$\dot{x} = f(x) + g(x)u \tag{4.2}$$

$$x(0) = x_0, \tag{4.3}$$

with state $x \in \mathbb{R}^n$, control input $u \in \mathbb{R}^m$, initial time t_0, final time t_f, $f : \mathbb{R}^n \to \mathbb{R}^n$, $g : \mathbb{R}^n \to \mathbb{R}^{n\times m}$ continuously differentiable in all arguments and the cost at the terminal time $\psi(x(t_f))$.

The calculus of variations solution can be viewed as applying the necessary conditions for constrained optimization, the only change is that the optimization is infinite dimensional. Therefore, Lagrange multipliers is used to combine the constraints (Equation (4.2)) to the cost function (Equation (4.1)). To this end, we define the modified cost function using the Lagrange multipliers $\lambda(t) \in \mathbb{R}^n$ as

$$\bar{J} = \psi(x(t_f)) + \int_0^{t_f} [q(x(t)) + u(t)^T u(t) + \lambda^T(t)(f(x(t)) + g(x(t))u(t) - \dot{x})]dt \tag{4.4}$$

Defining the *Hamiltonian* H using what is referred to as a Legendre transformation,

$$H(x(t), u(t), \lambda(t)) = q(x(t)) + u(t)^T u(t) + \lambda^T(t)(f(x(t)) + g(x(t))u(t), \tag{4.5}$$

and integrating the last term on the right side of Equation (4.4) by parts to obtain

$$\bar{J} = \psi(x(t_f)) + \lambda^T(t_f)x(t_f) + \lambda^T(0)x(0) + \int_0^{t_f} [H(x(t), u(t), \lambda(t)) + \dot{\lambda}^T(t)x(t)]dt. \tag{4.6}$$

From the theory of Lagrange multipliers, the problem of determining the control function $u(t)$, that minimizes the original cost function Equation (4.1) subject to the constraints Equation (4.2) has been transformed to the problem of finding an unconstraint stationary points of Equation (4.6).

Next, consider the equation for variations of Equation (4.6) with respect to $x(t)$ and $u(t)$

$$\delta \bar{J} = \left[\left(\frac{\partial \psi}{\partial x} - \lambda^T \right) \delta x \right]_{t=t_f} + [\lambda^T \delta x]_{t=0} + \int_0^{t_f} \left[\left(\frac{\partial H}{\partial x} + \dot{\lambda}^T \right) \delta x + \frac{\partial H}{\partial u} \delta u \right] dt. \tag{4.7}$$

For a stationary point, it is required that this be equal to zero for all allowable variations. First, consider the variation δx, to make the coefficients of δx in Equation (4.7) vanish, $\lambda(t)$ have to be chosen according to

$$\dot{\lambda}^T = -\frac{\partial H}{\partial x}, \qquad 0 \leq t \leq t_f, \tag{4.8}$$

with boundary condition

$$\lambda^T(t_f) = \left. \frac{\partial \psi}{\partial x} \right|_{t=t_f}. \tag{4.9}$$

Equation (4.7) becomes

$$\lambda^T(0)\delta x(0) + \int_0^{t_f} \left[\frac{\partial H}{\partial u} \delta u \right] dt. \tag{4.10}$$

Since the initial condition is given and fixed, then $\delta x(0) = 0$. Also, since for a stationary point the variation must be zero for arbitrary $\delta u(t)$, the following must be satisfied

$$\frac{\partial H}{\partial u} = 0 \qquad 0 \leq t \leq t_f. \tag{4.11}$$

Equations (4.8), (4.9) and (4.11), plus the original dynamics and initial condition represent necessary conditions for optimality known as the *Euler-Lagrange equations*. These equations are used to design the control $u(t)$ that minimizes the cost function, and can be summarized as follows:

$$\dot{x} = f(x) + g(x)u \tag{4.12}$$

$$\dot{\lambda} = -\left(\frac{\partial H}{\partial x} \right)^T \tag{4.13}$$

$$\frac{\partial H}{\partial u} = 0, \tag{4.14}$$

with boundary conditions

$$x(0) \qquad \text{given} \tag{4.15}$$

$$\lambda(t_f) = \left(\frac{\partial \psi}{\partial x}\right)^T \Bigg|_{t=t_f}. \tag{4.16}$$

The optimizing control action $u^*(t)$ is determined by

$$u^*(t) = \arg\min_u H(x^*(t), u, \lambda^*(t)), \tag{4.17}$$

where $x^*(t)$ and $\lambda^*(t)$ denote the solution corresponding to the optimal trajectory.

The Lagrange multiplier $\lambda(t)$ is a dynamical variable that satisfies its own dynamical equation (4.13), known as *costate* or *adjoint* equation that progresses backward in time (by defining the backward time variable $\tau = t_f - t$ it follows that $d\tau = -dt$), with the final condition $\lambda(t_f)$ given in Equation (4.16).

Properties of the Euler-Lagrange solution

- *Open-Loop*: The optimal trajectory is explicitly solved as a function of time, not as a feedback law.
- *Local*: The solution is only valid for the particular initial condition $x(0)$. The problem is resolved whenever a new initial condition is given.
- *Necessary*: Since the Euler-Lagrange equations specify the conditions for the existence of a stationary point, they represent necessary conditions for an optimal trajectory.

4.1.2 Dynamic Programming: Hamilton-Jacobi-Bellman equations

Consider the nonlinear optimal control problem

$$\min_{u(\cdot)} J = \int_0^\infty (q(x) + u^T u) dt \tag{4.18}$$

subject to

$$\dot{x} = f(x) + g(x)u \tag{4.19}$$

$$x(0) = x_0, \tag{4.20}$$

for $q : \mathbb{R}^n \to \mathbb{R}$ positive semi-definite and $\mathbf{C^1}$ and the description of the other terms are consistent with those in the previous section. The desired solution is a state feedback control

law. Suppose the system $[f(x), q(x)]$ is *zero-state detectable*, i.e., for all $x \in \mathbb{R}^n$, $q(\phi(t,x)) = 0 \Rightarrow \phi(t,x) \to 0$ as $t \to \infty$ where $\phi(t,x)$ is the state transition function of the system $\dot{x} = f(x)$ with initial condition $x(0) = x$.

To derive the Hamilton-Jacobi-Bellman (HJB) partial differential equation (PDE) solution to the nonlinear optimal control problem, we adopt the dynamic programming technique described in [17]. First, we will present the *principle of optimality* definition, then apply this concept to the optimal control problem so as to derive the HJB PDE.

Definition 4.1.1 Principle of Optimality[1].
If $u^*(\tau)$ is optimal over the interval $[t, t_f]$, starting at state $x(t)$, then $u^*(\tau)$ is necessarily optimal over the subinterval $[t + \triangle t, t_f]$ for any $\triangle t$ such that $t_f - t \geq \triangle t > 0$.

The assumption underlying the principle of optimality is that the system can be characterized by its state $x(t)$ at time t, this summarizes the effect of all inputs $u(\tau)$ prior to time t. Therefore, the concept of dynamic programming is applying the principle of optimality to formulate an optimization problem as a recurrence relation. In the case of an optimal control problem, if one considers a value function which associates to every point in state space the optimal cost starting from that point, then we can write a recurrence relation in terms of the optimal value function which is valid for the entire state space. If this relation can be solved, then the value function obtained is associated with an entire family of optimal control problems, each with a different initial point.

Let us illustrate this idea by solving the nonlinear optimal control problem in Equations (4.18)-(4.20). Let $V^*(x_0)$ be the minimum of the cost function over all admissible trajectories $(x(t), u(t))$ where x begins at point x_0:

$$V^*(x_0) = \min_{u(\cdot)} \int_0^\infty (q(x(t)) + u^T(t)u(t))dt \tag{4.21}$$

subject to

$$\dot{x} = f(x(t)) + g(x(t))u(t) \tag{4.22}$$

$$x(0) = x_0. \tag{4.23}$$

If no such trajectory exists, then $V^*(\cdot) = +\infty$. The value function or Bellman's function of the optimal control problem is given as $V^* : \mathbb{R}^n \to \mathbb{R}_+ \cup \{\infty\}$. An optimal trajectory is a pair $(x(t), u(t))$ with a starting point x_0 and achieves optimal cost $V^*(x_0)$.

[1]The *principle of optimality* is utilized by assuming that the control is piecewise smooth and left continuous.

To apply the principle of optimality, consider $V^*(x)$ given by Equation (4.21), and let $u(t)$ be defined as the control signal over the interval $[t, \infty)$. By the additive properties of integrals and the principle of optimality

$$V^*(x(t)) = \min_{u(t)} \left\{ \int_t^{t+\triangle t} [q(x(\tau)) + u^T(\tau)u(\tau)]d\tau + V^*(x(t+\triangle t)) \right\}. \tag{4.24}$$

This implies that the optimal cost at $x(t)$ is given by the minimum of the cost it takes to move to $x(t+\triangle t)$ plus the cost incurred thus far. By using the principle of optimality the problem of finding an optimal control over the interval $[t, \infty)$ has been reduced to finding an optimal control over the reduced interval $[t, t+\triangle t]$.

Next, when $\triangle t$ is small, the integral in (4.24) can be approximated by $[q(x(t)) + u^T(t)u(t)] \triangle t$. Applying a multivariable Taylor-series expansion of $V^*(x(t+\triangle t))$ about $x(t)$, with $x(t+\triangle t) - x(t)$ approximated by $[f(x(t)) + g(x(t))u(t)] \triangle t$, yields

$$V^*(x) = \min_u \left\{ [q(x) + u^T u] \triangle t + V^*(x) + \left(\frac{\partial V^*}{\partial x} \right) [f(x) + g(x)u] \triangle t + o(\triangle t) \right\}, \tag{4.25}$$

where $\frac{\partial V^*}{\partial x}$ denotes the gradient of V^* with respect to the vector x, and $o(\triangle t)$ denotes higher-order terms in $\triangle t$. If we take limit as $\triangle t \to 0$ and cancelling $V^*(x)$ on both sides, we obtain

$$\min_{u(t)} \left\{ [q(x(t)) + u^T(t)u(t)] + \left(\frac{\partial V^*}{\partial x} \right) [f(x(t)) + g(x(t))u(t)] \right\} = 0. \tag{4.26}$$

The boundary condition for this equation is given by $V^*(0) = 0$ where $V^*(x)$ must be positive for all x. Equation (4.26) is one form the HJB equations. In many cases, this is not the final form of the equation. Two more steps can often be performed to reach a more convenient representation of this equation.

1) First, the indicated minimization is performed, leading to a control law of the form

$$u^* = -\frac{1}{2} g^T(x) \frac{\partial V^{*T}}{\partial x}. \tag{4.27}$$

2) The second step is to substitute Equation (4.27) back into Equation (4.26), and solve the

resulting nonlinear PDE

$$\frac{\partial V^*}{\partial x} f(x) - \frac{\partial V^*}{\partial x} g(x) g^T(x) \frac{\partial V^{*T}}{\partial x} + q(x) = 0 \tag{4.28}$$

for $V^*(x)$.

Equation (4.28) is what we often refer to as the HJB equation. The actual calculation of the optimal control action proceeds in an opposite fashion to the steps given above. First the HJB equation (Equation (4.28)) is solved for V^*, then this is substituted into Equation (4.27) where we obtain the optimal control action that achieves this minimal cost.

Properties of the Hamilton-Jacobi-Bellman solution

- *Closed-Loop*: The solution is a state feedback control law as given in Equation (4.27).
- *Global*: The solution provides the optimal control trajectory from every initial condition. Hence, it solves the optimal control problem for every initial condition, all at once.
- *Sufficient*: The solution of the HJB equation provides a sufficient condition for the solution to the corresponding optimal control problem.

Remark: In general, the HJB equation (4.28) is computationally intractable. This is the reason behind the existence of the discipline of nonlinear optimal control. The field of nonlinear optimal control can be thought of as the development of computationally tractable sub-optimal solutions to the optimal control problem.

4.2 7D Optimal Control Formulation

We draw our attention back to the formulation of an optimal treatment control to modulate inflammatory response to endotoxins. The control of inflammatory response is vital in the overall scheme of treating a critically ill animal or human. Optimal control techniques enable us to develop appropriate therapeutic regiment that can steer the model to a healthy state in reasonable time.

In this work, we seek to find a treatment strategy that minimizes the cost function given by

$$J = \int_{t_0}^{t_f} [Q_N N(t)^2 + Q_D D(t)^2 + Q_Y Y_{IL10}(t)^2 + R_{IL6} IL6Dose(t)^2 + R_{IL10} IL10Dose(t)^2] dt, \tag{4.29}$$

subject to

$$\frac{dP(t)}{dt} = -d_p \cdot P(t) \tag{4.30}$$

$$\frac{dN(t)}{dt} = k_N \cdot \frac{\mathbf{\Gamma(t)}}{x_N + \mathbf{\Gamma(t)}} - d_N \cdot N(t) \tag{4.31}$$

$$\frac{dD(t)}{dt} = k_D \cdot \frac{N(t)^6}{x_D^6 + N(t)^6} - d_D \cdot D(t) \tag{4.32}$$

$$\frac{dIL6(t)}{dt} = k_{IL6} \cdot \frac{N(t)^4}{x_{IL6}^4 + N(t)^4} \cdot \mathbf{\Omega(t)} - d_{IL6} \cdot IL6(t) + IL6Dose(t) \tag{4.33}$$

$$\frac{dTNF(t)}{dt} = k_{TNF} \cdot N(t)^{1.5} \mathbf{\Phi(t)} - d_{TNF} \cdot TNF(t) \tag{4.34}$$

$$\frac{dIL10(t)}{dt} = k_{IL10} \cdot \frac{N(t)^3}{x_{IL10}^3 + N(t)^3} \cdot \mathbf{\Psi(t)} - \mathbf{\Theta(t)} + Y_{IL10}(t) + s_{IL10} + IL10Dose(t) \tag{4.35}$$

$$\frac{dY_{IL10}(t)}{dt} = k_{IL102} \cdot \frac{D(t)^4}{x_{IL102}^4 + D(t)^4} - d_{IL102} \cdot Y_{IL10}(t), \tag{4.36}$$

with initial conditions

$$\begin{aligned} &P(0) = 3,\ 6,\ \text{or } 12; \quad N(0) = 0; \quad D(0) = 0; \quad IL6(0) = 0. \\ &TNF(0) = 0; \quad IL10(0) = \frac{s_{IL10} \cdot x_{IL10d}}{d_{IL10} \cdot x_{IL10d} - s_{IL10}}; \quad Y_{IL10}(0) = 0. \end{aligned} \tag{4.37}$$

Here, $\mathbf{\Gamma(t)}$, $\mathbf{\Omega(t)}$, $\mathbf{\Phi(t)}$, $\mathbf{\Psi(t)}$ and $\mathbf{\Theta(t)}$ are defined in Section 2.2.2. $IL6Dose(t)$ and $IL10Dose(t)$ are the treatment therapies (control variables) added to the 7D model. The addition of the treatment therapies in Equations (4.33) and (4.35) allow proper regulation of the pro- and anti- inflammatory responses. The source term $IL6Dose(t)$ represents the treatment therapy for interleukin-6 ($IL6$) whereas the treatment therapy for interleukin-10 ($IL10$) is the source term $IL10Dose(t)$. No treatment control was added to TNF; this is to avoid increasing the complexity of the control problem because an initial investigation on the addition of a control term did not alter the solution (the control remained at the zero level for the entire duration of the horizon). For this reason, we anticipate that modulating the effects of $IL6$ and $IL10$ will lead to tractable concentration levels of TNF.

The cost function (4.29) demonstrate our desire to minimize the activated phagocytic cells

(N), tissue damage marker (D), tissue damage driven IL-10 promoter (Y_{IL10}), IL6 treatment dose $IL6Dose(t)$, and IL10 treatment dose $IL10Dose(t)$. The parameters Q_N, Q_D and Q_Y in Equation (4.29) are the weight constants for the activated phagocytic cells (N), tissue damage marker (D) and tissue damage driven IL-10 promoter (Y_{IL10}), respectively. The weight constants associated with the control variables are R_{IL6} and R_{IL10}. Note that $IL6Dose(t)$ and $IL10Dose(t)$ are bounded so that dosing cannot be negative as well as limiting the maximum dose required; this is important because the treatment therapy can only be infused into the system but cannot be extracted and we need to avoid overdosing. Hence, we find an optimal control pair $(IL6Dose(t)^*, IL10Dose(t)^*)$ such that

$$J(IL6Dose^*, IL10Dose^*) = \min\{J(IL6Dose, IL10Dose)|(IL6Dose, IL10Dose) \in F\}$$

subject to Equations (4.30)-(4.36), and

$$F = \{(IL6Dose(t), IL10Dose(t))|0 \leq IL6Dose(t) \leq b_1,\ 0 \leq IL10Dose(t) \leq b_2\}.$$

To this end, we rewrite Equation (4.29) as

$$J(u) = \int_{t_0}^{t_f} L(y, u, t)dt \tag{4.38}$$

and formulate the Hamiltonian (H) as

$$H(y, u, \lambda, t) = L(y, u, t) + \lambda^T f(y, u, t), \tag{4.39}$$

where $y = [P(t), N(t), D(t), IL6(t), TNF(t), IL10(t), Y_{IL10}(t)]^T$ denote the respective states, the control inputs are $u = [IL6Dose(t), IL10Dose(t)]^T$, and λ is a costate variable which arises from using the Lagrange multiplier method since our problem is a constrained optimization. It can then be shown ([84, 100]) that the solution u^* to Equation (4.39) satisfies

$$\dot{y} = \frac{\partial H}{\partial \lambda} = f \tag{4.40}$$

$$-\dot{\lambda} = \frac{\partial H}{\partial y} = \frac{\partial f^T}{\partial x}\lambda + \frac{\partial L}{\partial y}, \tag{4.41}$$

and

min H with respect to $u \leq F$ as

$$H(y^*, u^*, \lambda^*, t) \leq H(y^*, u, \lambda^*, t), \tag{4.42}$$

where Equations (4.40) and (4.41) are the state and costate system, and (4.42) is the famous Pontryagin's Minimum Principle; notice that * denotes optimality. In summary, we aim to find u^* that is within the admissible (constraint) control region specified by F that satisfied Equations (4.40), (4.41) and (4.42).

4.2.1 7D Optimal Control Problem: Existence of a Solution

We will mirror the procedure used in [37] to show the existence of a solution to our optimal control problem. First, we present the following results on existence theorem due to [51].

Consider a control problem of the form

$$J(x_0, u) = \phi(e) \tag{4.43}$$

subject to

$$\dot{x} = f(t, x(t), u(t)), \qquad t_0 \leqq t \leqq t_1, \tag{4.44}$$

where $x(t) \in E^n$ is the system state and $u(t) \in U$ the control applied at time t End conditions are imposed imposed of the type $e \in S$, where $e = (t_0, t_1, x(t_0), x(t_1))$ and S is a given subset of E^{2n+2}. The cost $J(x_0, u)$ is of *Mayer* type, and for each $(t, x) \in E^{n+1}$ let

$$F(t, x) = \{f(t, x, u) : u \in U\}.$$

Assumptions 4.2.1 ((2.4) in Chapter 3, [51])
f is continuous; moreover, there exist positive constants C_1, C_2 such that

a) $|f(t, x, u)| \leqq C_1(1 + |x| + |u|)$,

b) $|f(t, x', u) - f(t, x, u)| \leqq C_2|x' - x|(1 + |u|)$ *for all* $t \in E^1$, x', $x \in E^n$, *and* $u \in U$.

In stating an existence theorem, let $\mathcal{F}$ denote the class of all (x_0, u) such that u is a Lebesgue-integrable function on an interval $[t_0, t_1]$ with values in U.

Theorem 4.2.1 (Theorem 2.1 in Chapter 3, [51])
Suppose that Assumptions 4.2.1 hold, and moreover that:

a) $\mathcal{F}$ is not empty,

b) U is compact,

c) S is compact and ϕ is continuous on S,

d) $F(t,x)$ is convex for each $(t,x) \in E^{n+1}$.

Then there exist (x^*, u^*) minimizing $J(x_0, u)$ on $\mathcal{F}$.

Corollary 4.2.1 (Corollary 2.2 in Chapter 3, [51])
Let $\mu = \inf J(x_0, u)$ and $\mu_1 > \mu$. In Theorem 4.2.1 assumption (c) can be replayed by:

c') ϕ is continuous on S; there exists a compact $S' \subset S$ such that $e \in S$ and $J(x_0, u) \leqq \mu_1$ imply $e \in S'$.

Theorem 4.2.1 can be extended in two ways. First, instead of the *Mayer* for in Equation (4.43), we suppose that

$$J(x_0, u) = \int_{t_0}^{t_1} L(t, x(t), u(t))dt + \phi(e), \tag{4.45}$$

where the cost $J(x_0, u)$ is said to be of *Bolza* type. Second, the control U is allowed not to be compact. Define

$$\tilde{F}(t,x) = \{\tilde{z} : z = f(t,x,u), z_{n+1} \geqq L(t,x,u), u \in U\},$$

where $z = (z_1, \ldots, z_n) \in E^n$ and $\tilde{z} \in E^{n+1}$.

Theorem 4.2.2 (Theorem 4.1 in Chapter 3, [51])
Suppose that Assumptions 4.2.1 hold, that L is continuous, and moreover that:

a) $\mathcal{F}$ is not empty,

b) U is closed,

c) S is compact and ϕ is continuous on S,

d) $\tilde{F}(t,x)$ is convex for each $(t,x) \in E^{n+1}$,

e) $L(t,x,u) \geqq g(u)$, where g is continuous and $|u|^{-1}g(u) \to +\infty$ as $|u| \to \infty$, $u \in U$.

Then there exist (x^*, u^*) minimizing $J(x_0, u)$ on $\mathcal{F}$.

Some of the assumptions in the theorem can be replaced by others, more easily verified. For example, if U is compact then e) follows.

Corollary 4.2.2 (Corollary 4.1 in Chapter 3, [51])
In Theorem 4.2.2 any of the assumptions c), d), e) can be replaced by the corresponding c'), d'), e') where:

c') Same as Corollary 4.2.1.

d') U is convex, $f(t,x,u) = \alpha(t,x) + \beta(t,x)u,\ L(t,x,\cdot)$ is convex on U

e') $L(t,x,u) \geqq c_1|u|^\beta - c_2,\ c_1 > 0,\ \beta > 1.$

To show the existence of an optimal solution u^* to our control problem at least for the saturated system (of Equations (4.30)-(4.36)), we will show that our optimal control problem satisfy the following conditions:

1) f is is continuous and Lipschitz continuous with respect to y.

2) The set of admissible controls, F is closed and convex.

3) L is continuous and convex on $F\ \forall\ t \in \mathbb{R}$ and $y \in \mathbb{R}^n$.

4) $|f(y,u,t)| \leq c(1 + |y|)$.

5) $L \geq c_1||u||^\beta - c_2,\ c_i > 0,\ i = 1,2,\ \beta > 1.$

These conditions stem from merging Theorem 4.2.2 and Corollary 4.2.2 (see also [37]).

To show 1) : In Section 3.9.1 we proved that the saturated 7D system is Lipschitz continuous. Since the treatment therapies in (4.33) and (4.35) are source terms, the result in Section 3.9.1 remains valid.

To show 2) : The admissible control defined by the set $F = \{(IL6Dose(t), IL10Dose(t))|0 \leq IL6Dose(t) \leq b_1,\ 0 \leq IL10Dose(t) \leq b_2\}$ is closed and convex by definition.

To show 3): $L(y,u,t) = Q_N N(t)^2 + Q_D D(t)^2 + Q_Y Y_{IL10}(t)^2 + R_{IL6} IL6Dose(t)^2 + R_{IL10} IL10Dose(t)^2$ is quadratic in u, hence it is convex on F.

To show 4): The proof in Section 3.9.1 establishes that the nonlinear terms in the saturated 7D system are bounded; therefore, there exists a c that satisfied condition (4).

To show 5):

$$\begin{aligned} L(y,u,t) &= Q_N N(t)^2 + Q_D D(t)^2 + Q_Y Y_{IL10}(t)^2 + R_{IL6} IL6Dose(t)^2 + R_{IL10} IL10Dose(t)^2 \\ &\geq \min\{R_{IL6}, R_{IL10}\}||u||^2 + Q_N N(t)^2 + Q_D D(t)^2 + Q_Y Y_{IL10}(t)^2 \\ &\geq \min\{R_{IL6}, R_{IL10}\}||u||^2 + Q_N N(t)^2 + Q_D D(t)^2 - Q_Y Y_{IL10}(t)^2 \\ &\geq \min\{R_{IL6}, R_{IL10}\}||u||^2 - Q_Y Y_{IL10}(t)^2 \\ &\geq \min\{R_{IL6}, R_{IL10}\}||u||^2 - Q_Y \max\{Y_{IL10}(t)^2\} \end{aligned}$$

Therefore, condition 5) holds for $\beta = 2$, $c_1 = \min\{R_{IL6}, R_{IL10}\}$ and $c_2 = \max\{Y_{IL10}(t)^2\}$. This condition is relatively easy to show since all the terms in $L(y,u,t)$ are quadratic and are nonnegative. Hence, we have established the existence of an optimal solution for our saturated system (Equations (4.30)-(4.36)).

4.3 Optimal Control Problem: Numerical Results

According to [128], there are essentially three numerical techniques for solving optimal control problems:

1) Solve the two-point boundary value problem given by the necessary conditions, with solution of the local Hamiltonian optimization problem at each time step.

2) Complete discretization of the problem, converting it into a finite dimensional nonlinear program.

3) Finite parameterization of the control trajectory, again converting the problem into a nonlinear program, but with the objective and constraint functions evaluated by integration of the system equations and their gradients with respect to the control parameters by integration of the adjoint equations or sensitivity equations.

Method 1) was utilized in [2] to derive HIV therapeutic strategies that uses two types of dynamic treatments representing reverse transcriptase inhibitors (RTIs) and protease inhibitors (PIs). In [37], method 3) was adopted in the treatment of individuals infected with HIV. More specifically, this work considers treatment schedules that can control the infection (HIV). Several commercial and non-commercial softwares have been developed to solve optimal control problems numerically. The Professional Optimal Control Software (PROPT), General Pseudospectral Optimal Control Software (GPOPS), Sparse Optimal Control Software (SOCS), and Recursive Integration Optimal Trajectory Solver 95 (RIOTS_95) are some optimal control

solvers developed thus far. In some situations, researches prefer to develop customized codes for solving their respective optimal control problems.

We will use GPOPS version 2.4 [57, 117] to solve our formulated optimal control problem. GPOPS is an open source MATLAB software for solving highly complex multiple-phase optimal control problems. It uses the Legendre-Gauss and Legendre-Gauss-Radau pseudospectral methods. The pseudospectral method is a direct transcription that transcribes the continuous optimal control problem into a discrete nonlinear programming problem (NLP). This can then be solved by well-developed nonlinear programming algorithms [18] (this approach resembles "method 2)" described above). GPOPS employes a third party nonlinear programming solver to solve the discrete NLP. The third party solvers GPOPS adopts are SNOPT (Sparse Nonlinear OPTimizer) and IPOPT (Interior Point Optimizer). In this work we will use SNOPT [133].

4.3.1 GPOPS

Gauss Pseudospectral Optimization Software (GPOPS) is a MATLAB program for solving multiple-phase optimal control problems of the form.

Given a set of P phases, minimize the cost functional

$$J = \sum_{p=1}^{P} \left[\mathbf{\Phi}^{(p)}(\mathbf{x}^{(p)}(t_0), t_0, \mathbf{x}^{(p)}(t_f), t_f; \mathbf{q}^{(p)}) + \int_{t_0^{(p)}}^{t_f^{(p)}} \mathcal{L}^{(p)}(\mathbf{x}^{(p)}(t), \mathbf{u}^{(p)}(t), t; \mathbf{q}^{(p)}) dt \right]$$

subject to

$$\dot{\mathbf{x}}^{(p)} = \mathbf{f}^{(p)}(\mathbf{x}^{(p)}, \mathbf{u}^{(p)}, t; \mathbf{q}^{(p)}), \qquad (p = 1, \ldots, P),$$

with inequality path constraints

$$\mathbf{C}_{\min}^{(p)} \leq \mathbf{C}^{(p)}(\mathbf{x}^{(p)}(t), \mathbf{u}^{(p)}(t), t; \mathbf{q}^{(p)}) \leq \mathbf{C}_{\max}^{(p)}, \qquad (p = 1, \ldots, P),$$

boundary conditions

$$\phi_{\min} \leq \phi^{(p)}(\mathbf{x}^{(p)}(t_0), t_0^{(p)}, \mathbf{x}^{(p)}(t_f), t_f^{(p)}; \mathbf{q}^{(p)}) \leq \phi_{\max}, \qquad (p = 1, \ldots, P),$$

and phase continuity (linkage) constraints

$$\mathbf{P}_{\min}^{(s)} \leq \mathbf{P}^{(s)}(\mathbf{x}^{(p_l^s)}(t_f), t_f^{(p_l^s)}; \mathbf{q}^{(p_l^s)}, \mathbf{x}^{(p_u^s)}(t_0), t_0^{(p_u^s)}; \mathbf{q}^{(p_u^s)}) \leq \mathbf{P}_{\max}^{(\mathbf{s})}, \begin{cases} p_l, p_u \in [1, \ldots, P] \\ s = 1, \ldots, L \end{cases}.$$

Here, $\mathbf{x}^{(\mathbf{p})}(t) \in \mathbb{R}^{n_p}$, $\mathbf{u}^{(\mathbf{p})}(t) \in \mathbb{R}^{m_p}$, $\mathbf{q}^{(\mathbf{p})} \in \mathbb{R}^{q_p}$ and $t \in \mathbb{R}$ denote the state, control, static parameters and time in phase $p \in [1, \ldots, P]$, respectively. L is the number of phases to be linked, $p_l^s \in [1, \ldots, P]$, $(s = 1, \ldots, L)$ are the "left" phase numbers, and $p_u^s \in [1, \ldots, P]$, $(s = 1, \ldots, L)$ the "right" phase numbers.

GPOPS employed the *Gauss Pseudospectral Method* (GPM). The GPM is an orthogonal collocation method based on using global polynomial approximations to the dynamic equations at a set of *Legendre-Gauss* (LG) collocation points. It has been shown that the optimality conditions of the nonlinear programming problem (NLP) is equivalent to the discretized optimality conditions of the continuous control problem which is not true for other pseudospectral methods. The theory of the GPM can be found in [18, 65]; however, no knowledge of the GPM is required for using GPOPS.

The organization of GPOPS is as follows. Note that the user must specify the optimal control problem to be solved by writing MATLAB functions that define the following functions in each phase of the problem:

1) the cost functional

2) the right-hand side of the differential equations and the path constraints (i.e., the differential-algebraic equations)

3) the boundary conditions (i.e., event conditions)

4) the linkage constraints (i.e., how the phases are connected).

In addition, the user must also specify the lower and upper limits on every component of the following quantities:

1) initial and terminal time of the phase

2) the state at the following points in time:

   - at the beginning of the phase
   - during the phase
   - at the end of the phase

3) the control

4) the static parameters

5) the path constraints

6) the boundary conditions

7) the phase duration (i.e., total length of phase in time)

8) the linkage constraints (i.e., phase-connect conditions).

We refer the reader to [57, 117] for a complete review of how to use GPOPS. It should be noted that this routine belongs to the *direct method* category. For completeness, we present a brief review of the GPM in Appendix C.

4.3.2 SNOPT

SNOPT is a general-purpose package for constrained optimization. It can be used to solve both linear and nonlinear functions subject to bounds on the variables and sparse linear or nonlinear constraints. It is suitable for large-scale linear and quadratic programming and for linearly constrained optimization as well as for general nonlinear programs of the form:

$$\begin{aligned} \min_{x} \quad & f_0(x) \\ \text{subject to} \quad & l \leq \begin{pmatrix} x \\ f(x) \\ A_L x \end{pmatrix} \leq u, \end{aligned}$$

where x is an n-vector of variables, l and u are lower and upper bounds, $f_0(x)$ is a smooth scalar cost function, A_L is a sparse matrix, and $f(x)$ is a vector of smooth nonlinear constraint functions $\{f_i(x)\}$. There is an option that can replace "min" in the cost function to a "max" if the problem is to be maximized.

SNOPT employs a particular sequential quadratic programming (SQP) algorithm that exploits sparsity in the constraint Jacobian and maintains a limited-memory quasi-Newton approximation to the Hessian of the Lagrangian [56]. Search directions are obtained from quadratic programming subproblems that minimize a quadratic model of the Lagrangian function subject to linearized constraints. An augmented Lagrangian merit function is reduced along each search direction to ensure convergence from any starting point. A tutorial on how to use SNOPT and

additional information on the SQP algorithm can be found in [56, 133]. A brief overview of the one of the simplest SQP methods (*Local SQP method*) is discussed in Appendix D.

4.4 Numerical Results

In order to use GPOPS, we need to provide bounds on the states and the controls. For our problem, we define the constraints as

$$0 \leq P(t) \leq P(t)_{\max} \tag{4.46}$$
$$0 \leq N(t) \leq N(t)_{\max} \tag{4.47}$$
$$0 \leq D(t) \leq D(t)_{\max} \tag{4.48}$$
$$0 \leq IL6(t) \leq IL6(t)_{\max} \tag{4.49}$$
$$0 \leq TNF(t) \leq TNF(t)_{\max} \tag{4.50}$$
$$0 \leq IL10(t) \leq IL10(t)_{\max} \tag{4.51}$$
$$0 \leq Y_{IL10}(t) \leq Y_{IL10}(t)_{\max}. \tag{4.52}$$

The bounds on the control are chosen to conform with what was done in the literature [39]. The maximum dose amount of pro-inflammatory therapy $IL6Dose(t)$ permitted is calculated as the difference between the current level of $IL6(t)$ and the maximum permitted level of $IL6(t)$, given by $IL6(t)_{\max}$. Likewise, the maximum dose amount of anti-inflammatory therapy $IL10Dose(t)$ permitted is calculated as the difference between the current level of $IL10(t)$ and the maximum permitted level of $IL10(t)$, given by $IL10(t)_{\max}$. As endotoxin challenge levels $3\,mg/kg$, $6\,mg/kg$, and $12\,mg/kg$ were administered to rats during the experimentation, each level represents an initial condition for endotoxin concentration $P(t)$ (i.e., $P(0) = 3,$ or 6, or 12, see (4.37)). Therefore, there are three optimal control problems to be solved and each problem has separate bounds. Since the magnitudes of the states in the cost function (4.29) are on different scales, we balance them by specifying their weight constants as

$$Q_N = 1.0 \times 10^{-12},\ Q_D = 25 \text{ and } Q_{Y_{IL10}} = 3.2 \times 10^{-6}.$$

For the same reason, the treatment therapy weight constants are

$$R_{IL6} = 1.8 \times 10^{-3} \text{ and } R_{IL10} = 2.5 \times 10^{-2}.$$

4.4.1 Numerical Results for endotoxin challenge level 3 mg/kg

The initial condition is given as

$$P(0) = 3\,mg/kg,\ N(0) = 0\,cell\,count,\ D(0) = 0,\ IL6(0) = 0\,pg/ml,$$

$$TNF(0) = 0\,pg/ml, IL10(0) = 12.302\,pg/ml,\ Y_{IL10}(0) = 0.$$

It is noted that non-accessible tissue damage marker $D(t)$ and tissue damage driven non-accessible IL-10 promoter $Y_{IL10}(t)$ are dimensionless [126]. The upper bound values for the state constraints in (4.46)-(4.52) are as follows

$$P(t)_{\max} = 3,\ N(t)_{\max} = 3.0 \times 10^7,\ D(t)_{\max} = 6,\ IL6(t)_{\max} = 1.5 \times 10^4,$$

$$TNF(t)_{\max} = 3000,\ IL10(t)_{\max} = 300,\ Y_{IL10}(t)_{\max} = 1.4 \times 10^4.$$

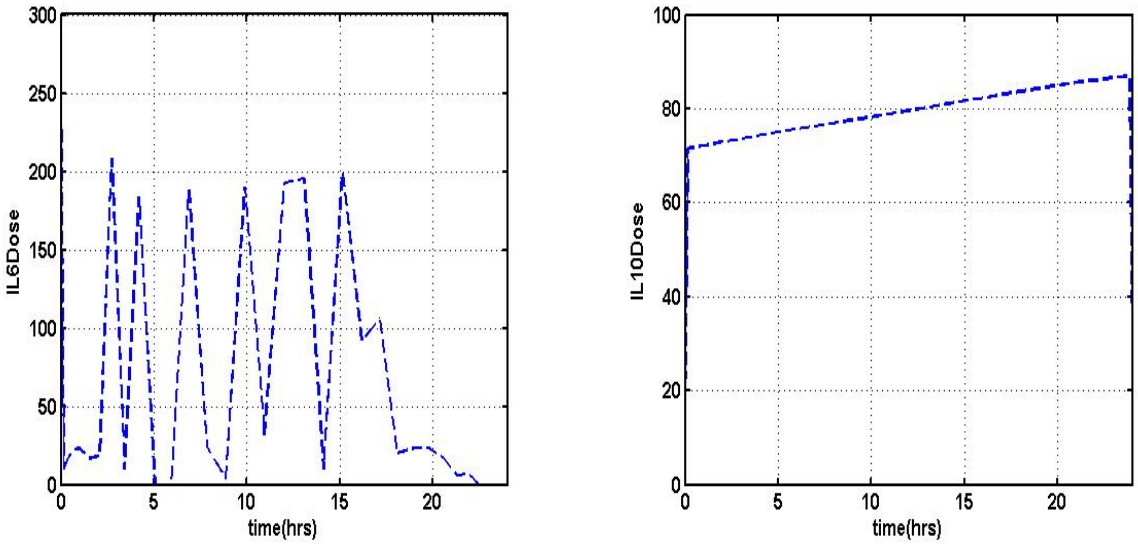

Figure 4.1: Optimal treatment control ($IL6Dose$ and $IL10Dose$) at $3\,mg/kg$ endotoxin level

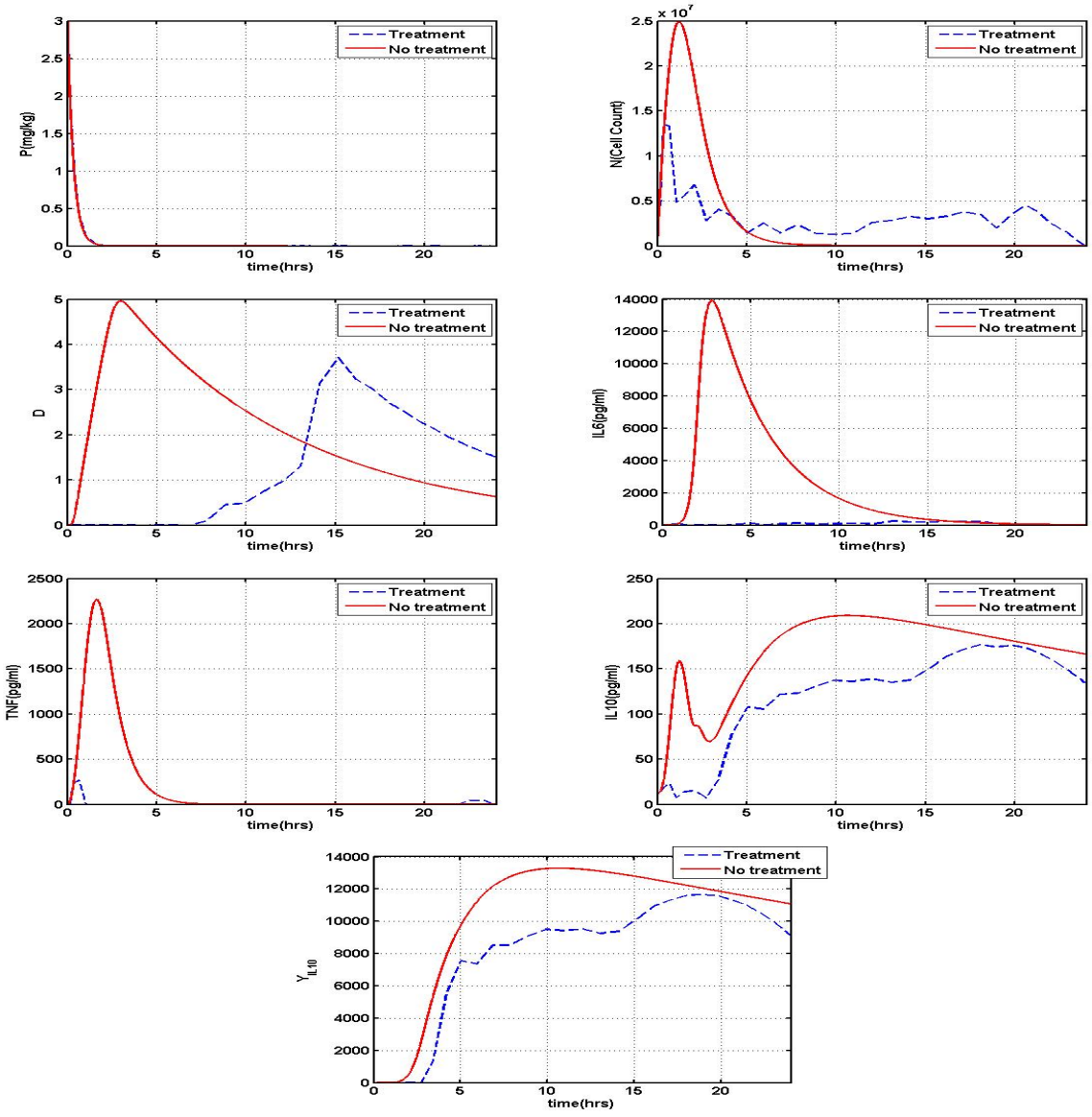

Figure 4.2: Model solution under optimal treatment control (- -); model solution with no treatment control (—) at $3\,mg/kg$ endotoxin level.

The optimal treatment control functions are depicted in Figure 4.1. The pro-inflammatory treatment dose IL6Dose(t) shows a rapid up-down movements for most of the durations in the horizon. These movements indicate the changes in the dose levels of IL6Dose(t) that is required. IL10Dose(t) depicts a steady rise in the dose level until the final hour.

The model response under the current treatment regiment together with the response with no

treatment are described in Figure 4.2. Perhaps an interesting observation is how the response for all the states were affected by the treatment therapy. Some states showed significant reductions in their response when compared with their corresponding levels without any treatments. Endotoxin concentration (P) levels basically remained unchanged indicating that the therapy had no effect. This is logical since it already decays exponentially. Though tissue damage (D) reduced by about 1.5 from its non treatment levels, it's peaked occurred at a much later time unlike the solution with no treatment. The behavior of $IL10(t)$ can be attributed mainly to $Y_{IL10}(t)$ irrespective of treatment. Observe that both $IL10(t)$ and $Y_{IL10}(t)$ have similar trajectories from the 4^{th} hour which is not surprising since we know from [126] that the second surge in $IL10(t)$ is due to tissue damage. From the results obtained we see that the optimal control methodology successfully lower the effects of the states. Finally, Figure E.2 contains the plots of the states under optimal treatment strategy. These plots illustrate a more lucid descriptions of the model response to the treatment dose.

4.4.2 Numerical Results for endotoxin challenge level 6 mg/kg

The only difference between the initial condition specified in Section 4.4.1 and in this section is the endotoxin concentration given by

$$P(0) = 6\, mg/kg.$$

The upper bound values for the state constraints in (4.46)-(4.52) are

$$P(t)_{\max} = 6,\ N(t)_{\max} = 3.0 \times 10^7,\ D(t)_{\max} = 6,\ IL6(t)_{\max} = 2.0 \times 10^4,$$

$$TNF(t)_{\max} = 4000,\ IL10(t)_{\max} = 450,\ Y_{IL10}(t)_{\max} = 2.5 \times 10^4.$$

Figure 4.3 illustrates the optimal treatment therapy at $6\, mg/kg$ endotoxin challenge level. $IL6Dose$ exhibited a sharp spike in the early hours before dropping to about 250 until the 5^{th} hour. Although the dose level displayed a little surge afterwards, it tapered off gradually for the rest of the horizon to zero. This implies that the regiment for $IL6$ is to administer a high dose of $IL6Dose$ around the early hours, subsequent doses would be significantly reduced and no additional dose should be given from the 19^{th} hour. At the onset, $IL10Dose$ sprout to about 180 before holding steady around that level for the rest of the horizon. Therefore, the dose level for $IL10$ is about the same for the entire horizon.

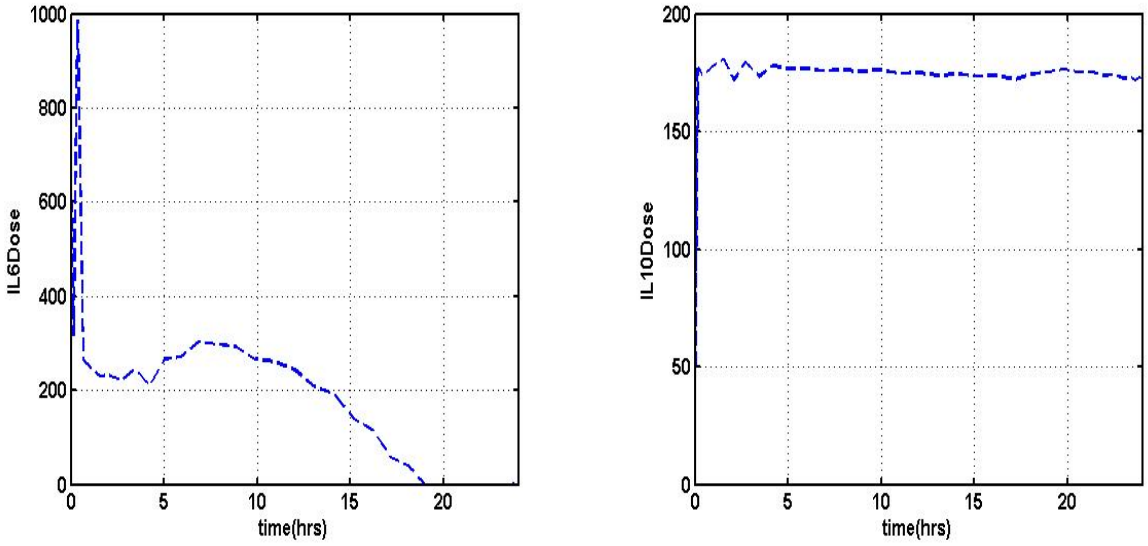

Figure 4.3: Optimal treatment control ($IL6Dose$ and $IL10Dose$) at $6\,mg/kg$ endotoxin level.

The model behavior under optimal control treatment strategy and without any treatment are depicted in Figure 4.4. The states response to treatment was not as effective as at the $3\,mg/kg$ concentration level as shown in Figure 4.2. The therapeutic response of total number of activated phagocytic cells N was unfavorable, unlike the other states that responded positively. The main reason why the level of N remained elevated is due to P. It is easy to observe that the activation of N is linked with the initial concentration of P and as the endotoxin levels stayed elevated so was N. Tissue damage D showed the most significant reduction under the treatment control. Finally, Figure E.3 depicted the model plots under optimal treatment strategy.

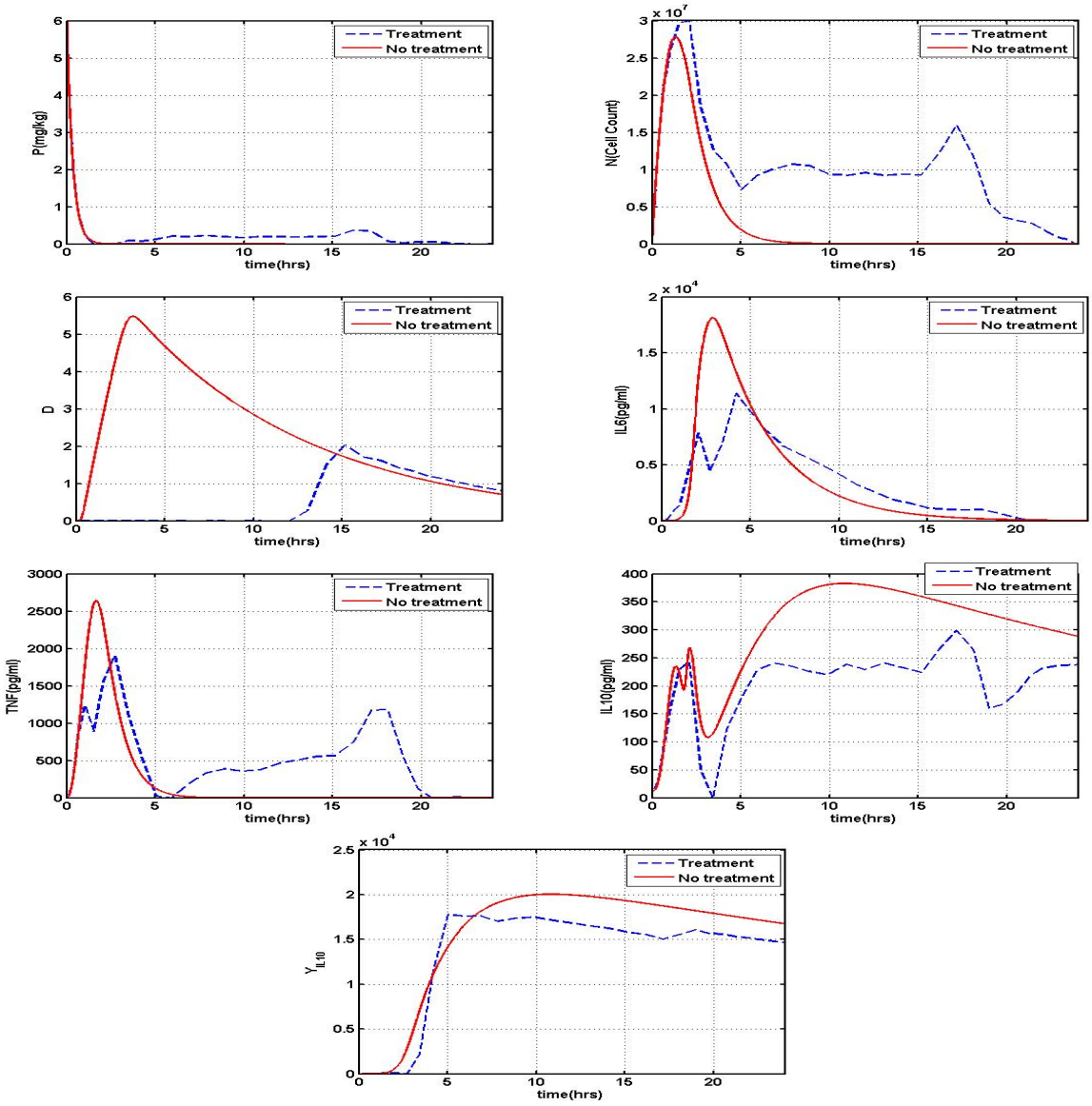

Figure 4.4: Model solution under optimal treatment control (- -); model solution with no treatment control (—) at $6\,mg/kg$ endotoxin level.

4.4.3 Numerical Results for endotoxin challenge level 12 mg/kg

The initial condition for the concentration of endotoxin challenge is given as

$$P(0) = 12\,mg/kg.$$

The initial condition for the other states remain unchanged from the previous sections. The upper bound values for the state constraints in (4.46)-(4.52) are

$$P(t)_{\max} = 12,\ N(t)_{\max} = 3.5 \times 10^7,\ D(t)_{\max} = 6.5,\ IL6(t)_{\max} = 2.0 \times 10^4,$$

$$TNF(t)_{\max} = 3000,\ IL10(t)_{\max} = 900,\ Y_{IL10}(t)_{\max} = 3.0 \times 10^4.$$

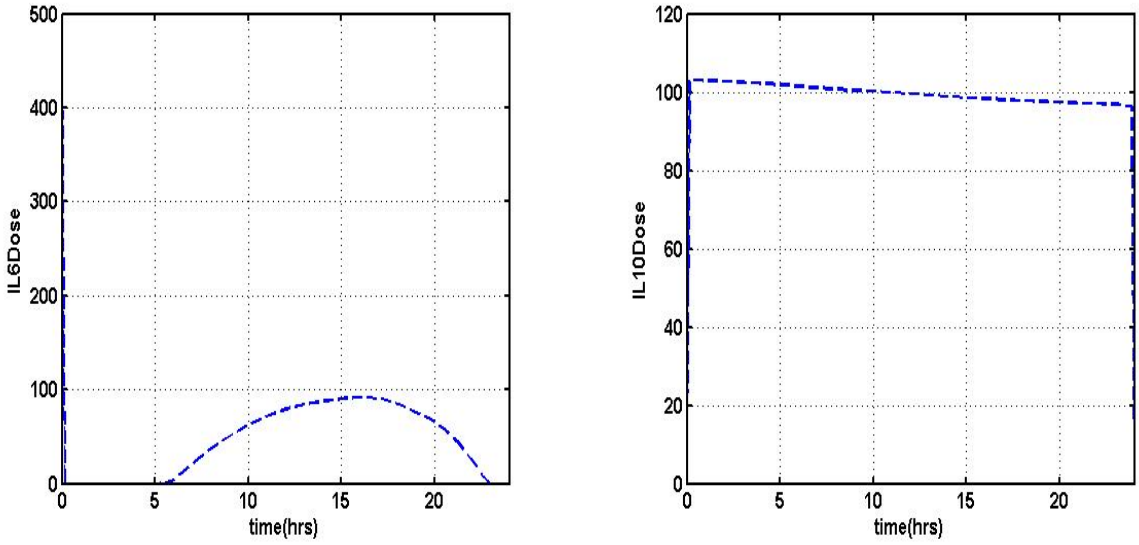

Figure 4.5: Optimal treatment control ($IL6Dose$ and $IL10Dose$) at $12\,mg/kg$ endotoxin level for 45 LG collocation points

As depicted in Figure 4.5, the presence of $IL6Dose$ treatment control was milder at this endotoxin concentration level. $IL10Dose$ remained high but displayed a marginal decline as time progressed. The model trajectory under treatment control in Figure 4.6 showed significant reduction; so, there is potential to design optimal therapeutic strategies to regulate inflammation. Finally, Figure E.4 depicts plots of the model state variables under treatment control.

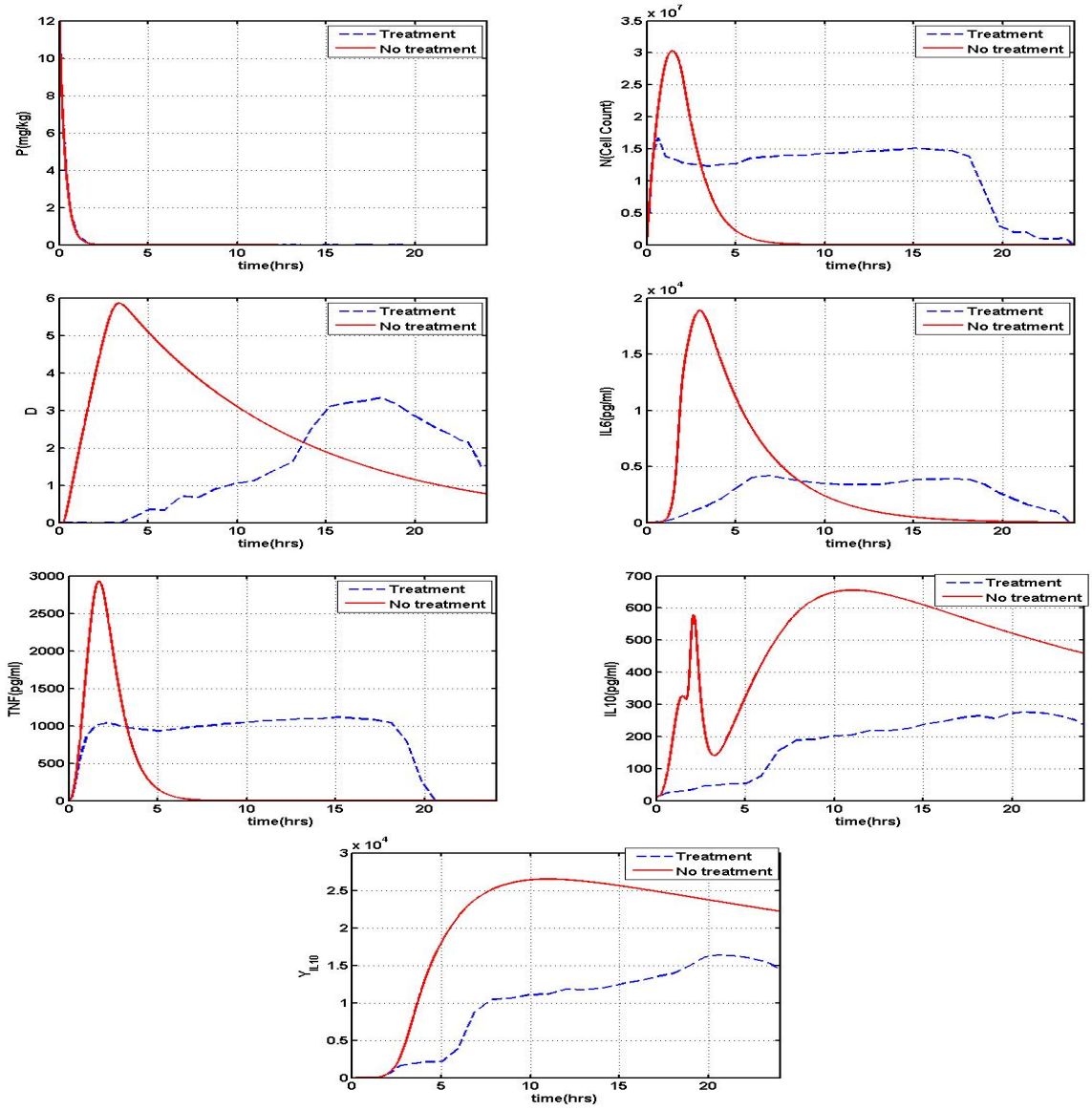

Figure 4.6: Model solution under optimal control methodology at $12\,mg/kg$ endotoxin level for 45 LG collocation points

Chapter 5

Model Predictive Control

5.1 Introduction

Model Predictive Control (MPC), also known as Receding Horizon Control (RHC) or Moving Horizon Control (MHC) refers to a family of feedback schemes that do not designate a particular control strategy, instead a range of control methods which make explicit use of a model of the process to obtain the control signal by minimizing an objective function [25]. MPC is a form of control in which the current control action is obtained by solving *on-line*, at each sampling instant, a finite horizon open-loop optimal control problem, using the current state of the system as the initial state. The optimization yields an optimal control sequence and the first control in this sequence is applied to the plant [94].

The basic differences among the various MPC algorithms are the process model, the cost function to be optimized, and their respective noises. Regardless of these differences, the MPC algorithms have been very successful and have gained wide acceptance in industrial applications. In addition, extensive scholarly research has been conducted in academia. The reason for such popularity is the ability of MPC designs to yield high performance control systems capable of operating without expert intervention for an extended periods of time [54]. In particular, we outline some advantages of MPC over other competing methods [25]:

- MPC is very attractive to scientist with limited knowledge of control as the concepts are very intuitive and at the same time the tuning is relatively easy.
- It can be used to control a wide range of processes, from those with relatively simple dynamics to more complex ones.

- The multivariate case can easily be dealt with.
- It intrinsically has compensation for dead times.
- It introduces feed forward control in a natural way to compensate for measurable disturbances.
- The resulting controller is an easy-to-implement control law.
- Its extension to the treatment of constraints is conceptually simple, and these can be systematically included during the design process.
- It is very useful when future references are known.
- It is a totally an open methodology based on certain basic principles which allows for future extensions.

There are a wide variety of applications of MPC scheme. Some of these areas include refinery, petrochemical, chemicals, aerospace, automotive, food processing, pulp and paper, metallurgy etc. More recently, MPC has a growing presence in biological processes. An excellent source for the multitude of industrial applications can be found in [114].

5.2 Historical Background

The first set of publications highlighting the emergence of MPC in the processing industry can be traced back to the late 1970s. Mainly, in [122, 123] where Model Predictive Heuristic Control (MPHC) was presented (MPHC is also known as Model Algorithmic Control (MAC)) and in 1979 engineers from Shell Oil [35, 109] discussed "Dynamic Matrix Control" with applications to a fluid catalytic cracker. A dynamic process model is explicitly used in both algorithms (impulse response in [122, 123] and step response in [35, 109]) to predict the effect of the future control actions of the manipulated variables on the output, hence the name "Model Predictive Control". The future moves of the variables are determined by minimizing the predicted error subject to operational constraints. The optimization is repeated at each sampling time based on up-to-date information or measurements from the plant. These formulations were primarily heuristic and algorithmic such that the numerical computations will be done using digital computers that were beginning to become popular at the time.

The Receding Horizon or Moving Horizon principle which is at the core of every MPC algorithm was proposed in 1963 [113], within the framework of "Open-Loop Optimal Feedback". The link between the closely related minimum time optimal control problem and linear programming

were first established in [144]. The popularity of MPC increased drastically from the 1980s, particularly in chemical process industries due to the simplicity of the algorithm and its use of the impulse or step response model. Later, MPC was formulated in the state space context [99]; this gave way for the use of well known theorems of the state space theory as well as facilitate their generalization to more complex processes such as multivariable processes, nonlinear processes, and systems with stochastic disturbances and noise in the measured variables. To this end, several predictive controller algorithms have been developed. Some of the algorithms developed are: Dynamic Matrix Control (DMC), Model Algorithmic Control (MAC), Predictive Functional Control (PFC), Generalized Predictive Control (GPC), Ydstie's Extended Horizon Adaptive Control (EHAC), and Extended Prediction Self Adaptive Control (EPSAC).

MPC has also been well studied in academia, some of the applications include under controlled conditions to a simple mixing tank and a heat exchanger [10], and coupled distillation column for the separation of a ternary mixture [82, 83]. An MPC comparison with conventional control schemes on a heat exchanger and an industrial autoclave was studied in [106]. Some of these applications are multivariable and involved constraints which are precisely the kinds of problems that motivated the development of MPC control algorithms [54].

5.3 MPC Methodology

In general, the methodology of every controller that is a part of the MPC family is formulated as solving on-line a finite horizon open-loop optimal control problem subject to system dynamics and constraints involving states and controls. The MPC strategy is represented in Figure 5.1 and the particular scheme we discuss is identical to those in [7, 47, 48].

From the measurement or information obtained at time t, the controller predicts the future dynamic behavior of the system over a prediction horizon T_p and determines (over a control horizon $T_c \leq T_p$) the input such that a predetermined open-loop performance objective functional is optimized. If there were no disturbances and no model-plant mismatch, and if the optimization problem could be solved over an infinite horizon, then the input signal found at $t = 0$ could be applied open-loop to the system for all $t \geq 0$. However, due to disturbances and model-plant mismatch the actual system behavior is different from the predicted one. To incorporate feedback, the optimal open-loop input is implemented only until the next sampling instant. The sampling time between the recalculation/measurement (new optimization) can vary in principle. Typically, it is fixed, i.e., the optimal control problem is re-evaluated after the sampling time δ. Using the new system state at time $t+\delta$, the whole procedure—prediction and optimization—is repeated; moving the control and prediction horizon forward.

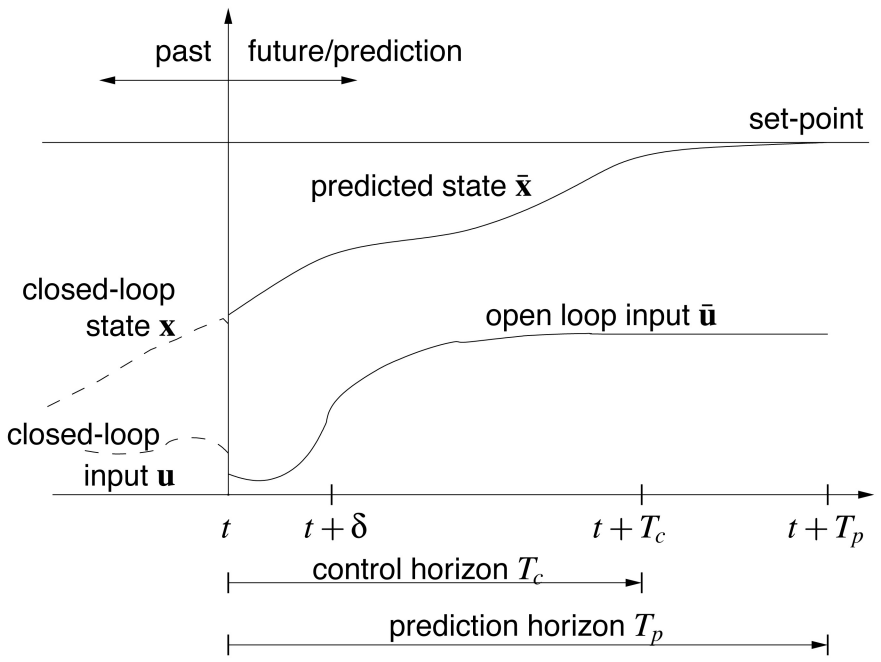

Figure 5.1: Model Predictive Control (MPC) strategy

A standard MPC algorithm operates in the following manner:

1) Obtain estimates of the states of the system.

2) Calculate an optimal input minimizing the desired cost function over the prediction horizon using the system model for prediction.

3) Implement the first part of the optimal input until the next sampling instant.

4) Continue with 2).

This strategy is implemented through a basic schematic diagram shown in Figure 5.2. The model is use to make future prediction of the process, based on past and current values as well as the proposed optimal future control actions. The optimizer is used to calculate these actions, taking into account the cost function as well as the constraints. The process model plays a decisive role in the controller in that the assigned model needs to be able to represent the process dynamics such that the future output can be precisely predicted.

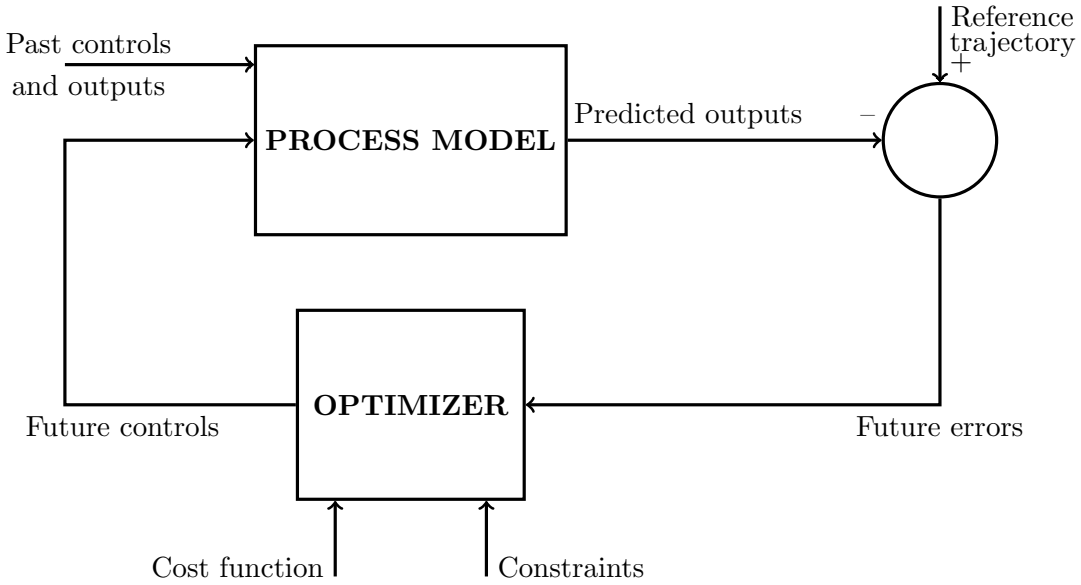

Figure 5.2: Schematic structure of Model Predictive Control (MPC)

5.4 Nonlinear Model Predictive Control (NMPC)

In general, industrial processes are nonlinear and it is necessary to distinguishes between linear and nonlinear model predictive control (NMPC). Linear MPC belongs to a family of MPC schemes that use linear models to predict the system dynamics and considers linear constraints on the states and inputs. NMPC refers to MPC schemes that are based on nonlinear models and/or consider a non-quadratic cost-functional and general nonlinear constraints [7].

Most MPC applications are based on the use of linear models since it originated in the late 70s and there are two main reasons why linear models are favored [25].

- The identification of a linear model based on process data is relatively easy.
- Linear models provide good results when the plant is operating in the neighborhood of the operating points.

In 1997, there were over 2,200 applications of MPC scheme that were implemented using linear models and most of these were in refinery and petrochemical [114]. And by 2003, more than 4,500 applications using linear models ranging from chemicals to aerospace industries were reported [116]. Although linear MPC approaches have been used in many applications, especially in process industries, most systems are inherently nonlinear by nature. With the quest for

higher product quality specifications, increasing productivity demands, tighter environmental regulations and demanding economical considerations in many industries, it has become imperative to operate systems closer to the boundary of the admissible operating region. Linear models are obviously not sufficient in describing the process dynamics under such increased specification levels; hence, the need to embrace nonlinear models can no longer be circumvented. Therefore, the inadequacies of linear models essentially motivates the use of nonlinear model predictive control.

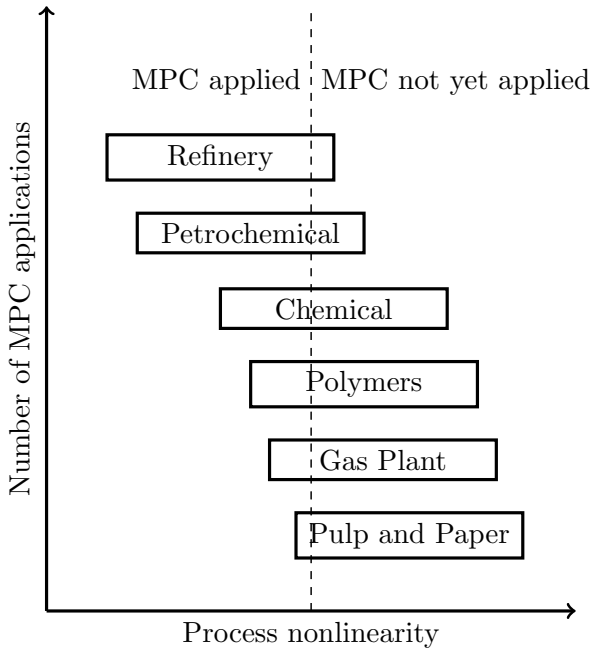

Figure 5.3: Distribution of MPC applications versus the degree of process nonlinearity [115].

More recently, there has been a surge in the applications of NMPC techniques in areas where MPC has not been traditionally applied [115]. Figure 5.3 shows a rough distribution of the number of MPC applications versus the degree of process nonlinearity. MPC scheme has not yet penetrated deeply into areas where process nonlinearities are strong and market demands require frequent changes in operating conditions. These are the areas that display the greatest opportunities for NMPC applications. In the biomedical processes there have been reports of great success in the application of NMPC. For example, [43, 52, 104] applied NMPC in the regulation of glucose supply in diabetic patients and an exploration of optimal dosing of anticancer agents. This scheme has also been used in HIV control [145]. In [37], NMPC was

applied on a model of HIV dynamics that incorporates drug resistance in a treatment schedule to control this infection. Lastly, [39] employed this scheme to find optimal therapeutic strategies to modulate inflammation. With the widespread success of NMPC in biomedical sciences, we will adopt an NMPC scheme in this work to obtain optimal treatment control for our reduced model of acute inflammatory response.

5.4.1 Theoretical Issues in NMPC

Despite the growing interest in the application of NMPC schemes, there are many theoretical difficulties that arise from the use of this scheme, at least conceptually. These are basically connected with the theoretical issues faced when working with nonlinear models. The key issues regarding the use of NMPC are [25]:

- The availability of nonlinear models from experimental data is an open issue, there is a lack of identification techniques for nonlinear processes.
- The optimization problem is nonconvex. Problems of this nature are much more difficult to solve than the QP problem.
- The difficulty of the optimization problem translates into an increase in computational time. This can limit the use of this technique.
- The study of crucial concepts such as stability and robustness is more complex in the case of nonlinear systems.

Some of these problems are partially solved. However, the most important theoretical issues facing NMPC are stability and robustness. For this reason, we will briefly outline how stability and robustness are currently handled in NMPC. We conclude this section with a description of a typical nonlinear mathematical system that can be used for most NMPC scheme. Consider the following continuous time nonlinear set of ordinary differential equations:

$$\dot{\mathbf{x}}(t) = \mathbf{f}(\mathbf{x}(t), \mathbf{u}(t)) \tag{5.1}$$

$$\mathbf{x}(0) = \mathbf{x}_0 \tag{5.2}$$

subject to

$$\mathbf{u}(t) \in \mathcal{U},\ \mathbf{x}(t) \in \mathcal{X}, \quad \forall\, t \geq 0 \tag{5.3}$$

where $\mathcal{U} \subseteq \mathbb{R}^m$ and $\mathcal{X} \subseteq \mathbb{R}^n$ denote the set of feasible inputs and the set of feasible states, respectively. The expression in (5.3) represents the inputs and states constraints. In practice, the finite horizon open-loop optimal control problem described in Equations (5.1)-(5.3) can be formulated as follows [48]:

$$\min_{\bar{\mathbf{u}}(\cdot)} J(\mathbf{x}(t), \bar{\mathbf{u}}(\cdot); T_c, T_p) = \int_t^{t+T_p} F(\bar{\mathbf{x}}(\tau), \bar{\mathbf{u}}(\tau)) d\tau \tag{5.4}$$

subject to

$$\dot{\bar{x}}(\tau) = \mathbf{f}(\bar{\mathbf{x}}(\tau), \bar{\mathbf{u}}(\tau)) \tag{5.5}$$

$$\bar{\mathbf{x}}(t) = \mathbf{x}(t) \tag{5.6}$$

$$\bar{\mathbf{u}}(\tau) \in \mathcal{U}, \quad \forall\, \tau \in [t,\, t + T_c] \tag{5.7}$$

$$\bar{\mathbf{u}}(\tau) = \bar{\mathbf{u}}(\tau + T_c), \quad \forall\, \tau \in [t + T_c,\, t + T_p] \tag{5.8}$$

$$\bar{\mathbf{x}}(\tau) \in \mathcal{X}, \quad \forall\, \tau \in [t,\, t + T_p] \tag{5.9}$$

where T_p and T_c are the prediction and the control horizon with $T_c \leq T_p$ (a number of NMPC algorithms set $T_c = T_p$). $\bar{\mathbf{u}}(\cdot)$ is the internal controller and $\bar{\mathbf{x}}(\cdot)$ is the solution of Equations (5.5) and (5.6) driven by $\bar{\mathbf{u}}(\cdot)$ such that $[t,\, t + T_p] \to \mathcal{U}$ with $\mathbf{x}(t)$ as the initial condition. It is necessary to make the distinction between the real system and the variables in the controller since the predicted values, even in the nominal undisturbed case will generally not be the same with the actual closed-loop values as the optimal input is recalculated (over a moving finite horizon T_c) at every sampling instance.

5.4.2 Stability

Stability is by far one of the most important issues surrounding finite horizon NMPC schemes. It is critical to know whether a finite horizon NMPC strategy does lead to stability of the closed-loop. The main issue facing a finite prediction and control horizon comes from knowing that the predicted open-loop and the resulting closed-loop behavior are, in general, different [48]. A perfect situation is for one to have an NMPC technique that successfully attain closed-loop stability independent of the performance of the parameters in the objective functional and has the ability to approximates the infinite horizon NMPC scheme as good as possible. Any NMPC scheme that successfully attain closed-loop stability independent of the performance of the parameters in the objective functional is usually referred to an NMPC approach with *guaranteed stability*. Different possibilities to achieve closed-loop stability for NMPC using finite horizon length have been proposed in the literature [4, 28, 40, 89].

Ideally the best way to achieve stability is the use of an infinite horizon cost, i.e., if the prediction horizon goes on without terminating [19, 73]. Based on Bellman's Principle of Optimality [15], it is clear that feasibility at one sampling instance implies feasibility and optimality at the next sampling instance in the nominal case. This basically means that the input and state trajectories computed as the solution of the NMPC optimization at a specific instance in time are equal to the closed-loop trajectories of the nonlinear system. This implies that the remaining parts of the trajectories after one sampling instance are the optimal solution at the next sampling instance, which also implies closed-loop stability [48]. As noted in several MPC literature, infinite horizon schemes are usually not applied in practice because the open-loop optimal control problem cannot be solved sufficiently fast.

Since we know that there are possibilities to achieve closed-loop stability for NMPC using a finite horizon, we will explore the approaches used to achieve closed-loop stability. A number of these approaches modify the setup of the NMPC scheme so that stability of the closed-loop can be guaranteed independently of the plant and performance specifications [48]. One way to make this work is by adding suitable equality or inequality constraints and/or suitable additional penalty terms to the cost functional. The sole purpose of adding these constraints known as *stability constraints* is to accomplish stability of the closed-loop [94, 95].

The zero terminal equality constraint is one of the simplest stability constraints to add at the end of the prediction horizon in order to enforce the stability of a finite prediction horizon. The *zero terminal equality constraint* is of the form

$$\bar{\mathbf{x}}(t + T_p; \mathbf{x}(t), t, \bar{\mathbf{u}}) = \mathbf{0} \tag{5.10}$$

The addition of Equation (5.10) to Equations (5.5)-(5.9) leads to stability of the closed-loop if the optimal control problem possesses a solution at $t = 0$. This is indeed true because the feasibility at one time instance leads to feasibility at the next time instance and a decrease in the value function. The main drawback with a zero terminal equality constraint is that the system must return to the origin in finite time; for this reason it is not compatible with some optimal control problems. The *tracking system problem* is one such example where this kind of stability constraints cannot be exercised since the final state is often nonzero. Moreover, the fact that the system must be brought to the origin in finite time can lead to feasibility problems for short prediction/control horizon lengths. Besides, on the numerical computational front, an exact satisfaction of a zero terminal equality constraint does require an infinite number of iterations in the nonlinear programming problem [28]. On the positive side, the zero terminal equality constraint is straightforward to apply and conceptually simple.

Other stability constraints have been proposed due to the limitations of the zero terminal

equality constraints. The *terminal region constraint* and the *terminal penalty term* $E(\bar{\mathbf{x}}(t+T_p)$ are two such constraints proposed. Both of these can be included in the NMPC algorithm or either one can be added. The terminal region constraint which is added at the end of the prediction horizon has the form

$$\bar{\mathbf{x}}(t+T_p) \in \Omega \subseteq \mathcal{X}, \tag{5.11}$$

and the terminal penalty term is added to the objective functional

$$J(\mathbf{x}(t), \bar{\mathbf{u}}(\cdot); T_p) = \int_t^{t+T_p} F(\bar{\mathbf{x}}(\tau), \bar{\mathbf{u}}(\tau))d\tau + E(\bar{\mathbf{x}}(t+T_p). \tag{5.12}$$

The terminal penalty term in Equation (5.12) is not a performance specification that can be chosen freely, rather E and the terminal region Ω in (5.11) are determined off-line such that stability is "enforced" [48]. The interested reader is refer to [28, 40, 41, 94] for a comprehensive overview of this subject as well as the different NMPC algorithms.

Finally, it is important to point out that a repeated minimization over a *finite horizon objective* in a receding horizon manner does not necessary lead to an optimal solution for the infinite horizon problem even if the same objective function is used. Rather, the two solutions will in general differ significantly if a short horizon is chosen. To this end, we see that short horizons are desirable from a computational point of view, but long horizons are required for closed-loop stability and in order to achieve the desired performance [48].

5.4.3 Robustness

In general, NMPC schemes do not require that the actual system is identical to the model used for prediction. In scenarios where the actual system is identical to the model used, we say that there is *no model/plant mismatch*; control systems that belong to this group are known as *nominal* systems. This is obviously an unrealistic assumption for practical applications and the progress of an NMPC algorithm that focuses on robustness issues. The presence of uncertainty in the characterization of a system raises the question of robustness, i.e., what is the possibility of maintaining certain properties such as stability and performance in the presence of uncertainty? Most studies on robustness consider unconstrained systems. If a Lyapunov function for the nominal closed-loop system maintains its descent property and if the disturbance (uncertainty) is sufficiently small, then stability is maintained in the presence of uncertainty [94]. However, when constraints on states and controls are present, it is necessary to ensure, that disturbances do not cause transgression of the constraints and this clearly adds

an extra level of complexity. Suppose we assume that a nonlinear system with uncertainty is given as

$$\dot{\mathbf{x}}(t) = \mathbf{f}(\mathbf{x}(t), \mathbf{u}(t), \mathbf{r}(t)), \tag{5.13}$$

where the uncertainty $\mathbf{r}(\cdot)$ satisfies $\mathbf{r}(\tau) \in \mathcal{R}(x, u)$ and $\mathcal{R}$ is assumed to be compact. The main impediment with robustness is the resulting difference between the predicted open-loop and actual closed-loop trajectory, this is also true in the case of nominal stability.

There are several approaches to the study of robustness that were discussed in [48, 90, 94]. On the other hand, it is worthwhile to mention that the robustness properties of the NMPC schemes designed for nominal stability is extensively studied in [75, 91]. There are at least three main robust NMPC formulations:

- **Robust NMPC solving an open-loop min-max problem:**
  The standard NMPC setup in this formulation is maintained but the cost function we seek to optimize is changed to the worse case disturbance "sequence" that can occur, i.e.,

$$J(\mathbf{x}(t), \bar{\mathbf{u}}(\cdot); T_p) = \max_{\bar{\mathbf{d}}(\cdot)} \int_t^{t+T_p} F(\bar{\mathbf{x}}(\tau), \bar{\mathbf{u}}(\tau)) d\tau + E(\bar{\mathbf{x}}(t+T_p) \tag{5.14}$$

$$\text{subject to} \tag{5.15}$$

$$\dot{\bar{x}}(t) = \mathbf{f}(\bar{\mathbf{x}}(t), \bar{\mathbf{u}}(t), \bar{\mathbf{d}}(t)) \tag{5.16}$$

$$\bar{\mathbf{x}}(t) = \mathbf{x}(t). \tag{5.17}$$

  The open-loop min-max optimal control problem is solved on-line. The main difficulty is that by adding stability constraints like in the nominal case could result in a situation where no feasible solution may be achieved. This arise from the fact that one input signal must "reject" all possible disturbances and guarantee the satisfaction of the stability constraints.

- $\mathbf{H_\infty - NMPC}$:
  The H_∞-NMPC ensures robustness by its the choice of a cost function, the key obstacle is that determining the controller requires solution of a nonlinear Hamilton-Jacobi-Isaacs (HJI) equation. To avoid this complexity, the NMPC cost function can be modified similar to the H_∞ problem and optimizing over a sequence of control laws robustly stabilizing finite horizon H_∞-NMPC formulations. The central impediment is the prohibitive computational time necessary.

- **Robust NMPC optimizing a feedback controller used during the sampling times:**
  The open-loop formulation of the robust stabilization problem can be seen as very conservative, since only open-loop control is used during the sampling times. By this we imply that the disturbances are not directly rejected in between the sampling instances. To overcome this problem it has been proposed not to optimize over the input signal. Instead of optimizing the open-loop input signal directly, a feedback controller is optimized, i.e., the decision variable $\bar{\mathbf{u}}$ is not considered as optimization variable instead a "sequence" of control laws $\mathbf{u_i} = \mathbf{k_i}(\mathbf{x})$ applied during the sampling times is optimized. Now the optimization problem has as optimization variables the parameterizations of the feedback controllers $\{\mathbf{k_1}, \cdots, \mathbf{k_N}\}$. While this formulation is very attractive since the conservatism is reduced, the solution is often prohibitively complex.

5.4.4 Output Feedback

One of the greatest hindrance in the application of NMPC is that at every sampling instant t_i the system state is required for prediction. Oftentimes, not all system states are directly accessible, by this we mean that only the output variables y are directly available for feedback.

$$y(t) = g(x(t), u(t)), \tag{5.18}$$

where $y(t) \in \mathbb{R}^p$ are the measured outputs and $g : \mathbb{R}^n \times \mathbb{R}^m \to \mathbb{R}^p$ maps the state and input into the output. This limitation is usually taken care of by using a state observer for the reconstruction of the states. Rather than using the optimal feedback, the following is applied:

$$u(t; \hat{x}(t_j)) = \bar{u}^*(t; \hat{x}(t_j)), \quad t \in [t_i, t_{j+1}), \tag{5.19}$$

i.e., replace the initial x in the optimal control problem by its estimate $\hat{x}$. The estimation error is an uncertainty, therefore robustness issues are not fully resolved and are involved though some perturbation results may be employed for the unconstrained case. Any state estimator may be employed, usually Kalman Filter (KF) can be used when the system is linear or Extended Kalman Filter (EKF)/Unscented Kalman Filter (UKF) when the system is nonlinear. However, due of lack of a general nonlinear separation principle, stability is not guaranteed, even if the state observer and the NMPC controller are both stable [7].

Meanwhile, the stability problem has been studied extensively by a number of researchers. However, the work by [92] established stability of the composite system (observer and model predictive control) when a weak detector is employed. Another result in [97] established stability

of the composite system when a moving horizon observer is employed; no uncertainty exists in the model so the state can be perfectly estimated using a record of input/output data over the interval $[t-T_0, t]$ where t is the current time. Furthermore, [47] presented a broad class of state feedback nonlinear model predictive controllers' conditions on the observer that guarantee that the closed-loop is semi-global stable.

Chapter 6

NMPC Numerical Results: Reduced 7D Model

One of the objectives of this thesis is to propose treatment control for inflammatory response to combat uncontrolled systemic inflammation. Most of the theoretical research on acute inflammation have focus on describing the fundamental mechanisms regarding inflammation and how inflammatory mediators interact with themselves at time progresses [29, 76, 140]. A key result emanating from this research affirms that successful therapeutic interventions require proper timing relative to the evolution of the inflammatory response [38, 120]. In Section 4.4 we discussed the results obtained by studying the 7D model under an open-loop optimal control treatment strategies. Optimal treatment levels $IL6Dose(t)$ and $IL10Dose(t)$ were computed for the specified initial conditions at $3\,mg/kg$, $6\,mg/kg$ and $12\,mg/kg$ endotoxin challenge levels. Although the open-loop controller revealed significant reduction in the states response to treatment, this technique may be deficient for the follow reasons:

- Some unmodelled effect can disturb the system, thus rendering the treatment schedule ineffective.
- In the event that a dose is missed, the open-loop control is no longer optimal.
- The open-loop optimal control does not make use of the periodic measurements taken at subsequence sampling times.

NMPC is a suitable feedback technique to handle these deficiencies since the control only depends on the current state of the system. In this chapter, we summarize the *in silico* simulation results from applying NMPC on the 7D model using three different cases of recalcu-

lation/measurement steps at $3\,mg/kg$, $6\,mg/kg$ and $12\,mg/kg$ endotoxin challenge levels. The cases represent the different structures we want the treatment schedule to vary and this will provide insights on how effective the states respond to different therapeutic schedule. The following are the cases we wish to examine:

1) Adapt recalculation/measurement steps that correspond to the actual time periods blood samples were taken from the rats. Since the elapse time between the last two observations was 12 hours, we will maintain the same 12 hours recalculation step after the 24^{th} hour. In this case, the recalculation step is considered unequal.

2) This case assumes hourly recalculation/measurement interval. Hence, it is a fixed recalculation step of every one hour.

3) The last case assumes every four hours recalculation/measurement step beginning from the 4^{th} hour. Prior to the 4^{th} hour the recalculation step will be the same as the first case, i.e., $t = 0, 1, 2, 4, 8, \ldots$.

Another reason for studying the NMPC technique across these cases of recalculation/measurement step is to establish a trade-off between the optimized dose regiment with respect to modulating inflammation and the complexity of the different recalculation steps we understudied. The "hourly recalculation/measurement step" is expected to be the most expensive case since it requires hourly treatment dose to be administered on the system. The "four hours recalculation/measurement step" is assumed the next expensive case since the system will receive treatment dose at times 0, 1, 2, 4 then every four hours. The least expensive case is the "unequal recalculation/measurement step". Note that as the states in the model and control are continuous function, the control and state values used at each recalculation step are a linear interpolation.

The *in silico* simulation horizon for the NMPC scheme will be 72 hours (3 days). We will examine the effect of the optimal therapeutic strategy over this horizon at all three cases of recalculation/measurement steps for each endotoxin challenge level. The model optimal feedback estimates will be used at each recalculation/measurement step since experimental data corresponding to the treatment time points are unavailable. However, we will concluded this chapter with an example illustrating how to incorporate clinical data with treatment information at every time point. Typically, in such situations a better way to implement NMPC is to combine it with Kalman filter to serve as a state estimator.

6.1 Acute Inflammation: NMPC Simulations

The acute inflammatory response model used in the NMPC scheme was described in Section 4.2; the same model was used for the open-loop optimal control problem in Chapter 4. At each recalculation step $IL6Dose(t)$ and $IL10Dose(t)$ treatment control doses are adjusted accordingly to modulate inflammatory responses and the maximum dose allowed is chosen to be consistent with what was described in Section 4.4 as well as in the literature [39], but with a minor modification. The maximum dose amount for each inflammatory therapy at a given recalculation step is calculated as the difference between the current concentration level of the inflammatory cytokine and the maximum allowable level of that cytokine. This calculation applied to both $IL6Dose(t)$ and $IL10Dose(t)$. The bounds on the states are consistent with the open-loop optimal control simulations. Stability constraints were not added in our NMPC algorithm because the 72 hours horizon was long enough to display steady state behaviors on the states at either the choice of recalculation step or the endotoxin challenge level.

6.1.1 NMPC Simulations at 3 mg/kg endotoxin challenge level

The NMPC simulated results at $3\,mg/kg$ endotoxin challenge level showing the control and state response for each of the three cases of recalculation steps are summarized below.

Figure 6.1 shows an exponential decay for the concentration of endotoxin levels across all the different cases of recalculation steps. This behavior is logical with the ODE describing the dynamics of $P(t)$ (Figures 6.8 and 6.9 in Section 6.1.2 illustrate identical behavior).

Figure 6.2 captures the treatment response of the total number of activated phagocytic cells $N(t)$ from the NMPC scheme. The rate of elimination of $N(t)$ is about the same for the different cases of recalculation step. However, notice that $N(t)$ was driven to equilibrium (zero) for only the "Unequal recalculation step". One would have expected the more expensive recalculation cases to achieve equilibrium faster. A comparison of the response of $N(t)$ in the open-loop optimal control simulation in Figure 4.2 and these plots show a significant reduction in the total number of activated phagocytic cells for the NMPC scheme than the open-loop optimal control.

The plots of tissue damage in Figure 6.3 revealed the most vivid changes in response to treatment at the three cases. As expected, the "One hour interval recalculation step" displayed the most significant reduction; indeed, it was the only case to achieve stable equilibrium before the end of the horizon. The "Four hours recalculation step" also showed substantial reduction in the response of $D(t)$. The magnitude of reduction achieved with the feedback NMPC scheme

is considerable when compared with the open-loop control solution (see Figure 4.2). Inflammatory response induce tissue damage and elevated levels of damage up-regeluates $N(t)$ as well as induce $Y_{IL10}(t)$. The interactions of $N(t)$, $D(t)$ and $Y_{IL10}(t)$ are visibly observed when analyzing the plots of the "Unequal recalculation step" in Figures 6.2, 6.3 and 6.7, respectively. Around the 25^{th} hour, $N(t)$ displayed a sudden surge (see "Top Left" plot in Figure 6.3), this triggered a corresponding surge in $Y_{IL10}(t)$ (see "Top Left" plot in Figure 6.7) as well as slightly up-regulated $N(t)$ (see "Top Left" plot in Figure 6.2).

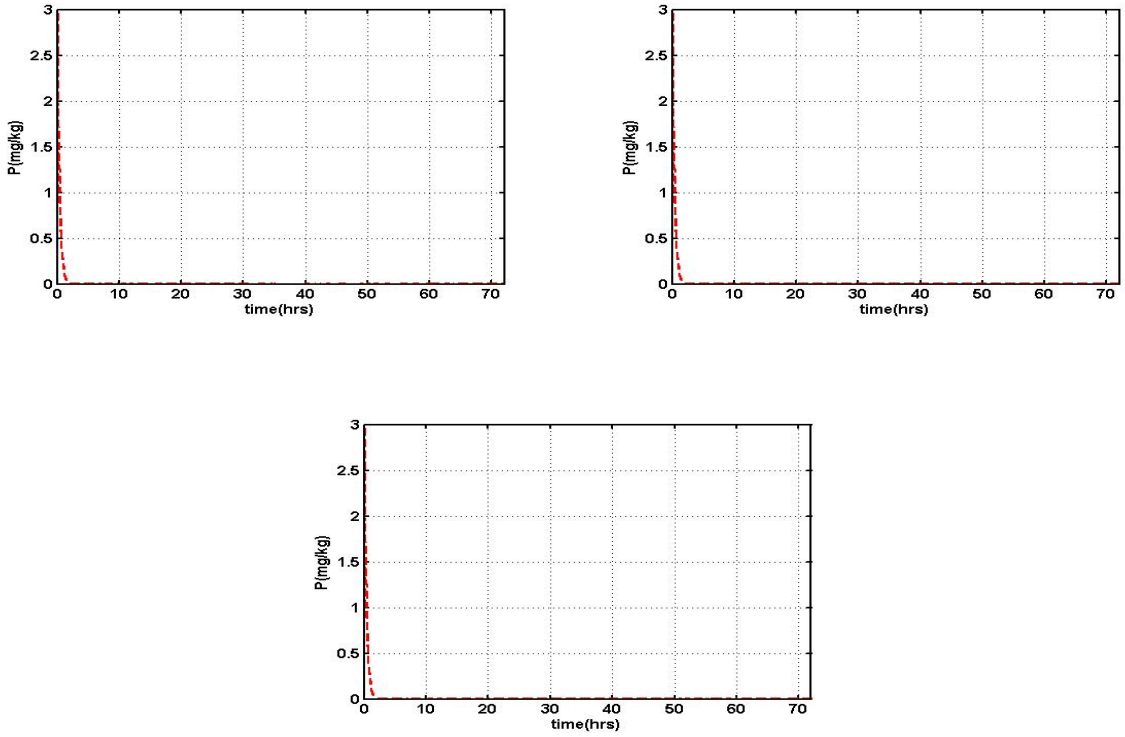

Figure 6.1: NMPC simulation of $P(t)$ at $3\,mg/kg$ endotoxin challenge level showing the three difference cases of recalculation step over a 72 hours (3 days) horizon:

Top Left: Unequal recalculation step.

Top Right: One hour interval recalculation step.

Bottom: Four hours recalculation step.

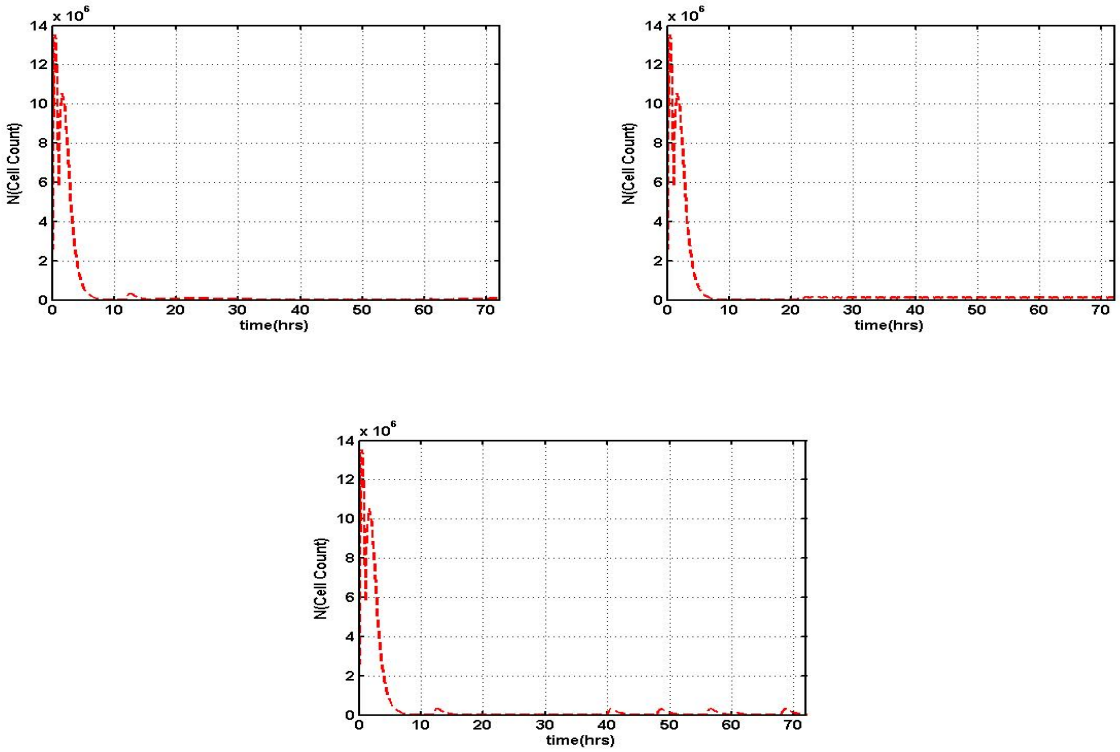

Figure 6.2: NMPC simulation of $N(t)$ at $3\,mg/kg$ endotoxin challenge level showing the three difference cases of recalculation step over a 72 hours (3 days) horizon:

Top Left: Unequal recalculation step.

Top Right: One hour interval recalculation step.

Bottom: Four hours recalculation step.

The plots in Figure 6.4 are a combination of the pro-inflammatory cytokine interleukin-6 ($IL6(t)$) and the pro-inflammatory therapy ($IL6Dose(t)$). The side-by-side plots display the response of interleukin-6 (on the left) to treatment and their corresponding pro-inflammatory therapeutic doses (right plots). The trajectories of $IL6Dose(t)$ correlate with the changes displayed in the dynamics of the $IL6(t)$; the treatment controller $IL6Dose(t)$ exhibited features that resembles the well known *bang-bang controller*, this characteristic can be linked to the nature of the numerical method which may not be the case in general. The frequent switches in the control behavior are in tune with the up-regulation and down-regulation of interleukin-6. From the top plots (the plot representing the "Unequal recalculation instance") one can see that the *bang-bang* phenomenon occurred more frequently during the early hours of the predictive horizon and by the 30^{th} hour the controller had switched to the "off" position which lasted

for the rest of the horizon; this conforms with the period when the effects of interleukin-6 had become almost nonexistence. The same pattern was captured in the "middle" and "bottom" plots; the only notable difference in these plots is that the *bang-bang* phenomenon continued until the end of the predictive horizon. These switches indicate the amount of pro-inflammatory therapeutic doses to administer. The "off" switch implies that no treatment dose is required and as the treatment schedule tries to regulate the pro-inflammatory response, it also attempts to use the minimum amount of dose needed. Lastly, "Unequal recalculation step" was the only case that successfully drove interleukin-6 to stable equilibrium.

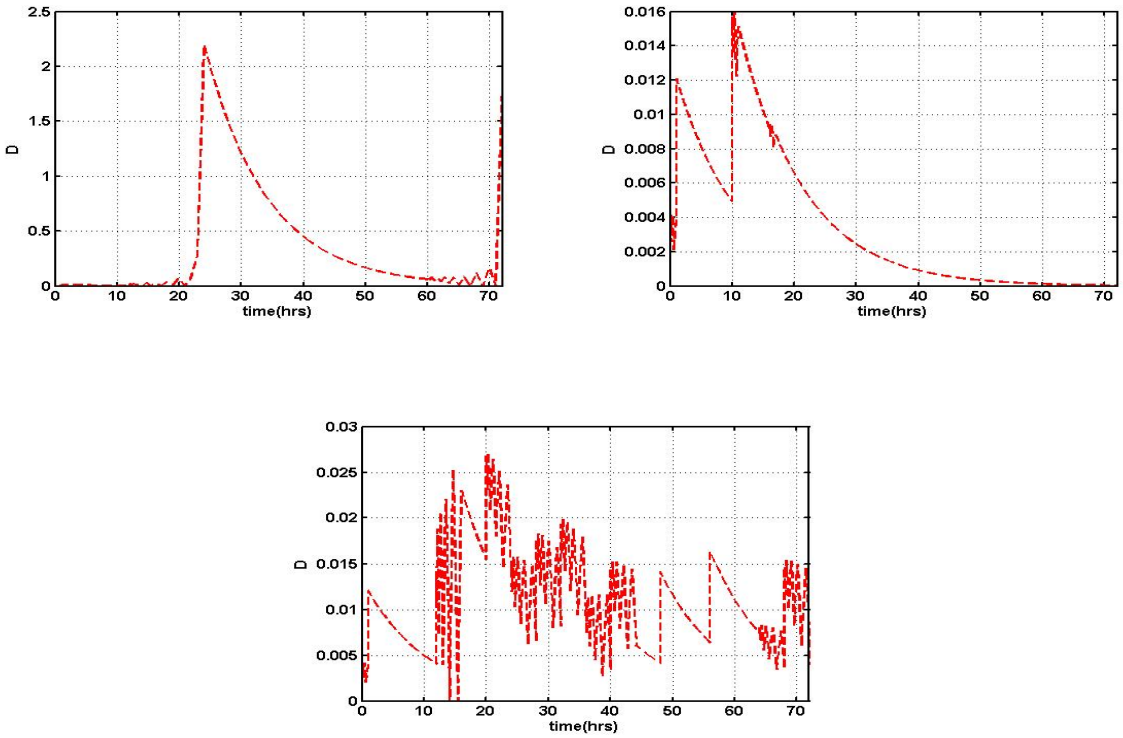

Figure 6.3: NMPC simulation of $D(t)$ at $3\,mg/kg$ endotoxin challenge level showing the three difference cases of recalculation step over a 72 hours (3 days) horizon:

Top Left: Unequal recalculation step.

Top Right: One hour interval recalculation step.

Bottom: Four hours recalculation step.

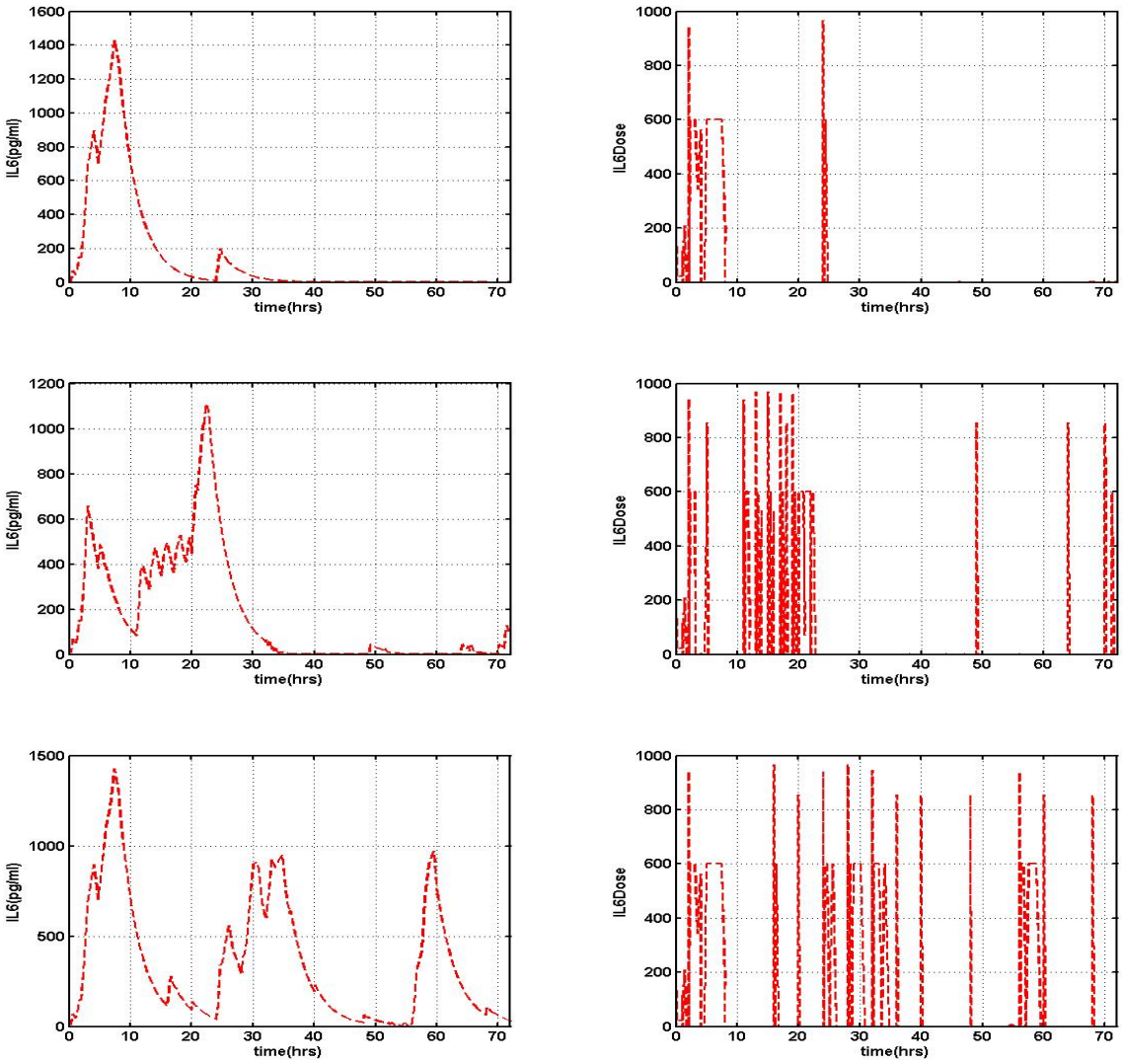

Figure 6.4: NMPC simulation of $IL6(t)$, and $IL6Dose(t)$ at $3\,mg/kg$ endotoxin challenge level showing the three difference cases of recalculation step over a 72 hours (3 days) horizon, the plots on the left are the states, whereas those on the right are the treatment control:

Top Left: Unequal recalculation step.

Top Right: One hour interval recalculation step.

Bottom: Four hours recalculation step.

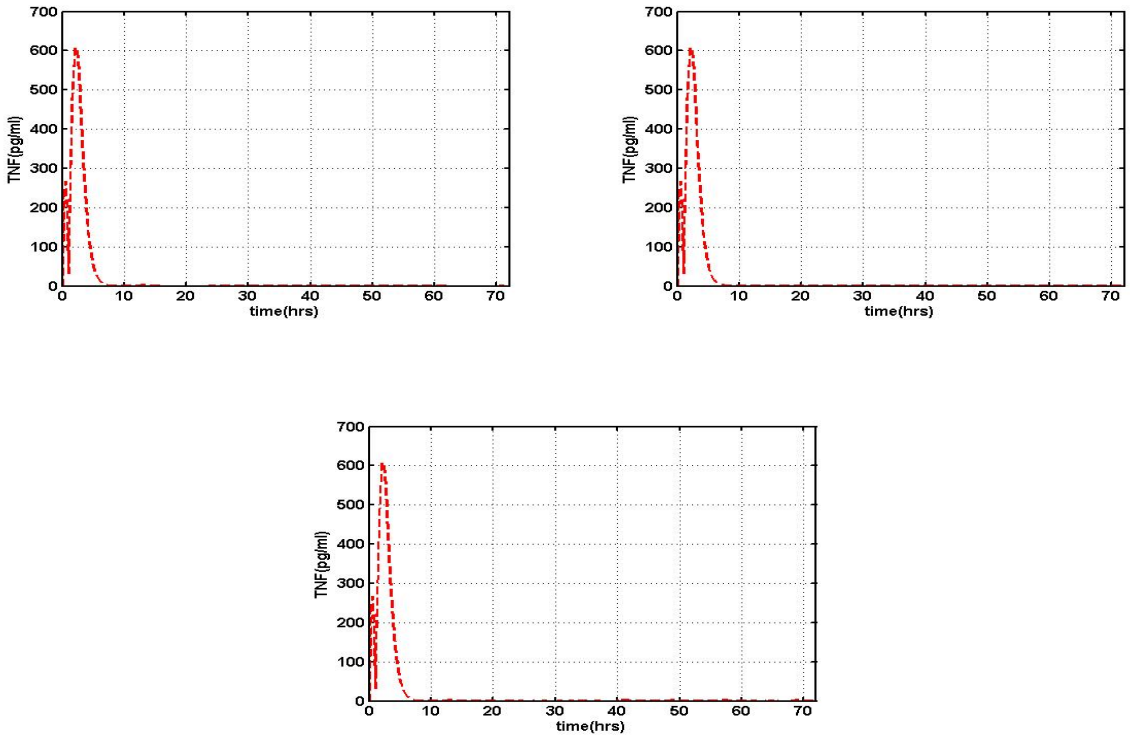

Figure 6.5: NMPC simulation of $TNF(t)$ at $3\,mg/kg$ endotoxin challenge level showing the three difference cases of recalculation step over a 72 hours (3 days) horizon:

Top Left: Unequal recalculation step.

Top Right: One hour interval recalculation step.

Bottom: Four hours recalculation step.

All three cases of recalculation step have identical *in silico* simulation results as depicted in Figure 6.5. The effects of the pro-inflammatory cytokine $TNF(t)$ was basically nonexistence after the 10^{th} hour when it achieved equilibrium. Perhaps it is interesting to note that this inflammatory response was neither one of the states in the cost function that we seek to minimize (Equation (4.29)) nor assigned a control variable but it quickly attained equilibrium. Lastly, the treatment response behavior of $TNF(t)$ is very similar to $N(t)$, this implies that both effects responded to treatment in an identical manner. This could be attributed to the fact that $N(t)$ was the most dominate state in the ODE describing $TNF(t)$.

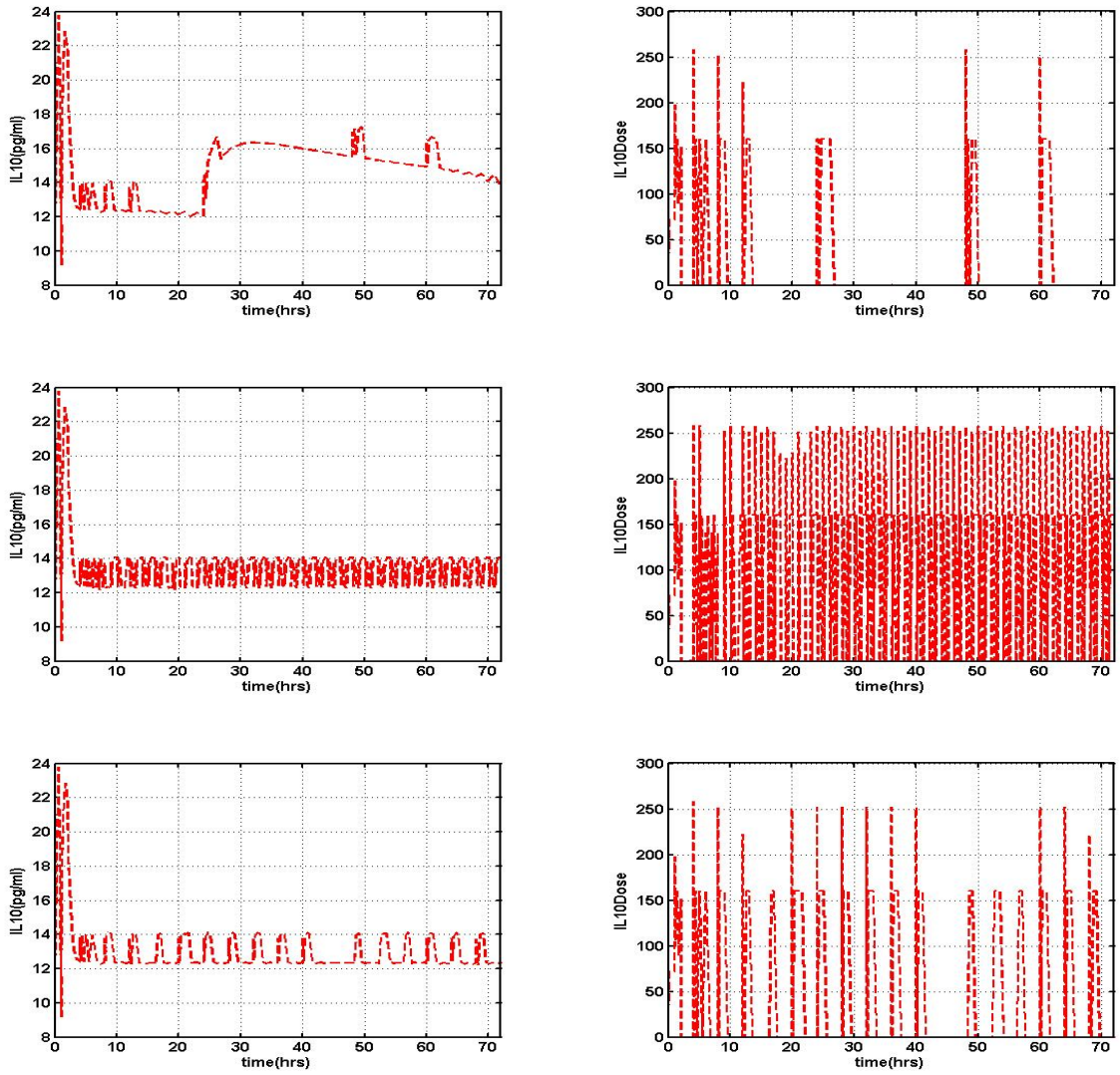

Figure 6.6: NMPC simulation of $IL10(t)$, and $IL10Dose(t)$ at $3\,mg/kg$ endotoxin challenge level showing the three difference cases of recalculation step over a 72 hours (3 days) horizon, the plots on the left are the states, whereas those on the right are the treatment control:

Top Left: Unequal recalculation step.

Top Right: One hour interval recalculation step.

Bottom: Four hours recalculation step.

$IL10Dose(t)$ displayed more *bang-bang* phenomenon in the controller as shown in Figure 6.6, especially in the "One hour interval recalculation step" case (middle plot). $IL10Dose(t)$ con-

sistently captured the frequent small up-down swing between $12\,mg/kg$ and $14mg/kg$ in the treatment response of interleukin-10 ($IL10(t)$) for both "One hour interval recalculation step" and "Four hours recalculation step". Lastly, $IL10(t)$ achieve equilibrium relatively early in the horizon, this is depicted in the middle and bottom plots.

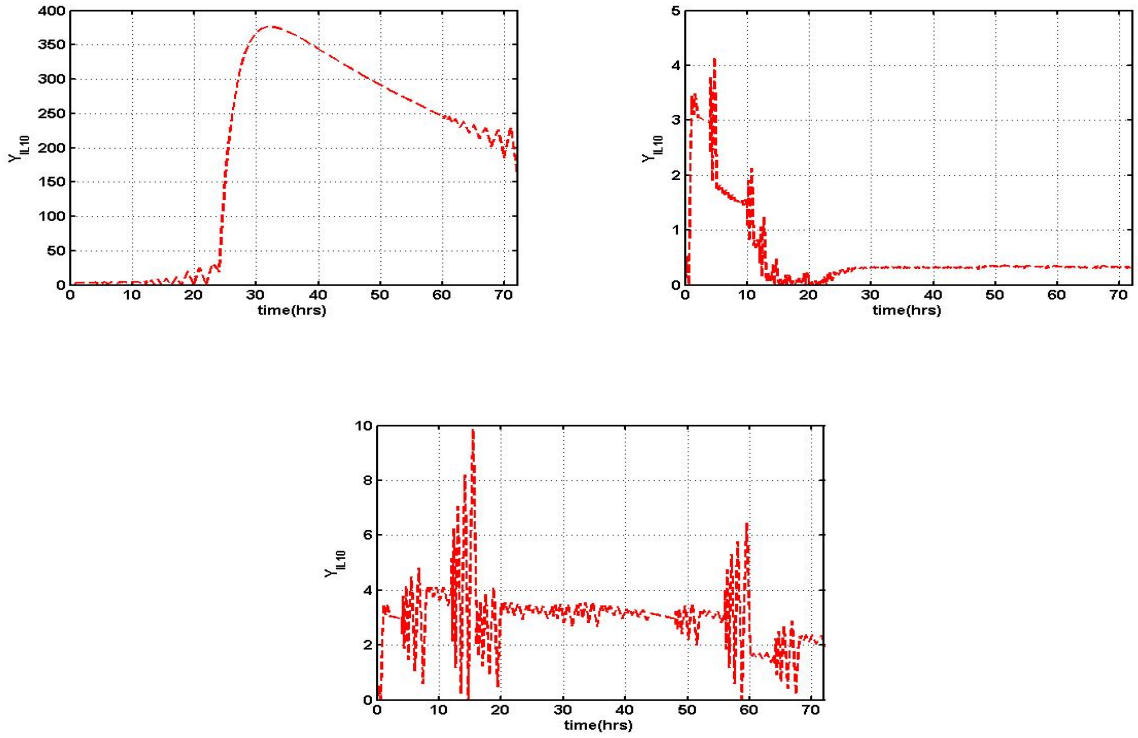

Figure 6.7: NMPC simulation of $Y_{IL10}(t)$ at $3\,mg/kg$ endotoxin challenge level showing the three difference cases of recalculation step over a 72 hours (3 days) horizon:

Top Left: Unequal recalculation step.

Top Right: One hour interval recalculation step.

Bottom: Four hours recalculation step.

In Figure 6.7, the response of $Y_{IL10}(t)$ demonstrated another vivid changes to treatment for the three different cases. Similar behavior also occurred for $D(t)$ in Figure 6.3. This shows that the tissue damage related states are more sensitive to the choice of recalculation step used. The plots show an enormous reduction in the effect of $Y_{IL10}(t)$ between the "unequal recalculation step" and other cases.

6.1.2 NMPC *in silico* simulations at 6 mg/kg and 12 mg/kg endotoxin challenge levels

This section focuses on the NMPC *in silico* simulation results at $6\,mg/kg$ and $12\,mg/kg$ endotoxin challenge levels, respectively. The plots for those states with no control variable are placed side-by-side for their respective endotoxin challenge levels and those on the left represent the $6\,mg/kg$ whereas those on the right denote $12\,mg/kg$. The plots of pro-inflammatory cytokine interleukin-6 ($IL6(t)$) and those of anti-inflammatory cytokine interleukin-10 ($IL10(t)$) are side-by-side with $IL6Dose(t)$ and $IL10Dose(t)$, respectively.

It is noted that the exponential decay of the concentration of endotoxin levels remained consistent as expected, regardless of the choice of recalculation step. Figures 6.8 and 6.9 depict the cascade of endotoxin levels at $6\,mg/kg$ and $12\,mg/kg$, respectively. The smooth rapid decrease in the response of $N(t)$ for "One hour recalculation step" in Figure 6.10 ($6\,mg/kg$ endotoxin level) was not captured by the other cases, rather they exhibited similar up-down swing as the level of $N(t)$ decreases. This implies that $N(t)$ is sensitive at $6\,mg/kg$ with respect to the choice of recalculation step. On the other hand, the $12\,mg/kg$ endotoxin level plots in Figure 6.11 illustrated an identical smooth rapid cascade across all the cases of recalculation step. Note that the treatment response of the concentration of $TNF(t)$ exhibited identical phenomenon similar to those in $N(t)$ (Figures 6.16, and 6.17), this similarity is not surprising since the same behavior was observed at $3\,mg/kg$ endotoxin concentration level.

The tissue damage related states ($D(t)$ and $Y_{IL10}(t)$ in Figures 6.12, 6.13, 6.20, and 6.21) displayed the most vivid treatment response changes and they are highly sensitive to the choice of recalculation step employed. The inflammatory response doses ($IL6Dose(t)$ and $IL10Dose(t)$ in Figures 6.14, 6.15, 6.18 and 6.19) showed great efficiency in regulating the concentration of interleukin-6 and interleukin-10. $IL10(t)$ achieved equilibrium in all the endotoxin challenge levels. Lastly, the NMPC scheme produced effective optimal treatment regiment to modulate inflammation better than the open-loop control *in silico* simulation.

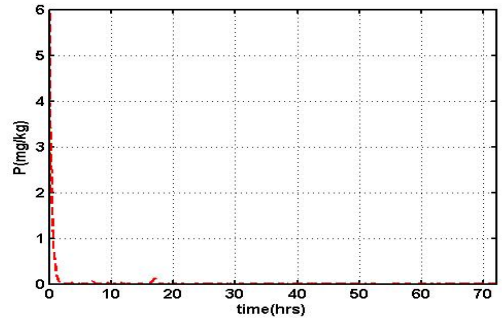

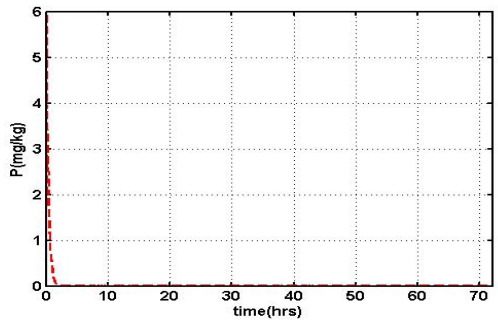

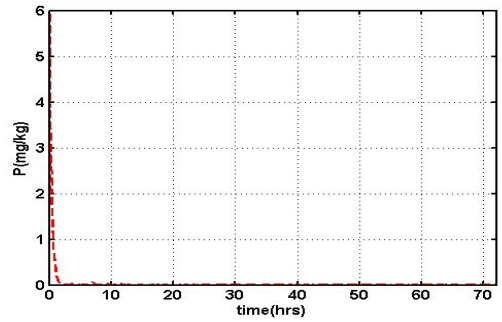

Figure 6.8: NMPC of $P(t)$ at $6\,mg/kg$.
Top: Unequal recalculation,
Middle: One hour recalculation,
Bottom: Four hours recalculation.

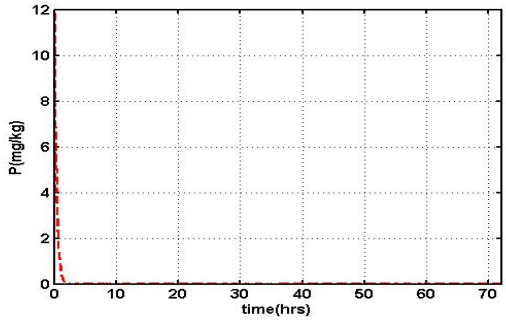

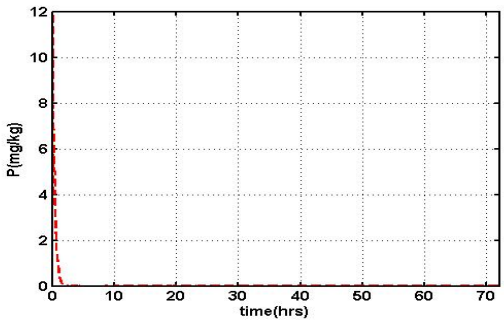

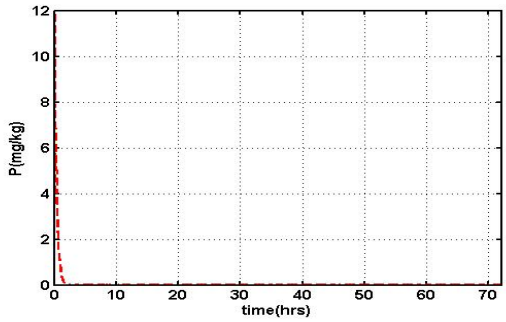

Figure 6.9: NMPC of $P(t)$ at $12\,mg/kg$.
Top: Unequal recalculation,
Middle: One hour recalculation,
Bottom: Four hours recalculation.

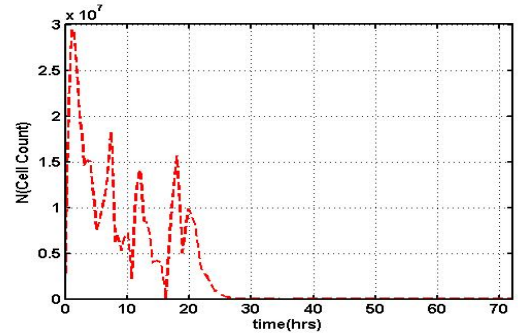

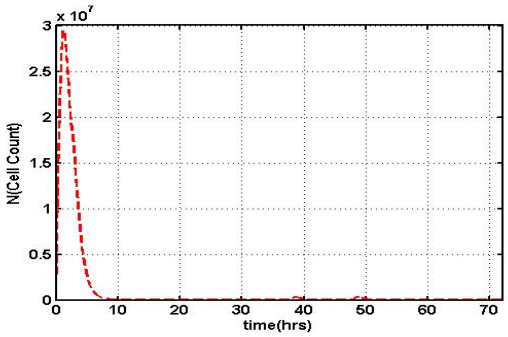

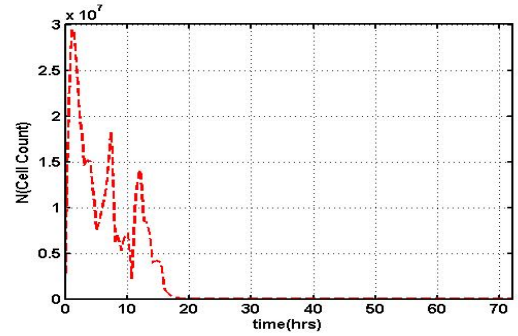

Figure 6.10: NMPC of $N(t)$ at $6\,mg/kg$.
Top: Unequal recalculation,
Middle: One hour recalculation,
Bottom: Four hours recalculation.

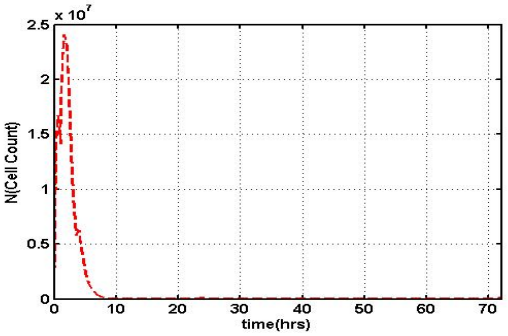

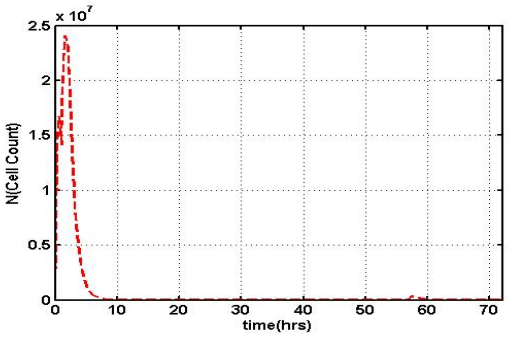

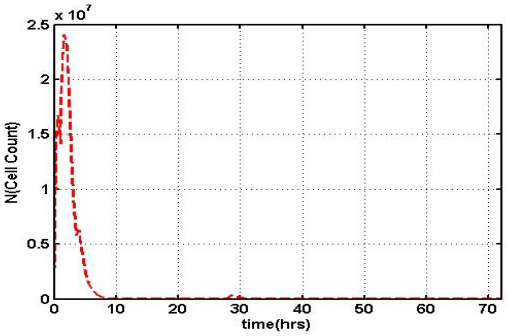

Figure 6.11: NMPC of $N(t)$ at $12\,mg/kg$.
Top: Unequal recalculation,
Middle: One hour recalculation,
Bottom: Four hours recalculation.

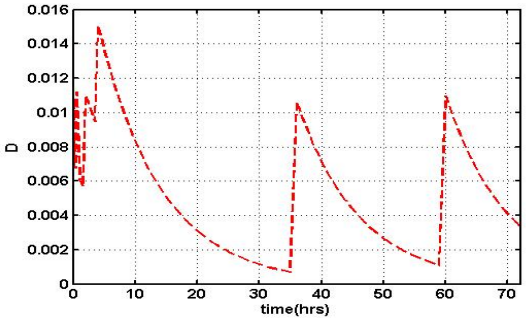

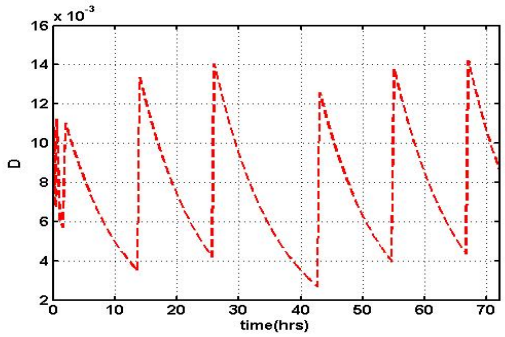

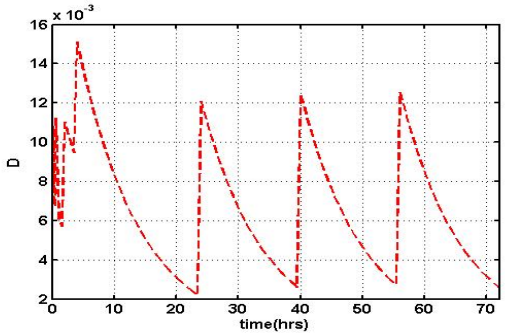

Figure 6.12: NMPC of $D(t)$ at $6\,mg/kg$.
Top: Unequal recalculation,
Middle: One hour recalculation,
Bottom: Four hours recalculation.

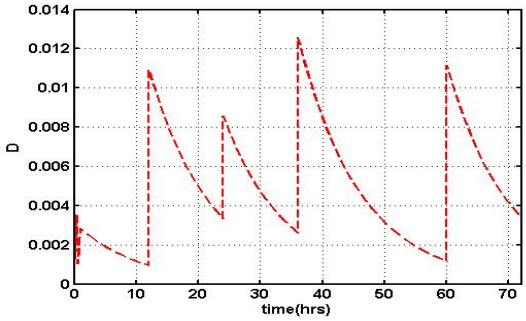

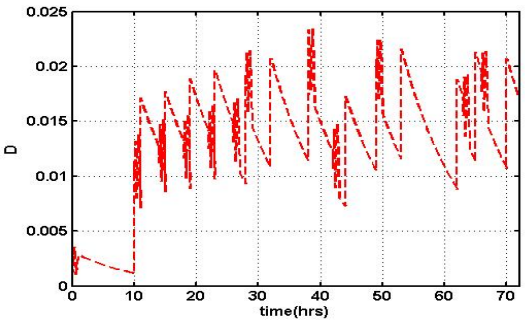

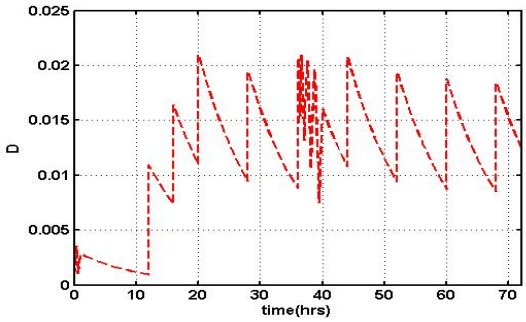

Figure 6.13: NMPC of $D(t)$ at $12\,mg/kg$.
Top: Unequal recalculation,
Middle: One hour recalculation,
Bottom: Four hours recalculation.

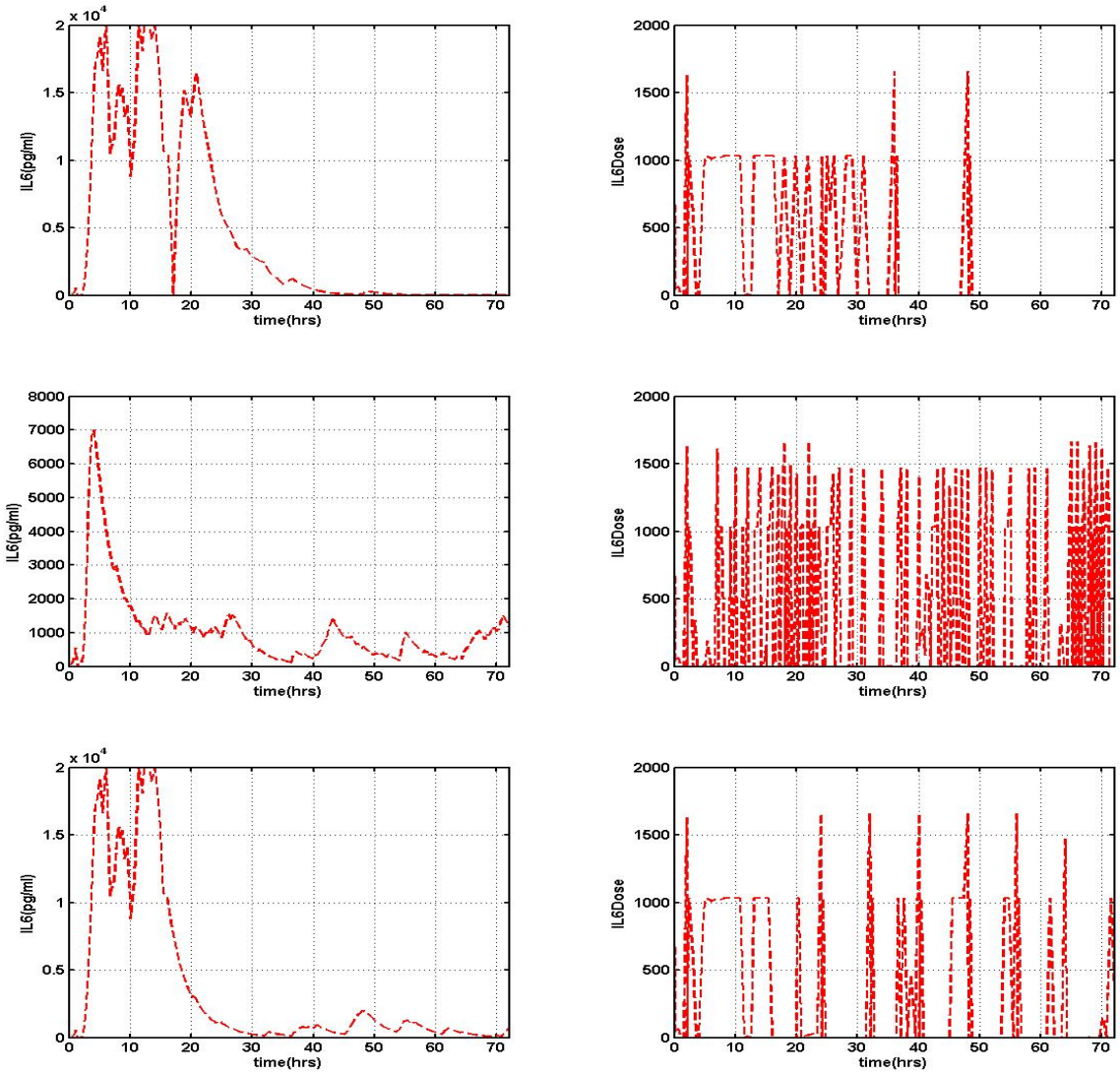

Figure 6.14: NMPC simulation of $IL6(t)$, and $IL6Dose(t)$ at $6\,mg/kg$ endotoxin challenge level showing the three difference cases of recalculation step over a 72 hours (3 days) horizon, the plots on the left are the states, whereas those on the right are the treatment control:

Top Left: Unequal recalculation step.

Top Right: One hour interval recalculation step.

Bottom: Four hours recalculation step.

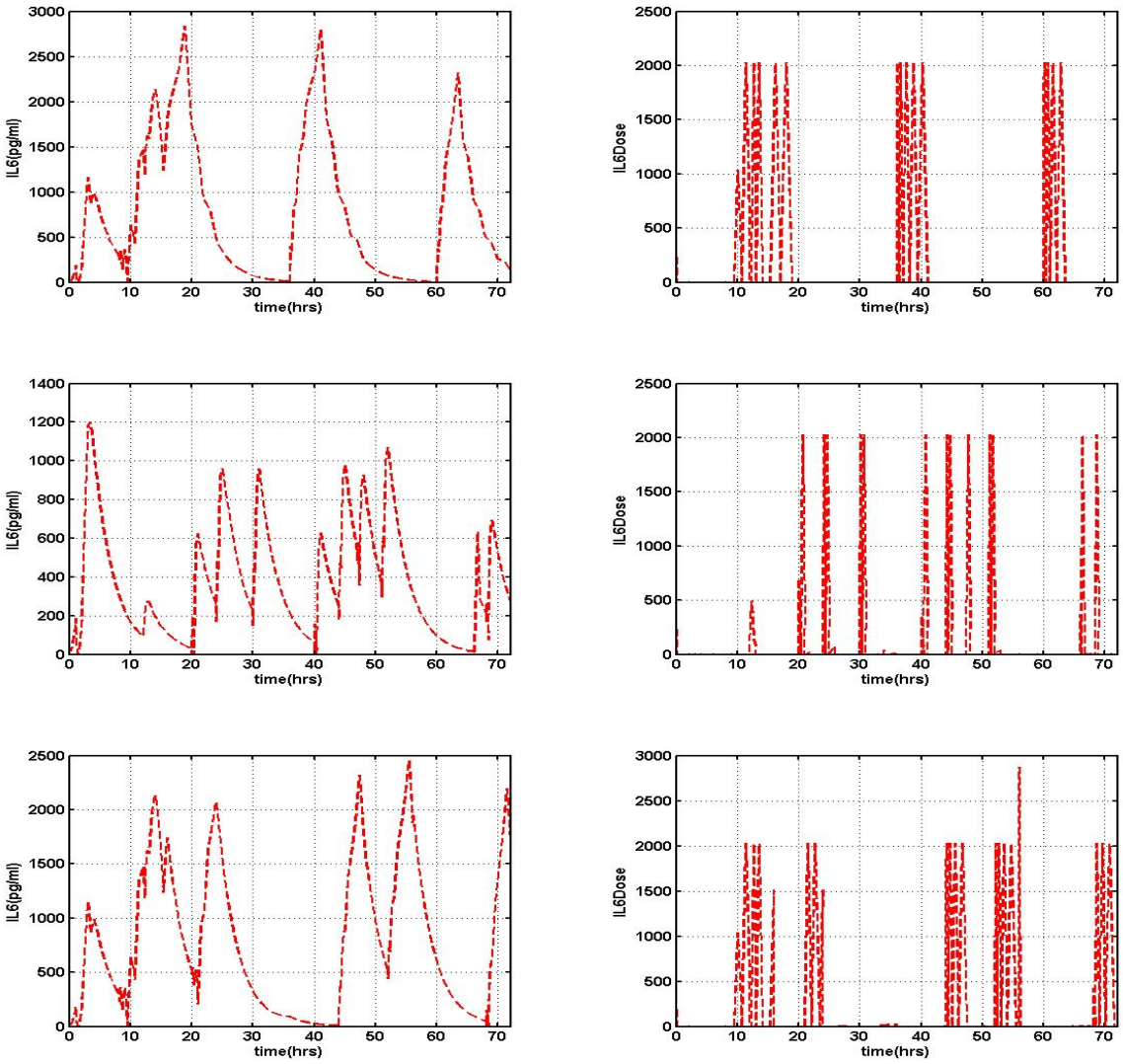

Figure 6.15: NMPC simulation of $IL6(t)$, and $IL6Dose(t)$ at $12\,mg/kg$ endotoxin challenge level showing the three difference cases of recalculation step over a 72 hours (3 days) horizon, the plots on the left are the states, whereas those on the right are the treatment control:

Top Left: Unequal recalculation step.

Top Right: One hour interval recalculation step.

Bottom: Four hours recalculation step.

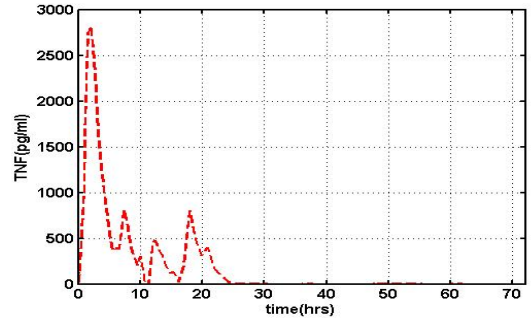

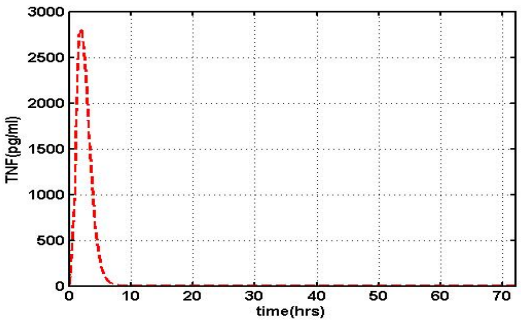

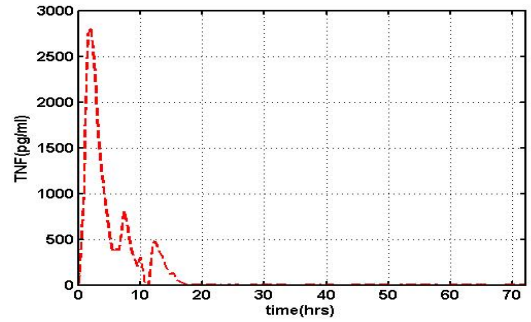

Figure 6.16: NMPC of $TNF(t)$ at $6\,mg/kg$.
Top: Unequal recalculation,
Middle: One hour recalculation,
Bottom: Four hours recalculation.

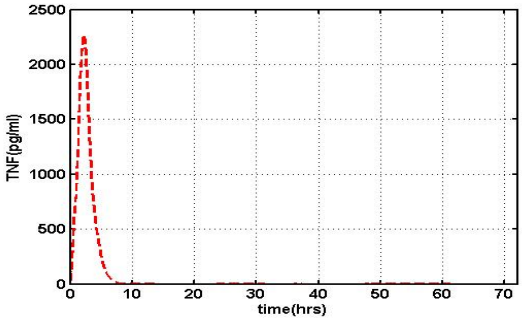

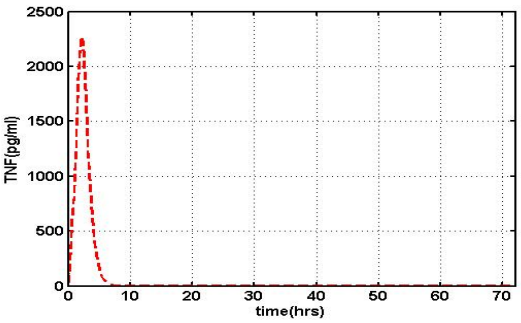

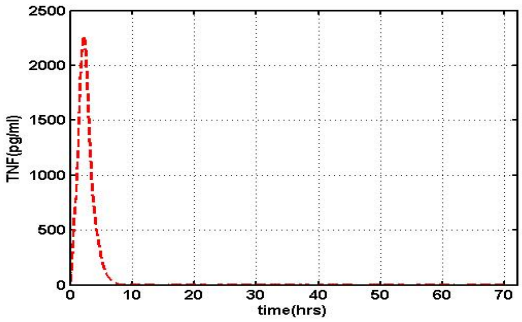

Figure 6.17: NMPC of $TNF(t)$ at $12\,mg/kg$.
Top: Unequal recalculation,
Middle: One hour recalculation,
Bottom: Four hours recalculation.

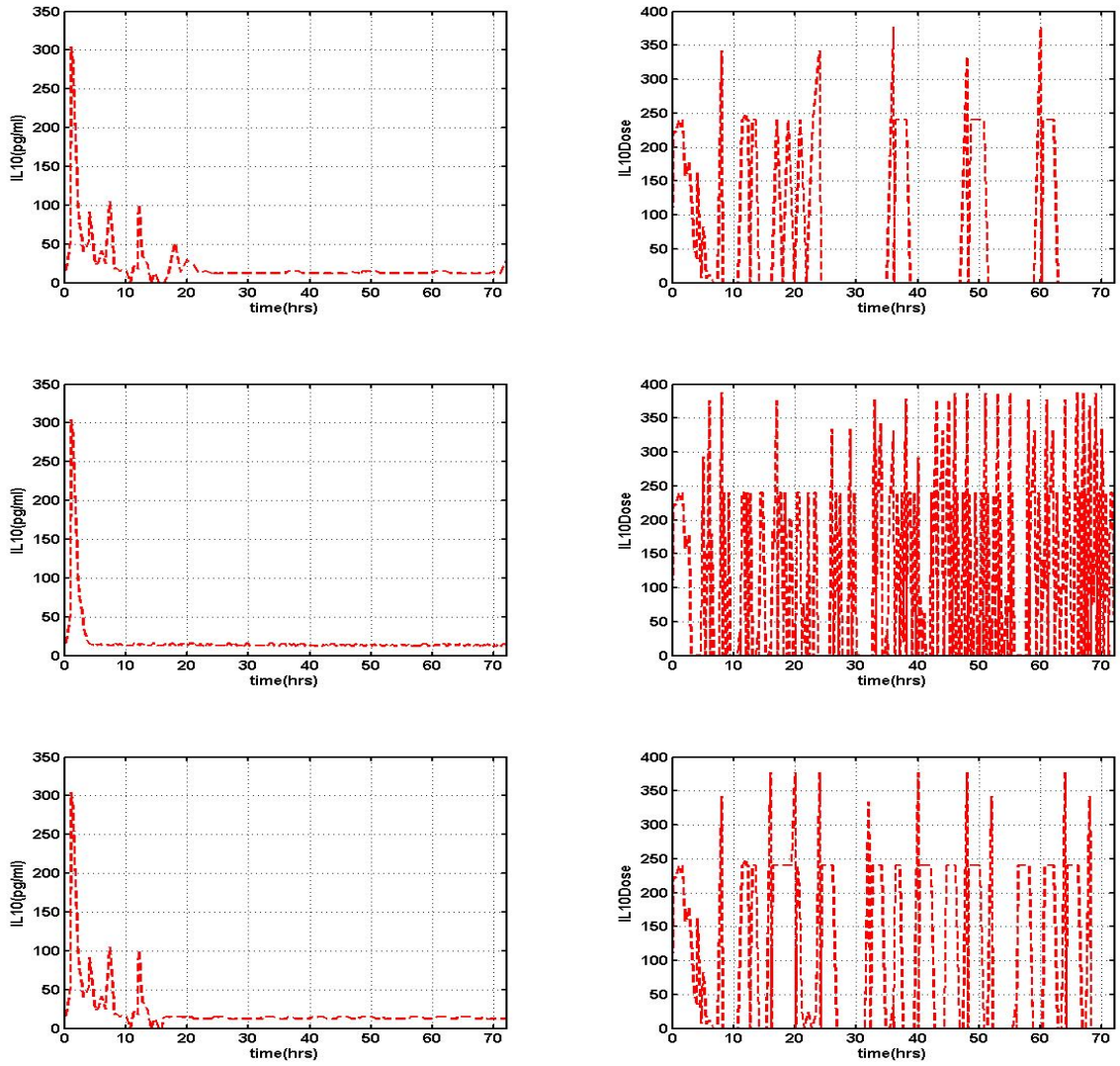

Figure 6.18: NMPC simulation of $IL10(t)$, and $IL10Dose(t)$ at $6\,mg/kg$ endotoxin challenge level showing the three difference cases of recalculation step over a 72 hours (3 days) horizon, the plots on the left are the states, whereas those on the right are the treatment control:

Top Left: Unequal recalculation step.

Top Right: One hour interval recalculation step.

Bottom: Four hours recalculation step.

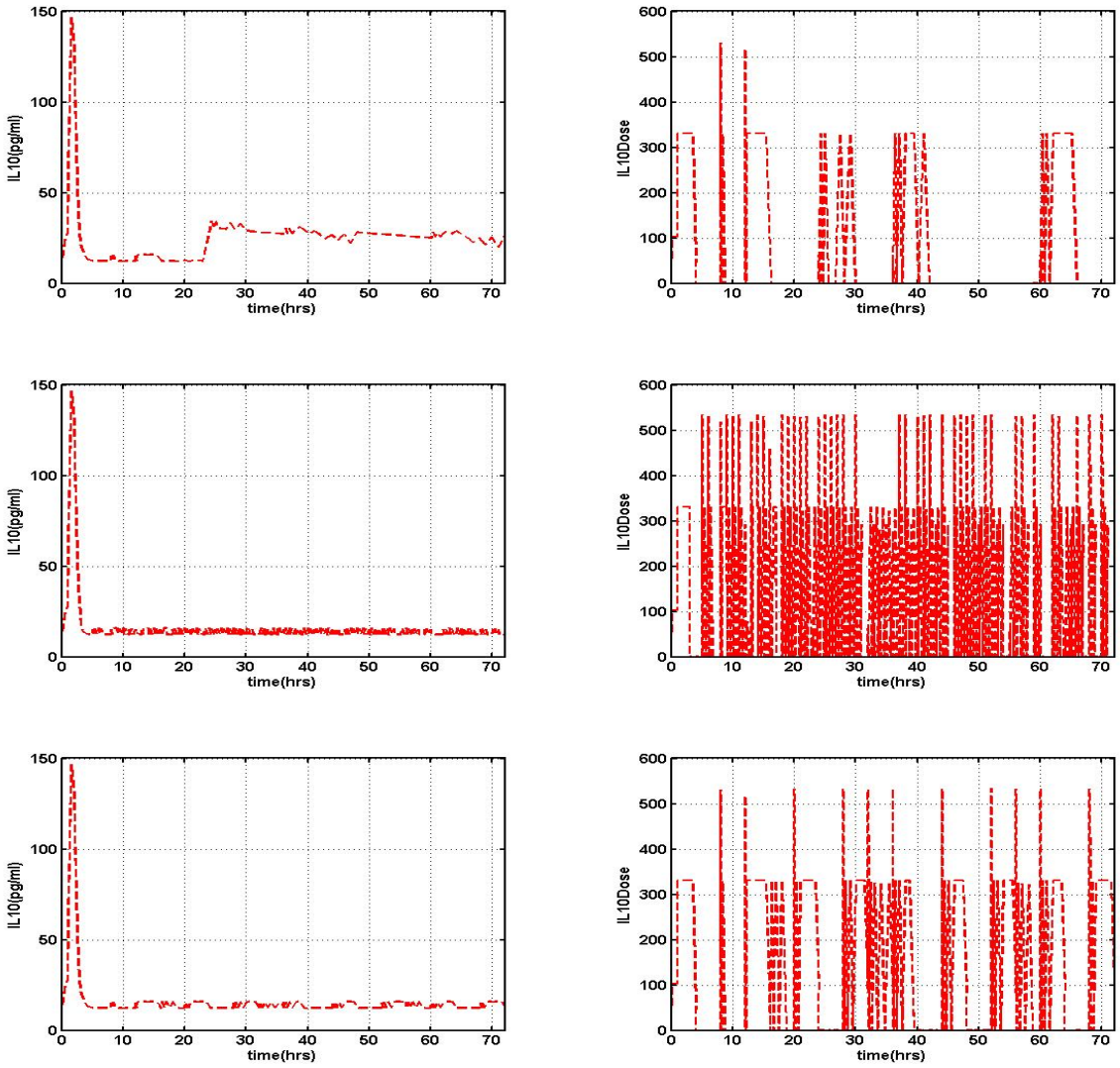

Figure 6.19: NMPC simulation of $IL10(t)$, and $IL10Dose(t)$ at $12\,mg/kg$ endotoxin challenge level showing the three difference cases of recalculation step over a 72 hours (3 days) horizon, the plots on the left are the states, whereas those on the right are the treatment control:

Top Left: Unequal recalculation step.

Top Right: One hour interval recalculation step.

Bottom: Four hours recalculation step.

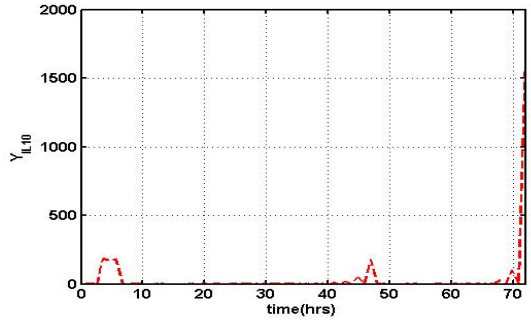

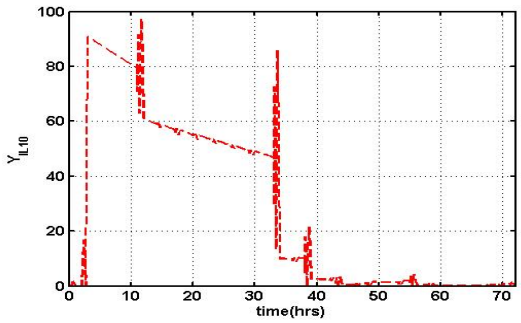

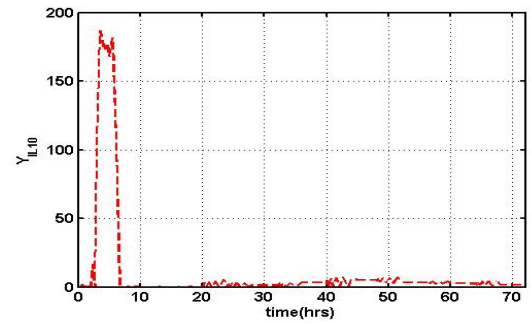

Figure 6.20: NMPC of $Y_{IL10}(t)$ at $6\,mg/kg$.
Top: Unequal recalculation,
Middle: One hour recalculation,
Bottom: Four hours recalculation.

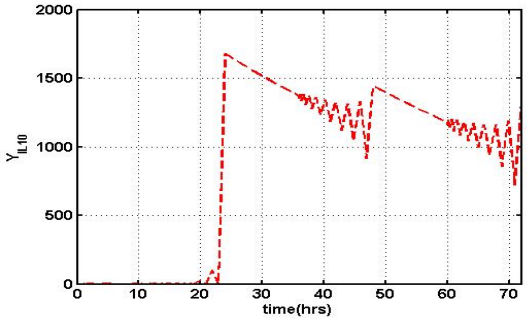

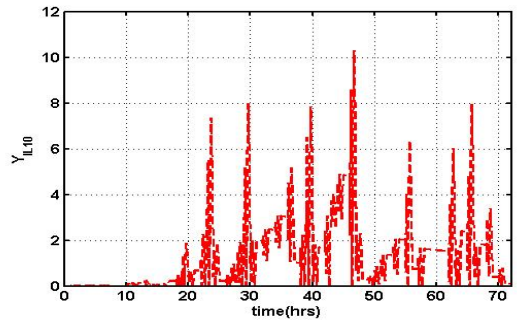

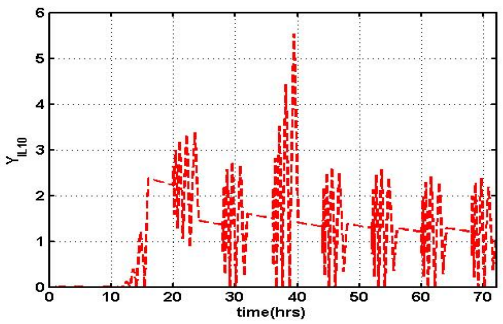

Figure 6.21: NMPC of $Y_{IL10}(t)$ at $12\,mg/kg$.
Top: Unequal recalculation,
Middle: One hour recalculation,
Bottom: Four hours recalculation.

6.2 NMPC and UKF

We conclude this chapter by demonstrating how Unscented Kalman Filter (UKF) can be incorporated in the NMPC scheme to filter the observed noisy states as well as estimate the unobserved states at each recalculation/measurement step. In practice, at the current recalculation/measurement step, measurements on the observed states will be taken based on the previously controlled step and Kalman filter or any other filter will be used to estimate the unobserved states in addition to filtering the noisy observed states.

6.2.1 Unscented Kalman Filter (UKF)

The UKF belongs to a family of filters known as *Sigma-Point Kalman Filter*. This class of filters uses statistical linearization to linearize a nonlinear function of a random variable via a linear regression between n points taken from a prior distribution of the random variable. The Extended Kalman Filter (EKF) is one of the widely used technique for performing recursive nonlinear estimation. Meanwhile, EKF only provides an approximation to optimal nonlinear estimation. The UKF, which was first proposed by [68, 69, 70], is an alternative filter with performance superior to that of the EKF.

The major difference between EKF and UKF comes from the way which the Gaussian random variables (GRV) are represented for propagating through system dynamics [141]. In the case of EKF, the state distribution is approximated by a GRV, which, in turn, is propagated analytically using a first-order linearlization of the nonlinear system. The problem with doing this is that it does lead to the introduction of large errors in the true posterior mean as well as the covariance of the transformed GRV may result in suboptimal performance and sometimes divergence of the filter. The UKF handle this problem by using a deterministic sampling technique. The state distribution is again approximated by a GRV but in this case by using a minimal set of carefully chosen points. These points completely represent the true mean and covariance of the GRV and when propagated via the true mean nonlinear system, captures the posterior mean and covariance accurately to second order for any nonlinearity unlike the EKF which only achieves first-order accuracy [141]. The computation of UKF does not require any explicit knowledge of the Jacobian or Hessian, and the complexity of EKF and UKF are the same order.

In this work, we implemented the UKF by using the *effective square-root* form. The standard Kalman implementation calculates the state (or parameter) covariance $\mathbf{P}_k$ recursively whereas the UKF requires taking the matrix square-root $\mathbf{S}_k\mathbf{S}_k^T = \mathbf{P}_k$, at each time step using Cholesky

factorization. In the square-root UKF (SR-UKF), $\mathbf{S}_k$ is propagated directly, therefore, avoiding the need to refactorize at each time step. This improves the numerical properties and yet maintained the same complexity as UKF. A complete review of the UKF and its extensions can be found in [141]. The SR-UKF algorithm for state estimation implemented in this work is presented in Appendix F and in [141]. Lastly, the MATLAB solver that implements this algorithm was developed by my colleague Brett Matzuka.

6.2.2 NMPC and UKF at 3 mg/kg endotoxin challenge level

We will add a 10% Gaussian noise to our *in silico* simulated results of the observed states; $IL6$, TNF and $IL10$ at $3\,mg/kg$ endotoxin challenge level and use them as clinical data. UKF will then be used to estimate the unobserved states; $P(t)$, $N(t)$, $D(t)$ and $Y_{IL10}(t)$ in addition to filtering the noisy observed states. The "four hours recalculation step" will be used as the recalculation/measurement step. By not assuming that all the states are observable, we succeed in creating a scenario that closely resembles the actual experiment done on rats in [126]. The key difference is that pseudo experimental data will be obtained at each recalculation/measurement step based on the last controlled step. Although we employed UKF as our state estimator, other choices of observer/estimator that can achieve good state estimation can also be used, and these have been widely studied in [5, 47, 92, 97].

The framework of our 7D ODE is given by

$$\dot{\mathbf{y}}(t) = \mathbf{F}(\mathbf{y}(t), \mathbf{u}(t), \mathbf{v}(t)) \tag{6.1}$$

$$\mathbf{z}(t) = \begin{pmatrix} IL6(t) \\ TNF(t) \\ IL10(t) \end{pmatrix} + \mathbf{w}(t), \tag{6.2}$$

where $\mathbf{y}$ represent the unobserved states of our reduced model, $\mathbf{u}$ denote the control variables, $\mathbf{v}$ the process noise, $\mathbf{z}$ denote the measured observations and $\mathbf{w}$ the observation noise which is gaussian with mean 0 and covariance $\mathbf{W}$. The process state Equation (6.1) is our usual 7D model with the addition of a *process noise* term. The measure observations Equation (6.2) represent our observed inflammatory cytokines with an *observation noise* term. The process noise that we assumed is based on the accuracy of the integrator and this will be a small value, $\mathbf{V} = 1.0 \times 10^{-6}\boldsymbol{I}_7$. Also, the observed noise covariance is $\mathbf{W} = 0.01\boldsymbol{I}_3$, where $\boldsymbol{I}_7$ and $\boldsymbol{I}_3$ are "7 by 7" and "3 by 3" identity matrices, respectively.

The plots in Figure 6.22 depict the responses of $P(t)$, $N(t)$ and $D(t)$ to treatment control when UKF was utilized in estimating the states. The *red dashed line* (- -) denote the NMPC

in silico simulation trajectories, whereas the UKF estimated points are represented in *black circles*. Notice that $P(t)$ and $N(t)$ were driven to their respective equilibrium positions before the 10^{th} hour. However, $D(t)$ remained slightly elevated.

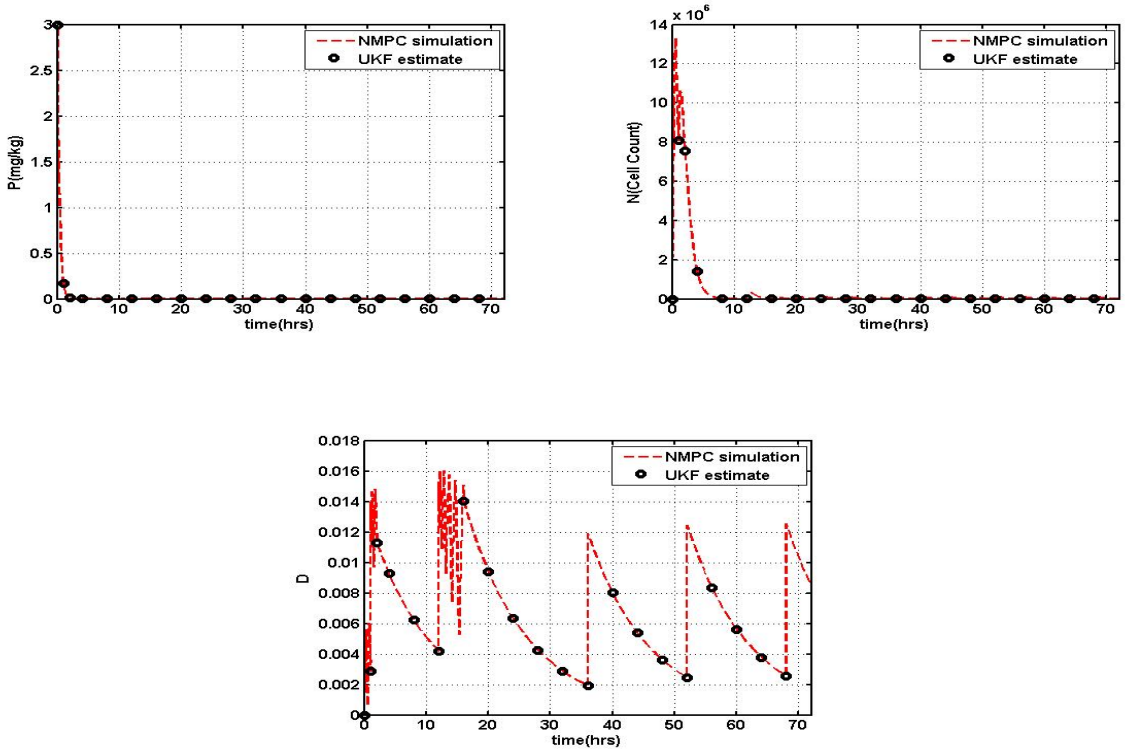

Figure 6.22: NMPC simulation combined with UKF for $P(t)$, $N(t)$, and $D(t)$ at $3\,mg/kg$ endotoxin challenge level using the "four hours recalculation step starting after the 4^{th} hour" over a 72 hours (3 days) horizon:

Top Left: Concentration of endotoxin level, $P(t)$.

Top Right: Total number of activated pahgocytic cells, $N(t)$.

Bottom: Tissue damage marker, $D(t)$.

The response of $IL6(t)$ to treatment as shown in Figure 6.23 appears to be the most significant when compared with the plots in Sections 6.1.1 and 6.1.2, where UKF was not used to filter the state. $IL6Dose(t)$ displayed the same consistent *bang-bang* phenomenon as in the previous sections.

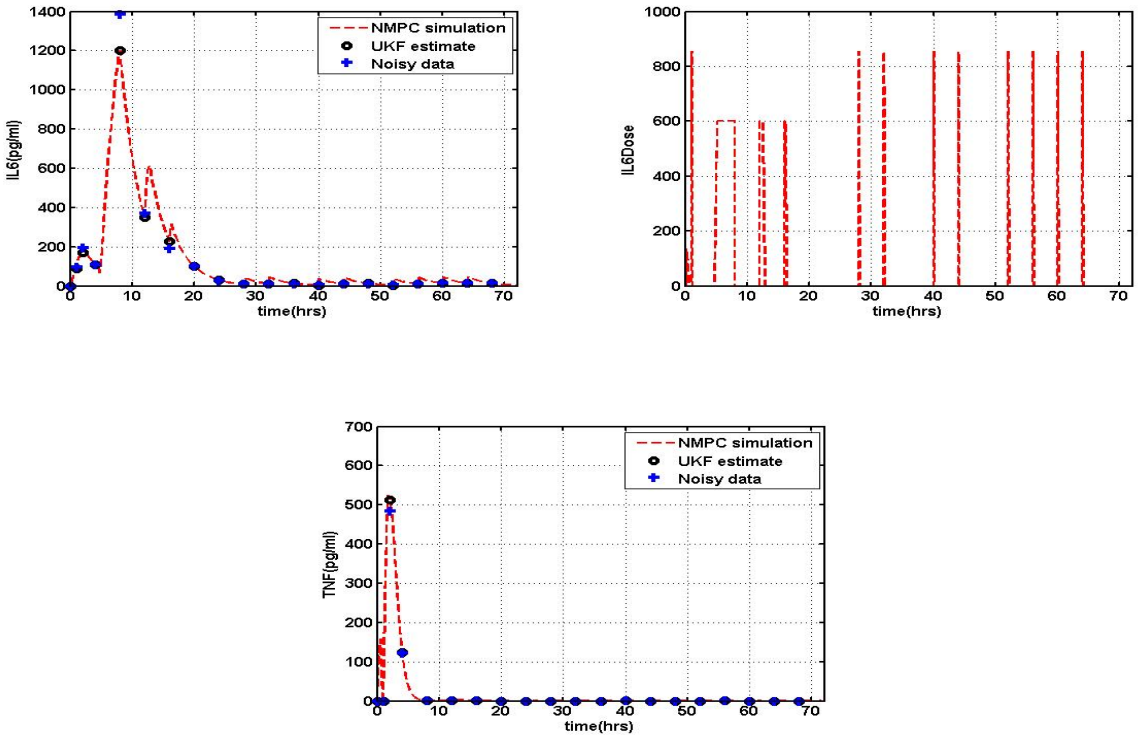

Figure 6.23: NMPC simulation combined with UKF for $IL6(t)$, $IL6Dose(t)$, and $TNF(t)$ at $3\,mg/kg$ endotoxin challenge level using the "four hours recalculation step starting after the 4^{th} hour" over a 72 hours (3 days) horizon:

Top Left: Concentration of pro-inflammatory cytokine, interleukin-6, $IL6(t)$.

Top Right: Treatment therapy dose for interleukin-6, $IL6Dose(t)$.

Bottom: Concentration of pro-inflammatory cytokine, tumor necrosis factor-α, $TNF(t)$.

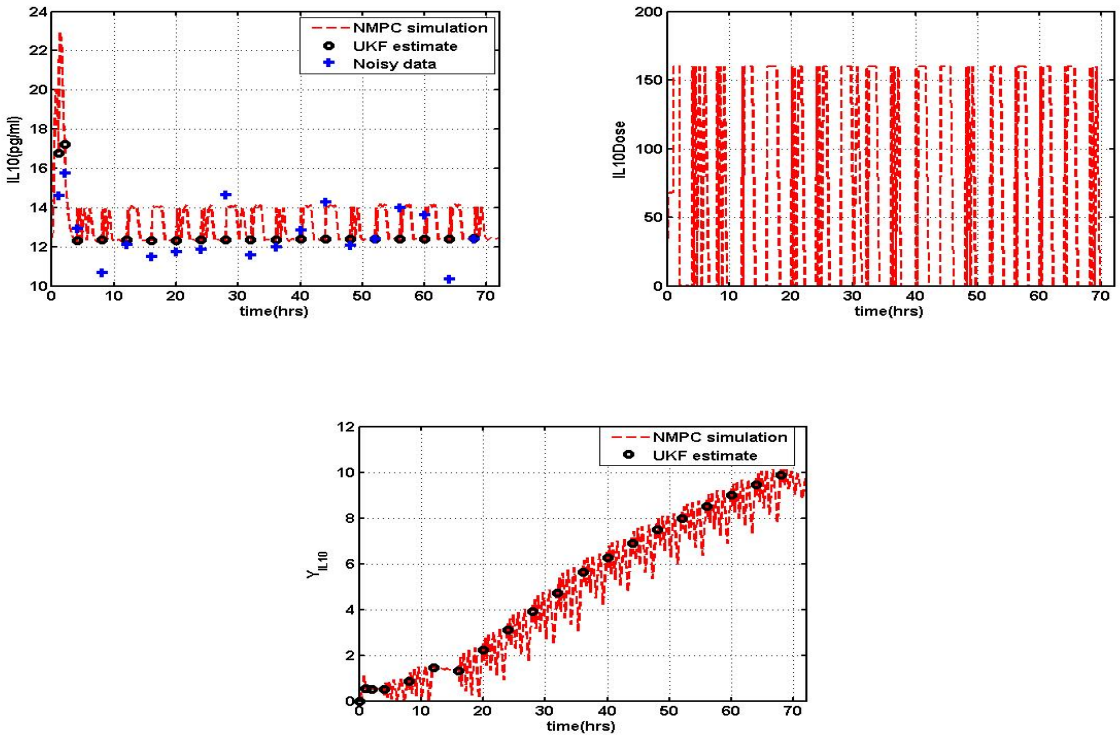

Figure 6.24: NMPC simulation combined with UKF for $IL10(t)$, $IL10Dose(t)$, and $Y_{IL10}(t)$ at $3\,mg/kg$ endotoxin challenge level using the "four hours recalculation step starting after the 4^{th} hour" over a 72 hours (3 days) horizon:

Top Left: Concentration of anti-inflammatory cytokine, interleukin-10, $IL10(t)$.

Top Right: Treatment therapy dose for interleukin-10, $IL10Dose(t)$.

Bottom: Tissue damage driven IL-10 promoter $TNF(t)$.

Figure 6.24 depicts an interesting characteristics of $Y_{IL10}(t)$. Although this state showed a substantial reduction from the pre-treatment levels, it appears to be increasing slowly. On the other had. $IL10(t)$ achieved equilibrium before the 10^{th} hour.

Chapter 7

Conclusions

7.1 Summary

The first phase of this work involved the development and validation of a mathematical model that can accurately predict acute inflammatory response to endotoxin challenge. In this phase, we compared the original 8D model developed in [126] with four different models we proposed. Two of those models were "modified 8D" models (8D-15 and 8D-21) and the other two were reduced 7D models (7D-15 and 7D-21). 7D was created by the elimination of a non-accessible state representing slow acting anti-inflammatory mediators ($CA(t)$). $CA(t)$ was removed based on the evidence presented in Section 2.2.1 while attempting to preserve the underlying biology reflecting known inflammatory physiology. This is necessary because when modeling biological processed with limited number of observations, over-fiting, over-parameterization and even the introduction of unjustified nonlinearities are extremely discouraged.

In order to construct models that accurately reproduced the experimental data on inflammatory cytokines; sensitivity analysis, subset selection and parameter estimation were all employed. Sensitivity analysis was used to identify those parameters that are sensitive to a slight perturbation for each of the cytokines. At the same time, since sensitivity analysis often identify parameters that are correlated, subset selection was employed for parameter identifiability analysis. The use of subset selection is critical in our research because our focus is identifying only the linearly independent sensitive parameters. The *SVD followed by QR with column pivoting* method described in [59] was used to achieve this goal. With the information garner thus far, we proposed four potential models to compare with the 8D model in [126]. Next, the normalized nonlinear least squares parameter estimation method was used to calibrate our models with available experimental data and the models parametrization were achieved using

the Nelder-Mead simplex method.

As it is our desire to identify the best model needed at the next phase of this work, all the competing models' curve fitting plots at $3\,mg/kg$ and $12\,mg/kg$ endotoxin challenge levels as well as model validation prediction plots at $6\,mg/kg$ endotoxin challenge level were closely examined. This stage of comparison proved inconclusive since a number of the models showed superior fits for a cross section of the plots considered and no model had a clear edge with respect to having a better curve fitting representation of the actual data. As a tiebreaker, AIC [3], as described in Section 2.3 was employed to compare the models quantitatively. AIC is a statistical model selection tool for quantifying the trade-off between model fit and model complexity, as measured by the total number of parameters. With a aid of AIC, we chose 7D-15 as the best model that satisfied this trade-off. Hence, 7D-15 became our model of choice for the next phase, for simplicity we shall refer to this model as 7D. We conclude this phase by proving the existence and uniqueness of a solution to 7D as well as conduct steady state and stability analysis

Since the control of inflammatory response is a key focal point in this work, this constitute the second and final phase of our research which was primarily to derive optimal therapeutic interventions for the control of acute inflammation triggered by endotoxins. Next, we studied the 7D model under an open-loop optimal control based treatment strategies. To identify specific therapy dosing characterization that can curb inflammatory responses, two source terms were added to the 7D ODE model in Section 2.2.2 to serve as treatment control variables. Specifically, $IL6Dose(t)$ was included in Equation (2.4) to form Equation (4.33), and $IL10Dose(t)$ was added to Equation (2.6) to form Equation (4.35). $IL6Dose(t)$ serves as the pro-inflammatory treatment dose needed to modulate interleukin-6 ($IL6(t)$) and $IL10Dose(t)$ is the anti-inflammatory treatment dose required to regulate interleukin-10 ($IL10(t)$). We also proved the existence a solution to our optimal control problem which was followed by the numerical results showing how efficient our methodology performed (Section 4.4).

The Nonlinear Model Predictive Control (NMPC) scheme was applied in this work to absorb any unexpected disturbances that is likely to occur in the system as time progresses; since the open-loop optimal control methodology lacks the ability to account for such disturbances. Three difference cases of recalculation/measurement steps at each endotoxin challenge level were used as time points to apply treatment doses on the 7D model while attempting to minimize total number of activated phagocytic cells ($N(t)$), tissue damage ($D(t)$), tissue damage driven non-accessible IL-10 promoter ($Y_{IL10}(t)$), and the inflammatory response doses $IL6Dose(t)$ and $IL10Dose(t)$ (Equation (4.29)). Simulation results capturing the level of response by the different states were summarized in Sections 6.1.1, and 6.1.2. A better way to implement NMPC

is to combine it with Unscented Kalman Filter (UKF). We demonstrated in Section 6.2.2 how this can be done by creating a pseudo clinical data after adding a 10% noise based on gaussian to our *in silico* simulated results that included therapeutic treatment received at each recalculation step.

7.2 Discussion

We successfully derived a reduced 7D model of acute inflammatory response to endotoxin challenge from the 8D model developed in [126]. In addition to reducing the dimension of the state space, the parameter space was also reduce from 46 to 40 parameters. We verified that the solutions of the 7D model demonstrated comparative or better overall performance in predicting the experimental data on inflammatory cytokines while maintaining relevant biological fidelity. The most significant challenge our 7D model faced was not capturing the dynamics of the anti-inflammatory cytokine as well as it consistently did with the pro-inflammatory cytokines.

The implementation of an NMPC scheme to derive optimal treatment therapies that can modulate inflammation was successfully conducted. The three therapeutic recalculation time points used in the NMPC scheme all significantly reduced the effects of the inflammation and tissue damage while controlling the states responses. Meanwhile, the "One hour recalculation step" is not biologically feasible since that can lead to too much blood loss in the rats which in turn can result in *hypovolemic shock*. The *in silico* simulation done at this recalculation instance only illustrates a theoretical improvement over the other recalculation intervals. A rather conservative but a more practical recalculation step will be to use the same time intervals corresponding to the periods actual data were obtained in the experiment done in [126].

In conclusion, although our findings in this work accomplished our goals, yet it raised many new pertinent questions that require further investigation. Some of the possible future directions in this work will be to come up with a better parameter estimation technique that can improve the model's predictability of interluekin-10, since the 7D mathematical model proposed is by no means perfect. Another potential aspect of future research could be to further reduced our model while maintaining the underlying biological relevance. In addition, it will be interesting to investigate whether varying the collocation points used in GPOPS can affect the numerical solution obtained. Finally, it is our desire to take our findings to the next level in some adaptive treatment procedure. One way is to involve medical practitioners on how we can implement our results through clinical study. This will enable us to incorporate *in vivo* experimental treatment data with an NMPC approach that includes a good Moving Horizon Estimation (MHE) for state estimation.

REFERENCES

[1] Adams, B. M., *Non-Parametric Parameter Estimation and Clinical Data Fitting with a Model of HIV Infection*, PhD thesis, North Carolina State University, July 2005.

[2] Adams, B. M., Banks, H. T., Kwon, H., Tran, H. T., *Dynamic Multidrug Therapies for HIV: Optimal and STI Control Approaches*, Technical Reports, Center for Research in Scientific Computation (CRSC), North Carolina State University, 2004.

[3] Akaike, H., *A bayesian extension of the minimum AIC procedure of autoregressive model fitting*, Biometrika, 66, 237-242,1979.

[4] Alamir, M., Bornard, G., *Stability of a truncated infinite constrained receding horizon scheme: The general discrete nonlinear case*, Automatica, 31(9), 1353-1356, 1995.

[5] Alamir, M., *Optimization based nonlinear observers revisited*, International Journal of Control, 72(13), 1204-1217, 1999.

[6] Alexander, C., Rietschel, E.T., *Bacterial lipopolysaccharides and innate immunity*, Journal of Endotoxin Research, 7(3), 167-202, 2001.

[7] Allgöwer, F., Findeisen, R. and Nagy, Z., *Nonlinear model predictive control: From theory to application*, J. Chin. Inst. Chem. Engrs. 35(3), 299-315, 2000.

[8] Allgöwer, F., Badgwell, T. A., Qin, J. S., Rawlings, J. B., Wright, S. J., *Nonlinear predictive control and moving horizon estimation–An introductory overview* In P. M. Frank, editor, Advances in Control, Highlights of ECC'99, 391-449, Springer, 1999.

[9] Angus, D., Linde-Zwirble, W., Lidicker, J., Clermont, G., Carcillo, J.,Pinsky, M., *Epidemiology of severe sepsis in the United States: analysis of incidence, outcome, and associated costs of care*, Critical Care Med. 29(7), 1303-1310, 2001.

[10] Arkun, Y., Hollett, J., Canney, W. M., Morari, M., *Experimental study of internal model control*, Industrial and Engineering Chemistry Process Design and Development, 25(1), 102-108, 1986.

[11] Attarian, A., *Open-source: Relative and General Sensitivity Analysis solver*, http://www4.ncsu.edu/ arattari/, October 2009.

[12] Banks, H.T., Tran, H.T., *Mathematical and Experimental Modeling of Physical and Biological Processes*, Chapman & Hall/CRC PRESS, 2009.

[13] Beeson, P.B., *Tolerance to bacterial pyrogens: I. Factors influencing its development*, Journal of Experimental Medicine, 86(1), 29-38, 1947.

[14] Bellingan, G., *Inflammatory cell activation in sepsis*, Br. Med. Bull., 55, 12-29, 1999.

[15] Bellman, R., *Dynamic Programming*, Princeton University Press, Princeton, New Jersey, 1957.

[16] Bellman, R., Åström K. J., *On structural identifiability*, Mathematical Biosciences, 7(3-4), 329-339, 1970.

[17] Bellman, R., *The Theory Dynamic Programming*, Proceedings of the National Academy of Sciences, USA, 38, 1952.

[18] Benson, D. A., *A Gauss Pseudospectral Transcription for Optimal Control* , PhD thesis, Massachusetts Institute of Technology, Cambridge, MA, February 2005.

[19] Bitmead, R. R., Gevers, M., Wertz, V., *Adaptive Optimal Control – The Thinking Man's GPC*, Prentice Hall, New York, 1990.

[20] Bochud, P.Y., Calandra, T., *Pathogenesis of sepsis: new concepts and implications for future treatment*, B. M. J., 326, 262-266, 2003.

[21] Bock, H., *Recent advances in parameter identification for ordinary differential equations*, In Deuflhard, P., Hairer, E. (Eds.), Progress in Scientific Computing, 2, Birkhuser, Boston, 95-121, 1983.

[22] Bone, R., Balk, R., Cerra, F., Dellinger, R., Fein, A., Knaus, W., Schein, R., Sibbald, W., *Definitions for sepsis and organ failure and guidelines for the use of innovative therapies in sepsis*, Chest 101(6), 1644-1655, The ACCP/SCCM Consensus Conference Committee, American College of Chest Physicians/Society of Critical Care Medicine, 1992.

[23] Bortz, D. M., *Modeling, analysis, and estimation of an in vitro HIV infection using functional differential equations*, PhD thesis, North Carolina State University, August 2002.

[24] Bozza, F. A., Salluh, J. I., Japiassu, A. M., Soares, M., Assis, E. F., Gomes, R. N., Bozza, M. T., Castro-Faria-Neto, H. C., Bozza, P. T., *Cytokines profiles as markers of disease severity in sepsis: a multiplex analysis*, Critical Care, 11(2), R49, 2007.

[25] Camacho, E. F., Bordons, C., *Model Predictive Control*, 2nd edition, Springer, 2004.

[26] Campbell, S. L., Haberman, R., *Introduction to Differential Equations with Dynamical Systems*, Princeton University Press, 2008.

[27] Cavaillon, J. M., *The nonspecific nature of endotoxin tolerance*, Trends in Microbiology, 3(8), 320-324, 1995.

[28] Chen, H., Allgöwer, F., *A quasi-infinite horizon nonlinear model predictive control scheme with guaranteed stability*, Automatica, 34(10), 1205-1218, 1998.

[29] Chow, C. C., Clermont, G., Kumar, R., Lagoa, C., Tawadrous, Z., Gallo, D., Betten, B., Bartels, J., Constantine, G., Fink, M. P., Billiar, T. R., Vodovotz, Y. *The Acute inflammatory response in diverse shock states*, Shock, 24, 74-84, 2005.

[30] Chu, Y., Hahn, J., *Parameter Set Selection for Estimation of Nonlinear Dynamic Systems*, AIChE Journal, 53, 2858-2870, 2007.

[31] Clarke, D. W., *Application of Generalized Predictive Control to Industrial Processes*, IEEE Control Systems Magazine, 122, 44-55, 1988.

[32] Cobelli, C., DiStefano, III J. J., *Parameter and structural identifiability concepts and ambiguities: a critical review and analysis*, AJP-Regulatory, Integrative and Comparative Physiology, 239(1), 7-24, 1980.

[33] Copeland, S., Warren, H.S., Lowry, S.F., Calvano, S.E., Remick, D., *Acute inflammatory response to endotoxin in mice and humans*, Clinical Diagnostic Laboratory Immunology, 12(1), 60-67, 2005.

[34] Cross, A.S., *Endotoxin tolerance-current concepts in historical perspective*, Journal of Endotoxin Research, 8(2), 83-98, 2002.

[35] Cutler, C. R., Ramaker, B. L., *Dynamic Matrix Control–A Computer Control Algorithm*, AIChE National meeting, Houston, Texas, 1979. Also in Automatic Control Conference, San Francisco, California 1980.

[36] Daun, S., Rubin, J., Vodovotz, Y., Roy, A., Parker, R., Clermont, G., *An ensemble of models of the acute inflammatory response to bacterial lipopolysaccharide in rats: Results from parameter space reduction*, Journal of Theoretical Biology, 253, 843-853, 2008.

[37] David, J. A., *Optimal Control, Estimation, and Shape Design: Analysis and Applications*, PhD thesis, North Carolina State University, July 2007.

[38] Day, J., Rubin, J., Vodovotz, Y., Chow, C., Reynolds, A., Clermont, G., *A reduced mathematical model of the acute inflammatory response II. Capturing scenarios of repeated endotoxin administration*, Journal of Theoretical Biology, 242, 237-256, 2006.

[39] Day, J., Rubin, J., Clermont, G., *Using nonlinear model predictive control to find optimal therapeutic strategies to modulate inflammation*, Submitted, preprint found in "http://www.math.pitt.edu/ rubin/pub/pub.html", November 2009.

[40] De Nicolao, G., Magni, L., Scattolini, R., *Stabilizing nonlinear receding horizon control via a nonquadratic terminal state penalty*, In Symposium on Control, Optimization and Supervision, CESA'96 IMACS Multiconference, pages 185-187, Lille, 1996.

[41] De Nicolao, G., Magni, L., Scattolini, R., *Stability and robustness of nonlinear receding horizon control*, In F. Allgöwer and A. Zheng, editors, Nonlinear Predictive Control, 3-23. Birkhäuser, 2000.

[42] DiStefano, III J. J., Cobelli, C., *On Parameter and Structural Identifiability: Nonunique Observability/Reconstructibility for Identifiable Systems, Other Ambiguities, and New Definitions*, IEEE Transactions on Automatic Control, 25(4), 830-833, 1980.

[43] Doyle, F., Jovanovic, L., Seborg, D., Parker, R. S., Bequette, B. W., Jeffrey, A. M., Xia, X., Craig, I. K., McAvoy, T., *A tutorial on biomedical process control*, Journal of Process Control, 17(7), 571-594, 2007.

[44] Ellwein, L., *Cardiovascular and Respiratory Regulation, Modeling and Parameter Estimation*, PhD thesis, North Carolina State University, August 2008.

[45] Eng, R.H., Smith, S.M., Fan-Havard, P., Ogbara, T., 1993. *Effect of antibiotics on endotoxin release from gram-negative bacteria*, Diagnostic Microbiology and Infectious Disease 16(3), 185-189, 1993.

[46] Engauge digitizer, *Open-source: Digitizing software which converts an image file showing a graph or map into numbers*, http://digitizer.sourceforge.net/, November 2009.

[47] Findeisen, R., Imsland, L., Allgöwer, F., Foss, B., *State and Output Feedback Nonlinear Model Predictive Control: An Overview*, European Journal of Control, 9(2-3),190-207, 2003.

[48] Findeisen, R., Allgöwer, F., *An Introduction to Nonlinear Model Predictive Control*, In Proc. 21st Benelux Meeting on Systems and Control, 2002, Veldhoven, Netherlands, 1-23, 2002.

[49] Fink, M., *Open-source: Automatic Differentiation code*, http://gosh.gmxhome.de/, October 2009.

[50] Fink, M., Attarian, A., Tran, H.T., *Subset Selection for Parameter Estimation in an HIV Model*, Proceedings in Applied Mathematics and Mechanics, 26 November 2007.

[51] Fleming, W. H., Rishel, R. W., *Deterministic and Stochastic Optimal Control*, Springer-Verlag, 1975.

[52] Florian, J. A. Jr., Eiseman, J. L., Parker, R. S., *Nonlinear model predictive control for dosing daily anticancer agents using a novel saturating-rate cell-cycle model*, Comput. Biol. Med., 38(3), 339-347, 2008.

[53] Freemanand, B. D., Natanson, C., *Anti-inflammatory therapies in sepsis and septic shock*, Expert Opin. Investig. Drugs, 9, 1651-1663, 2000.

[54] García, C. E., Prett, D. M., Morari, M., *Model Predictive Control: Theory and Practice — a Survey*, Automatica, 25(3), 335-348, 1989.

[55] Giannoudis, P. V., Smith, R. M., Perry, S. L., Windsor, A. J., Dickson, R. A., Bellamy, M. C., *Immediate IL-10 expression following major orthopaedic trauma: relationship to antiinflammatory response and subsequent development of sepsis*, Intensive Care Med., 26(8).

[56] Gill, P. E., Murray, W., Saunders, M. A., *SNOPT: An SQP Algorithm for Large-Scale Constrained Optimization*, SIAM REVIEW , 47, 1, 99-131, 2005.

[57] GPOPS., *Open-Source General Pseudospectral Optimal Control Software*, http://www.gpops.org/, April 2010.

[58] Golub, G.H., Van Loan, C.F., *Matrix Computations*, The Johns Hopkins University Press, third edition, 1996.

[59] Golub, G.H., Klema, V.C., Stewart, G.W., *Rank degeneracy and least squares problems*, Technical report, Stanford University, 1976.

[60] Gómez Ortega, J., Camacho, E. F., *Mobile Robot Navigation in a Partially Structured Environment using Neural Predictive Control*, Control Engineering Practice, 4, 1669-1679, 1996.

[61] Goris, R.J., Boekhorst, T.P., Nuytinck, J.K., Gimbrere, J.S., *Multiple-organ failure. Generalized autodestructive inflammation*, Arch. Surg., 120, 1109-1115, 1985.

[62] Gu, M., Eisenstat, S. C., *Efficient algorithms for computing a strong rank-revealing QR factorization*, SIAM Journal on Scientific Computing, 17(4), 848-896, 1996.

[63] Haykin, S., *Kalman Filters*, In S. Haykin, editor, Kalman Filtering and Neural Networks, 1-21, New York: Wiley, 2001.

[64] Heldt, T., *Computational Models of Cardiovascular Response to Orthostatic Stress*, PhD thesis, Massachusetts Institute of Technology, Cambridge, MA, September 2004.

[65] Huntington, G. T., *Advancement and Analysis of a Gauss Pseudospectral Transcription for Optimal Control Problems*, PhD thesis, Massachusetts Institute of Technology, Cambridge, MA, June 2007.

[66] Janeway, C., Travers, P., *Immunobiology: The Immune System in Health and Disease*, 3rd Edition, Current Biology Ltd., Garland, 1997.

[67] Janeway Jr., C.A., Travers, P., Walport, M., Shlomchik, M., *Immunobiology: The Immune System in Health and Disease*, 5th edition, Garland Publishing, New York, 2001.

[68] Julier, S. J., Uhlmann, J. K., Durrant-Whyte, H., *A new approach for filtering nonlinear systems* In Proceedings of the American Control Conference, 1628-1632, 1995.

[69] Julier, S. J., Uhlmann, J. K., *A general method for approximating nonlinear transformations of probability distributions*, Technical Report, RRG, Department of Engineering Science, University of Oxford, Oxford, United Kingdom, November 1996.

[70] Julier, S. J., Uhlmann, J. K., *A new extension of the Kalman filter to nonlinear systems*, In Proceedings of AeroSense: The 11th International Symposium on Aerospace/Defence Sensing, Simulation and Controls, 1997.

[71] Kalman, R. E., *Contributions to the theory of optimal control*, Boletin Sociedad Matematica Mexicana, 5, 102-119, 1960.

[72] Kamm, K., Vanderkolk, W., Lawrence, C., Jonker, M., Davis, A. T., *The effect of traumatic brain injury upon the challenge and expression of interleukin-1beta and interleukin-10 in the rat*, J. Trauma, 60(1), 152-157, 2006.

[73] Keerthi, S. S., Gilbert, E. G., *Optimal infinite-horizon feedback laws for a general class of constrained discrete time systems: Stability and moving-horizon approximations*, Journal of Optimization Theory and Applications, 57(2), 265-293, 1988.

[74] Kirk, D.E., *Optimal Control Theory: An Introduction*, Prentice-Hall Inc., 1970.

[75] Kleinman, B. L., *An easy way to stabilize a linear constant system*, IEEE Transactions on Automatic Control, 15(12), 692-692, 1970.

[76] Kumar, R., Clermont, G., Vodovotz, Y., Chow, C. C., *The dynamics of acute inflammation*, Journal of Theoretical Biology, 230, 145-155, 2004.

[77] Kwon, W. H., Pearson, A. E., *A modified quadratic cost problem and feedback stabilization of a linear system*, IEEE Transactions on Automatic Control, 22(5), 838-842, 1977.

[78] Kwon, W. H., Bruckstein, A. M., Kailath, T., *Stabilizing state-feedback design via the moving horizon method*, International Journal of Control, 37(3), 631-643, 1983.

[79] Iversen, M.H., Hahn, R.G., *Acute effects of vitamin A on the kinetics of endotoxin in conscious rabbits*, Intensive Care Med., 25 , 1160-1164, 1999.

[80] Lagoa , C. E., Bartels, J., Baratt, A., Tseng, G., Clermont, G., Fink, M. P., Billiar, T. R., Vodovotz, Y., *The role of initial trauma in the host's response to injury and hemorrhage: Insights from a correlation of mathematical simulations and hepatic transcriptomic analysis*, Shock, 26, 592-600, 2006.

[81] Lee, E. B., Markus, L., *Foundations of optimal control theory*, New York, Wiley, 1967.

[82] Levien, K. L., *Studies in the design and control of coupled distillation columns*, Ph.D. Thesis, University of Wisconsin, Madison, 1985.

[83] Levien, K. L., Morari, M., *Internal model control of coupled distillation columns*, AIChE Journal, 33(1), 83-98, 1987.

[84] Lewis, F., *Optimal Control*, John Wiley and Sons Inc, 1995.

[85] Li, R., Henson, M. A., Kurtz, K. J., *Selection of Model Parameters for Off-Line Parameter Estimation*, IEEE Transactions on Control Systems Technology, 12, 402-412, 2004.

[86] Linkers, D. A., Mahfonf, M., *Advances in Model-Based Predictive Control*, Chapter: Generalized Predictive Control in Clinical Anaesthesia, Oxford University Press, 1994.

[87] Ljung, L., *System Identification: Theory for the User*, Prentice Hall, Englewood Cliffs, NJ, 1999.

[88] Mackay, I., Rosen, F. S., *Advances in immunilogy*, N. Engl. J. Med., 343, 338-344, 2000.

[89] Magni, L., De Nicolao, G., Scattolini, R., *A stabilizing model-based predicitve control algorithm for nonlinear systems*, Auto, 37(10), 1351-1362, 2001.

[90] Magni, L., De Nicolao, G., Scattolini, R., Allgöwer, F., *Robust Receding Horizon Control for Nonlinear Discrete-Time Systems*, In Proceedings 15$^{\text{th}}$ IFAC World Congress, Barcelona, Spain, 2002.

[91] Magni, L., Sepulchre, R., *Stability margins of nonlinear receeding-horizon control via inverse optimality*, Systems and Control Letters, 32(4), 241-245, 1997.

[92] Magni, L., De Nicolao, G., Scattolini, R., *Output feedback receding-horizon control of discrete-time nonlinear systems*, In Proceedings of the IFAC nonlinear control systems design symposium, Enschede, Netherlands, 1998.

[93] Matzinger, P., *The danger model: a renewed sense of self*, Science, 296, 301-305, 2002.

[94] Mayne, D. Q., Rawlings, J. B., Rao, C. V., Scokaert, P. O. M., *Constrained model predictive control: Stability and optimality*, Automatica, 36, 789-814, 2000.

[95] Mayne, D. Q., *Nonlinear Model Predictive Control: Challenges and Opportunuties*, In F. Allgöwer and A. Zheng, editors, Nonlinear Predictive Control, 23-44, Birkhäuser, 2000.

[96] Meiss, J. D., *Differential Dynamical Systems*, SIAM, 2007.

[97] Michalska, H., Mayne, D. Q. (1995). *Moving horizon observers and observer-based control*, IEEE Transactions on Automatic Control, 40(6), 995-1006, 1995.

[98] Morrison, D.C., Ryan, J.L., *Endotoxins and disease mechanisms*, Annual Review of Medicine, 38, 417-432, 1987.

[99] Morari, M., *Advances in Model-Based Predictive Control*, Chapter in Model Predictive Control: Multivariate Control Technique of Choice in the 1990s, Oxford University Press, 1994.

[100] Naidu, D. S., *Optimal Control Systems*, CRC Press LLC, 2003.

[101] Nathan, C., *Points of control in inflammation*, Nature, 420,846-852, 2002.

[102] Nathan, C., Sporn, M., *Cytokines in context*, Journal of Cell Biology, 113(5), 981-986, 1991.

[103] Nocedal, J., Wright, S. J., *Numerical Optimization*, 2nd Edition, Springer, 2006.

[104] Parker, R. S., Doyle, F. J. III, Peppas, N. A., *The intravenous route to blood glucose control*, IEEE Eng. Med. Biol. Magazine, 20(1), 65-73, 2001.

[105] Parrillo, J.E., *Pathogenetic mechanisms of septic shock*, N. Engl. J. Med. 328(20), 1471-1477, 1993.

[106] Parrish, J. R., Brosilow, C. B., *Inferential control applications*, Automatica, 21, 527-538, 1985.

[107] Pinsky, M. R., *Sepsis: a pro- and anti-inflammatory disequilibrium syndrome*, Contrib. Nephrol., 132, 354-366, 2001.

[108] Pope, S.R., *Parameter Identification in Lumped Compartment Cardiorespiratory Models*, PhD thesis, North Carolina State University, Raleigh, NC, February 2009.

[109] Prett, D. M., Gillette, R. D., *Optimization and Constrained Multivariable Control of a catalytic cracking unit*, AIChE National meeting, Houston, Texas, 1979. Also in Automatic Control Conference, San Francisco, California 1980.

[110] Pretolani, M., *Interleukin-10: an anti-inflammatory cytokine with therapeutic potential*, Clin. Exp. Allergy, 29, 1164-1171, 1999.

[111] Primbs, J. A., *Nonlinear Optimal Control: A Receding Horizon Approach*, PhD thesis, California Institute of Technology, Pasadena, California, January 1999.

[112] Prince, J. M., Levy, R. M., Bartels, J., Baratt, A., Kane III, J. M., Lagoa, C., Rubin, J., Day, J., Wei, J., Fink, M. P., Goyert, S. M., Clermont, G., Billiar, T. R., Vodovotz, Y., *In silico and in vivo approach to elucidate the inflammatory complexity of CD14-deficient mice*, Mol. Med., 12, 88-96, 2005.

[113] Propoi, A. I., *Use of LP Methods for Synthesizing Sampled-Data Automatic Systems*, Automatic Remote Control, 24, 1963.

[114] Qin, S., Badgewell, T., *An overview of industrial model predictive control technology*, Chemical Process Control, 93(316), 232-256, 1997.

[115] Qin, S., Badgewell, T., *An Overview of Nonlinear Model Predictive Control Applications*, In F. Allgöwer and A. Zheng, Eds., Nonlinear Predictive Control, Birkhäuser, 369-392, 2000.

[116] Qin, S., Badgewell, T., *ÒA Survey of Industrial Model Predictive Control Technology*,Control Engineering Practice, 11(7), 733-764, 2003.

[117] Rao, A. V., Benson, D. A., Darby, C. L., Patterson, M. A., Francolin, C., and Huntington, G. T., *Algorithm 902: GPOPS, A MATLAB Software for Solving Multiple-Phase Optimal Control Problems Using The Gauss Pseudospectral Method* ACM Transactions on Mathematical Software, 37, 2 (to appear).

[118] Rawlings, J. B., *Tutorial Overview of Model Predictive Control*, IEEE Control Systems Magazine, 20(3), 38-52, 2000.

[119] Reid, J. G., *Structural Identifiability in Linear Time-Invariant Systems*, IEEE Transactions on Automatic Control, 22(7), 242-246, 1977.

[120] Reynolds, A., Rubin, J., Clermont, G., Day, J., Vodovotz, Y., Ermentrout, B., *A reduced mathematical model of the acute inflammatory response I. Derivation of model and analysis of anti-inflammation*, Journal of Theoretical Biology, 242, 220-236, 2006.

[121] Richalet, J., *Industrial Application of Model Based Predictive Control*, Automatica, 29(5), 1251-1274, 1993.

[122] Richalet, J., Rault, A., Testud, J. L., Papon,J., *Model Predictive Heuristic Control: Application to Industrial Processes*, Automatica, 14(2), 413-428, 1978.

[123] Richalet, J., Rault, A., Testud, J. L., Papon,J., *Algorithmic Control of Industrial Processes*, In 4th IFAC Symposium on Identification and System Parameter Estimation, Tbilisi, USSR, 1976.

[124] Rodriguez-Fernandez, M., Mendes, P., Banga, J. R., *A hybrid approach for efficient and robust parameter estimation in biochemical pathways*, BioSystems 83, 248-265, 2006.

[125] Rosenblum, Y. I., Johnson, R. C., Schmahail, T. J., *Preclinical safety evaluation of recombinant human interleukin-10*, Regulatory Toxicology and Pharmacology, 35(1), 56-71, 2002.

[126] Roy, A., Daun, S., Clermont, G., Rubin, J., Vodovotz, Y., Lagoa, C., Parker, R., *A mathematical model of acute inflammatory response to endotoxin challenge*, Mathematical Biosciences and Engineering, in press, 2009.

[127] Sanchez-Cantu, L., Rode, H.N., Christou, N.V., *Endotoxin tolerance is associated with reduced secretion of tumor necrosis factor*, Archives of Surgery, 124(12), 1432-1435, 1989.

[128] Sargent, R. W. H., *Optimal control*, Journal of Computational and Applied Mathematics, 124, 361-371, 2000.

[129] Schade, F.U., Flach, R., Flohe, S., Majetschak, M., Kreuzfelder, E., Dominguez-Fernandez, E., Borgermann, J., Obertacke, U., *Endotoxin tolerance*, In Brade, M., Opal, V. (Eds.), Endotoxin in Health and Disease. Marcel Dekker, New York, 751-767, 1999.

[130] Schittkowski, K., *Numerical Data Fitting in Dynamical Systems–A Practical Introduction with Applications and Software*, Kluwer Academic Publishers, 2002.

[131] Senaldi, G., Shaklee, C. L., Guo, J., Martin, L., Boone, T., Mak, T. W., Ulich, T.R., *Protection against the mortality associated with disease models mediated by TNF and IFN-γ in mice lacking IFN regulatory factor-1*, The Journal of Immunology, 163(12), 6820-6826, 1999.

[132] Shim, H., Han, S., Chung, C., Nam, S., Seo, J., *Optimal scheduling of drug treatment for HIV infection: Continuous dose control and receding horizon control* International Journal of Control, Automation and Systems, 1(3), 401-407, 2003.

[133] SNOPT, *Software for Large-Scale Nonlinear Programming*, http://www.cam.ucsd.edu/ peg/, April 2010.

[134] Sussmann, H. J., *From the brachystochrone to the maximum principle and back*, In Proceedings of the 35th IEEE Conference on Decision and Control, pages 1588-1593, Kobe, Japan, 1996.

[135] Thomas, Y. A. *Linear quadratic optimal estimation and control with receding horizon*, Electronics Letters, 11, 19-21, 1975.

[136] Timmer, J., *Modeling noisy time series: physiological tremor*, Int. J. Bifurcation Chaos 8(7), 1505-1516, 1998.

[137] Tricaud, C., Chen, Y., *Linear and Nonlinear Model Predictive Control Using A General Purpose Optimal Control Problem Solver RIOTS_95*, In 20$^{\text{th}}$ Chinese Control and Decision Conference, Yaitai, China, 2008.

[138] Vélez-Reyes, M., *Decomposed Algorithms for Parameter Estimation*, PhD thesis, Massachusetts Institute of Technology, Cambridge, MA, September 1992.

[139] Vodovotz, Y., Clermont, G., Hunt, C.A., Lefering, R., Bartels, J., Seydel, R., Hotchkiss, J., Ta'asan, S., Neugebauer, E., An, G., *Evidence-based modeling of critical illness: an initial consensus from the Society for Complexity in Acute Illness*, J. Crit. Care 22 (1), 77-84, 2007.

[140] Vodovotz, Y., Chow, C. C., Bartels, J., Lagoa, C., Prince, J. M., Levy, R. M., Kumar, R., Day, J., Rubin, J., Constantine, G., Billiar, T. R., Fink, M. P., Clermont, G., *In Silicon Models of Acute Inflammation in Animals*, Shock, 26(3), 235-244, 2006.

[141] Wan, E. A., van der Merwe, R., *The Unscented Kalman Filters*, In S. Haykin, editor, Kalman Filtering and Neural Networks, 221-280, New York: Wiley, 2001.

[142] Warner, A.E., DeCamp, M.M. Jr., Molina, R.M., Brain, J.D., *Pulmonary removal of circulating endotoxin results in acute lung injury in sleep*, Lab. Invest., 59 , 219-230, 1988.

[143] West, M. A., Heagy, W., *Endotoxin tolerance: A review*, Critical Care Medicine, 30(1), S64-S73, 2002.

[144] Zadeh, L. A., Whalen, B. H., *On Optimal Control and Linear Programming*, IRE Trans. Automatic Control, 7(4), 1962.

[145] Zurakowski, R., Messina, M., Tuna, S., Teel, A., *HIV treatment scheduling via robust nonlinear model predictive control*, Proceedings of the 5th Asian Control Conference, 25-32, 2004.

APPENDICES

Appendix A

8D Mathematical Model

The 8D ODEs describing the dynamics of the states are given below.

Endotoxin concentration ($P(t)$):

$$\frac{dP(t)}{dt} = -d_p \cdot P(t). \tag{A.1}$$

$P(t)$ decays exponentially with a rate equal to d_P. The decay rate was fixed at $3\,hr^{-1}$. The initial conditions for Equation (A.1) are either $3\,mg/kg$, $6\,mg/kg$, or $12\,mg/kg$ depending on the endotoxin dose level.

Total number of activated phagocytic cells ($N(t)$):
The equations representing activation of $N(t)$ are of the form:

$$\begin{aligned}
\frac{dN(t)}{dt} &= k_N \cdot \frac{R(t)}{x_N + R(t)} - d_N \cdot N(t) \qquad (A.2)\\
R(t) &= [k_{NP} \cdot P(t) + k_{ND} \cdot D(t)] \cdot fDN_{NCA}(t) \cdot fDN_{NIL10}(t) \cdot \gamma(t)\\
\gamma(t) &= (1 + k_{NTNF} \cdot fUP_{NTNF}(t)) \cdot (1 + k_{NIL6} \cdot fUP_{NIL6}(t))\\
fUP_{NTNF}(t) &= \frac{TNF(t)}{x_{NTNF} + TNF(t)}\\
fUP_{NIL6}(t) &= \frac{IL6(t)}{x_{NIL6} + IL6(t)}\\
fDN_{NCA}(t) &= \frac{x_{NCA}}{x_{NCA} + CA(t)}\\
fDN_{NIL10}(t) &= \frac{x_{NIL10}}{x_{NIL10} + IL10(t)}.
\end{aligned}$$

Resting phagocytic cells are activated by the presence of endotoxin in the system. Equa-

tion (A.2) represents the total number of activated phagocytic cells ($N(t)$). The initial condition for Equation (A.2) is $N(0) = 0$.

Tissue damage marker ($D(t)$):
The tissue damage caused by the inflammatory response to endotoxin challenge is modeled as follows:

$$\frac{dD(t)}{dt} = k_D \cdot \frac{N(t)^6}{x_D^6 + N(t)^6} - d_D \cdot D(t). \tag{A.3}$$

Parameters k_D and d_D represent the rate of generation and the rate of elimination of the non-measurable tissue damage marker. The initial condition for Equation (A.3) is $D(0) = 0$.

Anti-inflammatory moderator ($C_A(t)$):
$C_A(t)$ represents a combination of various inflammation inhibitory mediators, including the cytokine Transforming Growth Factor-$\beta 1$ ($TGF - \beta 1$) and cortisol. The equation representing $C_A(t)$ is given as:

$$\frac{dC_A(t)}{dt} = k_{CA} \cdot N(t) - d_{CA} \cdot C_A(t) + s_{CA}. \tag{A.4}$$

Parameters k_{CA} and d_{CA} represent the rate of $C_A(t)$ production/secretion and clearance, respectively. At basal conditions, the system is assumed to be slightly anti-inflammatory. This was achieved by introducing a constant, s_{CA}, into the ODE. Hence, at $t = 0$, $C(0) = \frac{s_{CA}}{d_{CA}}$

Concentration of interleukin-6 ($IL6(t)$):
The dynamics of $IL - 6$, which is a pro-inflammatory mediator, can be mathematically written as:

$$\begin{aligned}\frac{dIL6(t)}{dt} &= k_{IL6} \cdot \frac{N(t)^4}{x_{IL6}^4 + N(t)^4} \cdot [1 + k_{IL6TNF} \cdot fUP_{IL6TNF}(t) \\ &+ k_{IL6IL6} \cdot fUP_{IL6IL6}(t)] \cdot fDN_{IL6IL10}(t) \cdot fDN_{IL6CA}(t) \\ &- d_{IL6} \cdot IL6(t) \qquad \text{(A.5)} \\ fUP_{IL6TNF}(t) &= \frac{TNF(t)}{x_{IL6TNF} + TNF(t)} \\ fUP_{IL6IL6}(t) &= \frac{IL6(t)}{x_{IL6IL6} + IL6(t)} \\ fDN_{IL6IL10}(t) &= \frac{x_{IL6IL10}}{x_{IL6IL10} + IL10(t)} \\ fDN_{IL6CA}(t) &= \frac{x_{IL6CA}}{x_{IL6CA} + C_A(t)}.\end{aligned}$$

The initial condition for Equation (A.5) is $IL6(0) = 0$.

Concentration of tumor necrosis factor ($TNF(t)$):
The dynamics of $TNF - \alpha$, which is a pro-inflammatory mediator can be represented as follows:

$$\begin{aligned}\frac{dTNF(t)}{dt} &= k_{TNF} \cdot N(t)^{1.5} \cdot [1 + k_{TNFTNF} \cdot fUP_{TNFTNF}(t)] \\ &\cdot fDN_{TNFCA}(t) \cdot fDN_{TNFIL10}(t) \cdot fDN_{TNFIL6}(t) \\ &- d_{TNF} \cdot TNF(t) \qquad \text{(A.6)} \\ fUP_{TNFTNF}(t) &= \frac{TNF(t)}{x_{TNFTNF} + TNF(t)} \\ fDN_{TNFCA}(t) &= \frac{x_{TNFCA}^6}{x_{TNFCA}^6 + CA(t)^6} \\ fDN_{TNFIL10}(t) &= \frac{x_{TNFIL10}}{x_{TNFIL10} + IL10(t)} \\ fDN_{TNFIL6}(t) &= \frac{x_{TNFIL6}}{x_{TNFIL6} + IL6(t)}.\end{aligned}$$

The initial condition for Equation (A.6) is $TNF(0) = 0$.

Concentration of interleukin-10 ($IL10(t)$):
The dynamics of $IL10(t)$, which is a strong anti-inflammatory cytokine, can be represented mathematically by the following equations:

$$\begin{aligned}\frac{dIL10(t)}{dt} &= k_{IL10} \cdot \frac{N(t)^3}{x_{IL10}^3 + N(t)^3} \cdot [1 + k_{IL10IL6} \cdot fUP_{IL10IL6}(t) \\ &+ k_{IL10TNF} \cdot fUP_{IL10TNF}] - d_{IL10} \cdot fDN_{IL10d}(t) \cdot IL10(t) \\ &+ Y_{IL10}(t) + s_{IL10} \qquad \text{(A.7)} \\ fUP_{IL10IL6}(t) &= \frac{IL6(t)^4}{x_{IL10IL6}^4 + IL6(t)^4} \\ fUP_{IL10TNF} &= \frac{TNF(t)}{x_{IL10TNF} + TNF(t)} \\ fDN_{IL10d}(t) &= \frac{x_{IL10d}}{x_{IL10d} + IL10(t)}.\end{aligned}$$

The production of $IL10(t)$ in the basal state is represented by the constant s_{IL10} (as observed in experimental data). The initial condition for Equation (A.7) is $IL10(0) = \frac{s_{IL10} \cdot x_{IL10d}}{d_{IL10} \cdot x_{IL10d} - s_{IL10}}$.

Tissue damage driven non-accessible interleukin-10 promoter ($Y_{IL10}(t)$):

$$\frac{dY_{IL10}(t)}{dt} = k_{IL102} \cdot \frac{D(t)^4}{x_{IL102}^4 + D(t)^4} - d_{IL102} \cdot Y_{IL10}(t). \qquad \text{(A.8)}$$

The dynamics of $Y_{IL10}(t)$ are represented by the ODE (A.8). The rate of production of $Y_{IL10}(t)$ is represented by the parameter k_{IL102} coupled with a 4^{th} -order Hill equation which is driven by $D(t)$.

Detailed description of the the model parameters and the effects of the supporting functions in Equations (A.2) , (A.5), (A.6), and (A.7) can be found in [126].

Appendix B

7D Parameters and Plots

B.1 Reduced 7D Model Simulation Results

We display the plots of the reduced 7D model simulation for

$$P(t),\ N(t),\ D(t),\ IL6(t),\ TNF(t),\ IL10(t),\ \text{and}\ Y_{IL10}(t)$$

at $3\,mg/kg$, $6\,mg/kg$, and $12\,mg/kg$ endotoxin challenge levels respectively. The 7D model simulation plots at $3\,mg/kg$ endotoxin challenge level are displayed in Figure B.1. Figures B.2 and B.3 show plots at $6\,mg/kg$, and $12\,mg/kg$ endotoxin challenge levels, respectively.

Figure B.1: 7D model simulation results at $3\,mg/kg$ endotoxin challenge level for all the states.

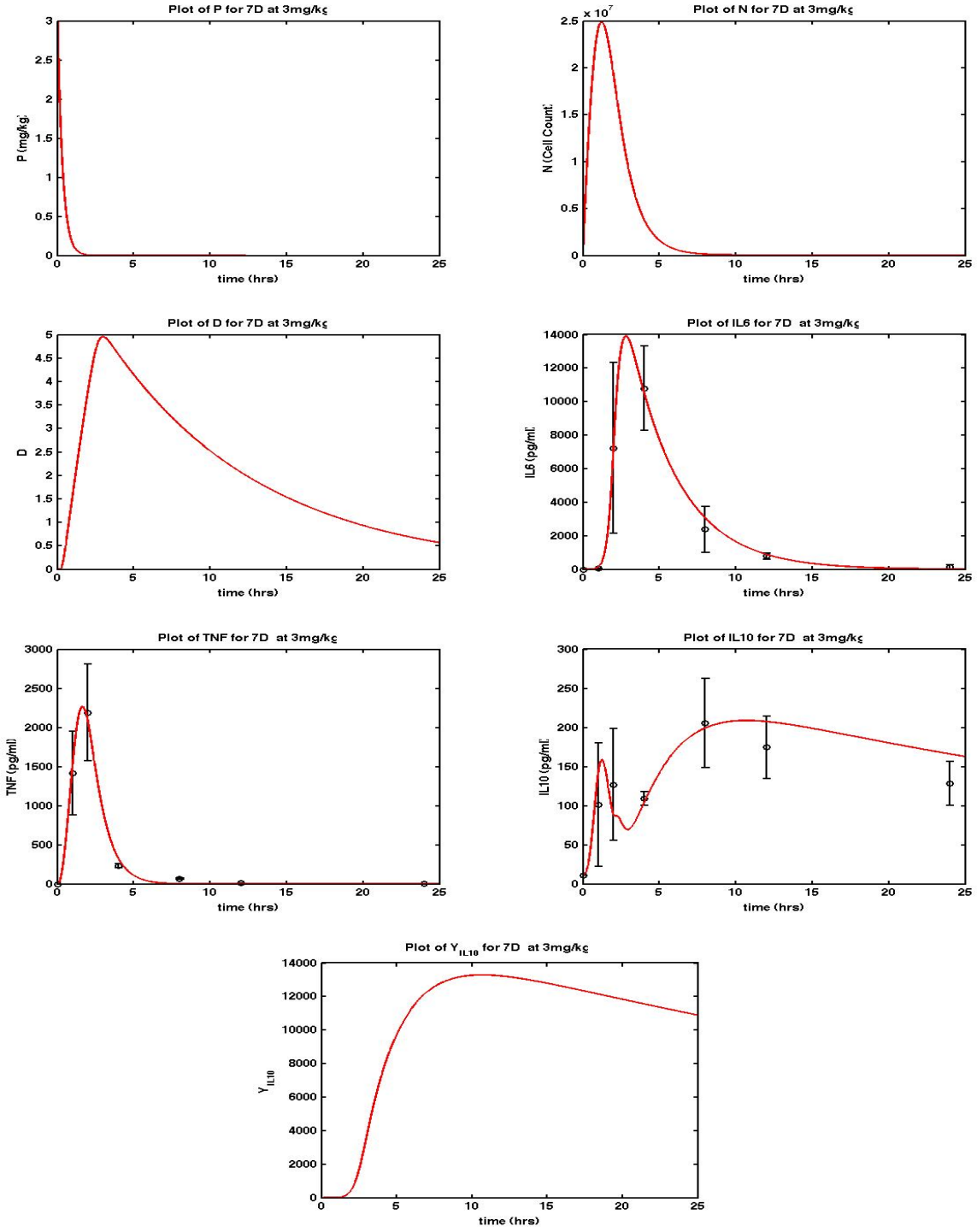

Figure B.2: 7D model simulation results at $6\,mg/kg$ endotoxin challenge level for all the states.

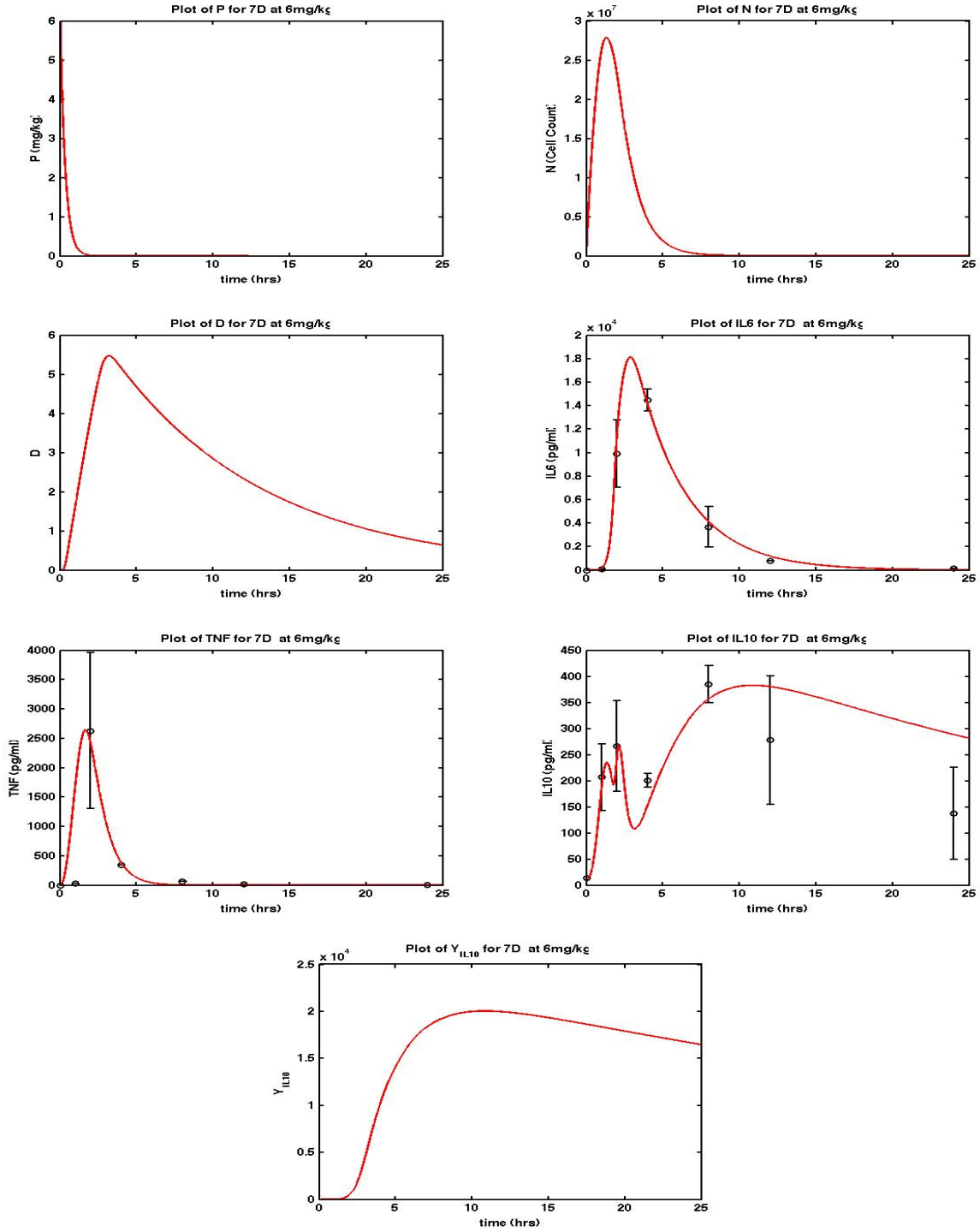

Figure B.3: 7D model simulation results at 12 mg/kg endotoxin challenge level for all the states.

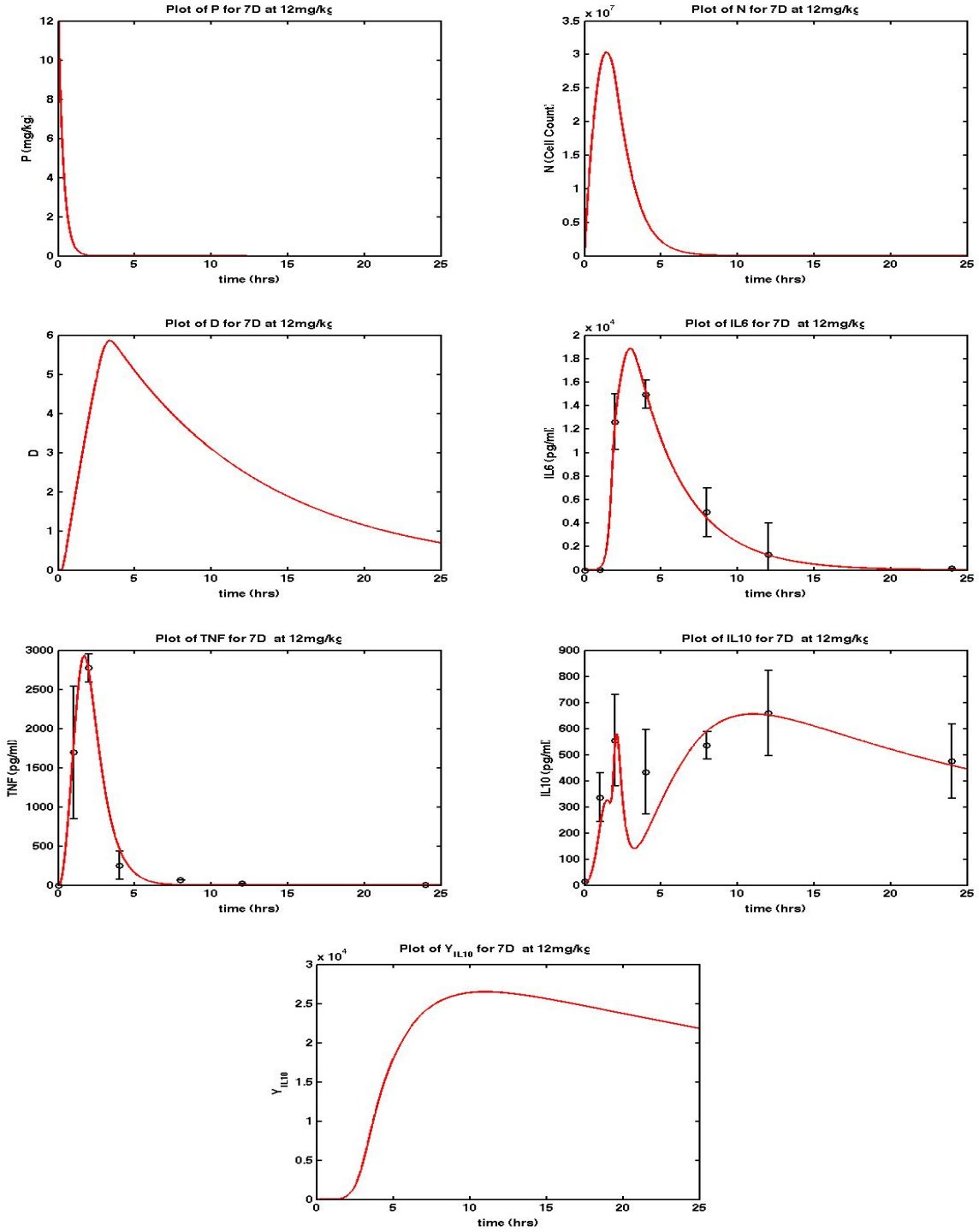

B.2 Reduced 7D Complete Parameter Values

Table B.1: Reduced 7D Model Parameters

No.	Parameter	Value	Unit	No.	Parameter	Value	Unit
1	d_P	3	hr^{-1}	21	k_{IL6IL6}	1.1191631e4	–
2	k_N	4.6297682e7	hr^{-1}	22	x_{IL6IL6}	1.987e5	$\frac{pg}{mL}$
3	x_N	14.177	$N-unit$	23	k_{TNF}	3.9e-8	$\frac{pg}{mL \cdot N-unit^{1.5}}$
4	d_N	1.004344813	hr^{-1}	24	d_{TNF}	1.651880958	hr^{-1}
5	k_{NP}	54.14849008	$\frac{N-unit \cdot kg}{mg}$	25	$x_{TNFIL10}$	2.2198e7	$\frac{pg}{mL}$
6	k_{ND}	0.013259	$\frac{N-unit}{D-unit}$	26	k_{TNFTNF}	1.0e-10	–
7	x_{NTNF}	1693.9509	$\frac{pg}{mL}$	27	x_{TNFTNF}	9.2969e6	$\frac{pg}{mL}$
8	x_{NIL6}	58080.742	$\frac{pg}{mL}$	28	x_{TNFIL6}	1.9446269e4	$\frac{pg}{mL}$
9	x_{NIL10}	147.68	$\frac{pg}{mL}$	29	$k_{IL10TNF}$	2.9951e-5	–
10	k_{NTNF}	12.94907	–	30	$x_{IL10TNF}$	1.1964e6	$\frac{pg}{mL}$
11	k_{NIL6}	2.71246	–	31	$k_{IL10IL6}$	4.1829	–
12	k_D	2.5247	$\frac{D-unit}{hr}$	32	$x_{IL10IL6}$	1.6942234e4	$\frac{pg}{mL}$
13	d_D	0.099359171	hr^{-1}	33	k_{IL10}	1.3374e5	$\frac{pg}{mL \cdot hr}$
14	x_D	1.1646809e7	$N-unit$	34	d_{IL10}	98.932	hr^{-1}
15	k_{IL6TNF}	4.4651	–	35	x_{IL10}	5.6323712e7	$N-unit$
16	x_{IL6TNF}	1.5125569e8	$\frac{pg}{mL}$	36	s_{IL10}	1187.2	$\frac{pg}{mL \cdot hr}$
17	k_{IL6}	9.0425e7	$\frac{pg}{mL \cdot hr}$	37	x_{IL10d}	488.5519610	$\frac{pg}{mL}$
18	d_{IL6}	0.308883173	hr^{-1}	38	k_{IL102}	1.3964e7	$\frac{Y_{IL10}-Unit}{hr}$
19	x_{IL6}	2.3833727e8	$N-unit$	39	d_{IL102}	0.016876136	hr^{-1}
20	$x_{IL6IL10}$	1.1818	$\frac{pg}{mL}$	40	x_{IL102}	37.454	$D-unit$

Appendix C

Gauss Pseudospectral Method (GPM)

The GPM is a collocation method that was originally developed by Benson [18] in an effort to correct the deficiencies of the Legendre Pseudospectral Method (LPM). In the interest of clarity, we begin with the following definitions.

Definition C.0.1 *A collocation method is a procedure of finding numerical solutions of differential and integral equations, the general approach is to choose a finite dimensional space of solutions together with a number of collocation points in the domain. The goal is to pick the solution that satisfies the equation of interest at the collocation points.*

Definition C.0.2 *The Legendre Pseudospectral Method (LPM) is a direct transcription method that converts a continuous optimal control problem into a discrete NLP. LPM uses a set of Lagrange-Gauss-Lobatto (LGL) points for collocation of the differential dynamic constraints of the optimal control problem [18].*

Suppose we aim to find the control that minimizes the Bolza cost functional

$$J = \mathbf{\Phi}(\mathbf{x}(t_0), t_0, \mathbf{x}(t_f), t_f) + \int_{t_0}^{t_f} \mathbf{g}(\mathbf{x}(t), \mathbf{u}(t), t)dt \tag{C.1}$$

subject to

$$\dot{\mathbf{x}}(t) = \mathbf{f}(\mathbf{x}(t), \mathbf{u}(t), t), \tag{C.2}$$

with boundary conditions

$$\phi(\mathbf{x}(t_0), t_0, \mathbf{x}(t_f), t_f) = \mathbf{0}, \tag{C.3}$$

and inequality path constraints

$$\mathbf{C}(\mathbf{x}(t), \mathbf{u}(t), t) \leq \mathbf{0}, \tag{C.4}$$

where $t \in [t_0,\ t_f]$, $\mathbf{x}(t) \in \mathbb{R}^n$ and $\mathbf{u}(t) \in \mathbb{R}^m$. Equations (C.1)-(C.4) constitute what is known as the continuous Bolza problem and the functions in the equations are defined as:

$$\begin{aligned}
\mathbf{\Phi} &: \mathbb{R}^n \times \mathbb{R} \times \mathbb{R}^n \times \mathbb{R} \to \mathbb{R} \\
\mathbf{g} &: \mathbb{R}^n \times \mathbb{R}^m \times \mathbb{R} \to \mathbb{R} \\
\mathbf{f} &: \mathbb{R}^n \times \mathbb{R}^m \times \mathbb{R} \to \mathbb{R}^n \\
\phi &: \mathbb{R}^n \times \mathbb{R} \times \mathbb{R}^n \times \mathbb{R} \to \mathbb{R}^q \\
\mathbf{\Phi} &: \mathbb{R}^n \times \mathbb{R}^m \times \mathbb{R} \to \mathbb{R}^c.
\end{aligned} \tag{C.5}$$

Gauss pseudospectral transcription converts the above continuous Bolza problem into a NLP, GPM approximates the states by using a basis of global interpolating polynomials which are established from a set of discrete points across the interval. Consider the transformation of t to $\tau \in [-1,\ 1]$ such that

$$t = \frac{t_f - t_0}{2}\tau + \frac{t_f + t_0}{2}.$$

Let $\mathcal{K} = \{\tau_1,\ \tau_2,\ \ldots,\ \tau_K\}$ be a set of K Legendre-Gauss (LG) points which correspond to the roots of the K^{th} degree Legendre polynomial, $P_K(\tau)$, where

$$P_K(\tau) = \frac{1}{2^K K!}\frac{d^K}{d\tau^K}\left[(\tau^2 - 1)^K\right].$$

The corresponding LG weights can be computed using

$$w_i = \frac{2}{(1 - \tau_i^2)\left[\dot{P}_K(\tau_i)\right]^2}, \quad \text{for } i = 1,\ \ldots,\ K,$$

where $\dot{P}_K$ is the derivative of the K^{th} degree Legendre polynomial.

The discretization points used in the GPM are the LG points combined with $\tau_0 = -1$ and $\tau_{K+1} = 1$, hence creating a $K + 2$ points ($\mathcal{K} \cup \{\tau_0,\ \tau_{K+1}\}$).

The discretization of the problem can be given in terms of τ such that the state is approximated using a basis of $K+1$ Lagrange interpolating polynomials $\mathcal{L}_i(\tau),\ \text{for } i = 0, \ldots, K.$

$$\mathbf{x}(\tau) \approx \mathbf{X}(\tau) = \sum_{i=0}^{K} \mathcal{L}_i(\tau)\mathbf{X}(\tau_i), \tag{C.6}$$

where

$$\mathcal{L}_i(\tau) = \prod_{j=0,\, j\neq i}^{K} \frac{\tau - \tau_j}{\tau_i - \tau_j}.$$

Similarly, the control is approximated at the K collocation points using a basis of K Lagrange interpolating polynomials $\tilde{\mathcal{L}}_i(\tau),\ \text{for } i = 1, \ldots, K.$

$$\mathbf{u}(\tau) \approx \mathbf{U}(\tau) = \sum_{i=1}^{K} \tilde{\mathcal{L}}_i(\tau)\mathbf{U}(\tau_i) \quad \text{for } \tau_i \in \mathcal{K}. \tag{C.7}$$

The cost functional in equation (C.1) is approximated via a Gauss quadrature as

$$J = \mathbf{\Phi}(\mathbf{X}_0,\, t_0,\, \mathbf{X}_f,\, t_f) + \frac{t_f - t_0}{2} \sum_{k=1}^{K} w_k g(\mathbf{X}_k,\, \mathbf{U}_k,\, \tau_k;\, t_0,\, t_f). \tag{C.8}$$

Taking the derivative of the state in equation (C.6) with respect to τ yields

$$\dot{\mathbf{x}}(\tau_k) \approx \dot{\mathbf{X}}(\tau_k) = \sum_{i=0}^{K} \dot{\mathcal{L}}_i(\tau_k)\mathbf{X}(\tau_i). \tag{C.9}$$

The derivative of each Lagrange polynomial at the LG points can be written in the form of a differentiation matrix $\mathbf{D} \in \mathbb{R}^{K\times K+1}$ as

$$\mathbf{D}_{ki} = \dot{\mathcal{L}}_i(\tau_k) = \sum_{l=0}^{K} \frac{\prod_{j=0,\, j\neq i,\, l}^{K} (\tau_k - \tau_j)}{\prod_{j=0,\, j\neq i}^{K} (\tau_i - \tau_j)}, \quad k = 1, \ldots, K;\ \ i = 0, \ldots, K. \tag{C.10}$$

The dynamic equation (C.2) is then transcribed into algebraic collocation constraint of the problem as

$$\sum_{i=0}^{K} \mathbf{D}_{ki}\mathbf{X}(\tau_i) - \frac{t_f - t_0}{2}\mathbf{f}(\mathbf{X}(\tau_k),\, \mathbf{U}(\tau_k),\, \tau_k;\, t_0,\, t_f) = \mathbf{0} \quad k = 1, \ldots, K. \tag{C.11}$$

Next, define the quadrature constraint

$$\mathbf{X}_f - \mathbf{X}_0 - \frac{t_f - t_0}{2} \sum_{i=1}^{K} w_k \mathbf{f}(\mathbf{X}(\tau_k),\, \mathbf{U}(\tau_k),\, \tau_k;\, t_0,\, t_f) = \mathbf{0}, \tag{C.12}$$

where $\mathbf{X}_0 = \mathbf{X}(\tau_0)$ and $\mathbf{X}_f = \mathbf{X}(\tau_f)$. Notice that equation (C.12) is an additional constraint in the discretiization since an additional variable was introduced. Also, (C.12) is a function on the right-hand side of the differential equation at each LG point, as such equation (C.10) can be solved for $\mathbf{f}$ and substitute the result into equation (C.12) to get

$$\mathbf{X}_f - \mathbf{X}_0 - \sum_{i=0}^{K} \sum_{k=1}^{K} w_k \mathbf{D}_{ki} \mathbf{X}(\tau_i) = \mathbf{0}. \tag{C.13}$$

As equation (C.13) is linear, it is implemented rather than equation (C.12). A lot of the details regarding the development of GPM have been omitted, the interested reason should see [18, 65] for a complete description of GPM.

Appendix D

Sequential Quadratic Programming (SQP)

The SQP methods tries to solve a NLP rather than convert it to a sequence of unconstrained minimization problems. The methods are particularly useful when solving problems with significant nonlinearities in the constraints. They are iterative methods that solve a quadratic programming (QP) problem at each iteration. We will give on overview of the framework for solving equality-constrained problems using the *Local SQP method* described in [103]. This reference is an excellent source for a complete review of SQP methods.

Consider the equality-constrained problem

$$\min f(x) \tag{D.1}$$

$$\text{subject to } g(x) = 0, \tag{D.2}$$

where $f : \mathbb{R}^n \to \mathbb{R}$ and $g : \mathbb{R}^n \to \mathbb{R}^m$ are smooth functions. The SQP technique is to model (D.1) and (D.2) as a QP subproblem at the current iterate x_k and then solve to obtain x^*. The next iterate becomes $x^* = x_{k+1}$. Applying Newton's method to the Karush-Kuhn-Tucker (KKT) optimality condition for (D.1) and (D.2) is the simplest derivation of SQP methods.

Define the Lagrangian function of (D.1) and (D.2) to be $\mathcal{L}(x, \lambda) = f(x) - \lambda^T g(x)$, where λ is the Lagrangian multiplier. Let

$$A(x)^T = [\nabla g_1(x), \nabla g_2(x), \ldots, \nabla g_m(x)],$$

such that $A(x)$ is the constraint jacobian and $g_i(x)$ is the i^{th} component of the vector in

(D.2). The first order (KKT) conditions for a system of $n+m$ equations in $n+m$ unknowns x and λ:

$$F(x,\lambda) = \begin{bmatrix} \nabla f(x) - A(x)^T\lambda \\ g(x) \end{bmatrix} = 0. \tag{D.3}$$

Any solution (x^*, λ^*) of (D.1) and (D.2) for which $A(x^*)$ has full rank satisfies (D.3) [103], using the Newton's method technique to solve (D.3), find the jacobian of (D.3) w.r.t x and λ;

$$F'(x,\lambda) = \begin{bmatrix} \nabla^2_{xx}\mathcal{L}(x,\lambda) & -A(x)^T \\ A(x) & 0 \end{bmatrix}.$$

The step for iterate (x_k, λ_k) is

$$\begin{bmatrix} x_{k+1} \\ \lambda_{k+1} \end{bmatrix} = \begin{bmatrix} x_k \\ \lambda_k \end{bmatrix} + \begin{bmatrix} p_k \\ p_\lambda \end{bmatrix}, \tag{D.4}$$

where p_k and p_λ solve the Newton-KKT system

$$\begin{bmatrix} \nabla^2_{xx}\mathcal{L}(x,\lambda) & -A(x)^T \\ A(x) & 0 \end{bmatrix} \begin{bmatrix} p_k \\ p_\lambda \end{bmatrix} = \begin{bmatrix} -\nabla f_k + A_k^T\lambda_k \\ -g_k \end{bmatrix}. \tag{D.5}$$

This iteration is well defined when the KKT matrix in (D.5) is nonsingular. If the following assumption from [103] holds at $(x,\lambda) = (x_k, \lambda_k)$ then the KKT matrix in (D.4) is nonsingular.

Assumptions D.0.1

(a) The constraint jacobian $A(x)$ has full row rank;

(b) The matrix $\nabla^2_{xx}\mathcal{L}(x,\lambda)$ is positive definite on the tangent space of the constraints, i.e., $d^T\nabla^2_{xx}\mathcal{L}(x,\lambda)d > 0 \;\forall\; d \neq 0$ such that $A(x)d = 0$.

Suppose equations (D.1) and (D.2) are reformulated using a quadratic program at iterate (x_k, λ_k) to be of the form:

$$\min_p \; f_k + \nabla f_k^T p + \frac{1}{2} p^T \nabla^2_{xx}\mathcal{L}_k p \tag{D.6}$$

$$\text{subject to } A_k p + g_k = 0. \tag{D.7}$$

If Assumptions D.0.1 hold for this problem, then it had a unique solution $(p_k,\, q_k)$ such that

equations (D.8) and (D.9) are satisfies.

$$\nabla^2_{xx}\mathcal{L}_k p_k + \nabla f_k - A_k^T q_k = 0 \tag{D.8}$$

$$A_k p_k + g_k = 0. \tag{D.9}$$

p_k and q_k can be identified with the solution of equation (D.5), and by subtracting $A_k^T \lambda_k$ from both sides of the first equation in (D.5), we get

$$\begin{bmatrix} \nabla^2_{xx}\mathcal{L}_k & -A(x)^T \\ A(x) & 0 \end{bmatrix} \begin{bmatrix} p_k \\ \lambda_{k+1} \end{bmatrix} = \begin{bmatrix} -\nabla f_k \\ -g_k \end{bmatrix}. \tag{D.10}$$

By nonsingularity of the coefficient matrix, $\lambda_{k+1} = q_k$, and p_k solves equations (D.5) and (D.6)-(D.7).

The next iterate (x_{k+1}, λ_{k+1}) can be defined either as the solution of (D.6)-(D.7) or be generated by the Newton's method (D.4). Algorithm D.0.1 shows the steps for solving (D.1)-(D.2) in its simplest form.

Algorithm D.0.1

Choose an initial pair (x_0, λ_0)*; set* $k \leftarrow 0$;
repeat *until a convergence test is satisfied.*
Evaluate f_k, ∇f_k, $\nabla^2_{xx}\mathcal{L}_k$, g_k, *and* A_k;
Solve equations (D.6)-(D.7) *to obtain* p_k *and* q_k*;*
Set $x_{k+1} \leftarrow x_k + p_k$ *and* $\lambda_{k+1} \leftarrow q_k$;
end(repeat)

Appendix E

7D Optimal Control Results

Figure E.1: Optimal treatment control functions at different endotoxin concentrations. Top plots denote $3\,mg/kg$, middle plots are $6\,mg/kg$ and bottom plots represent $12\,mg/kg$.

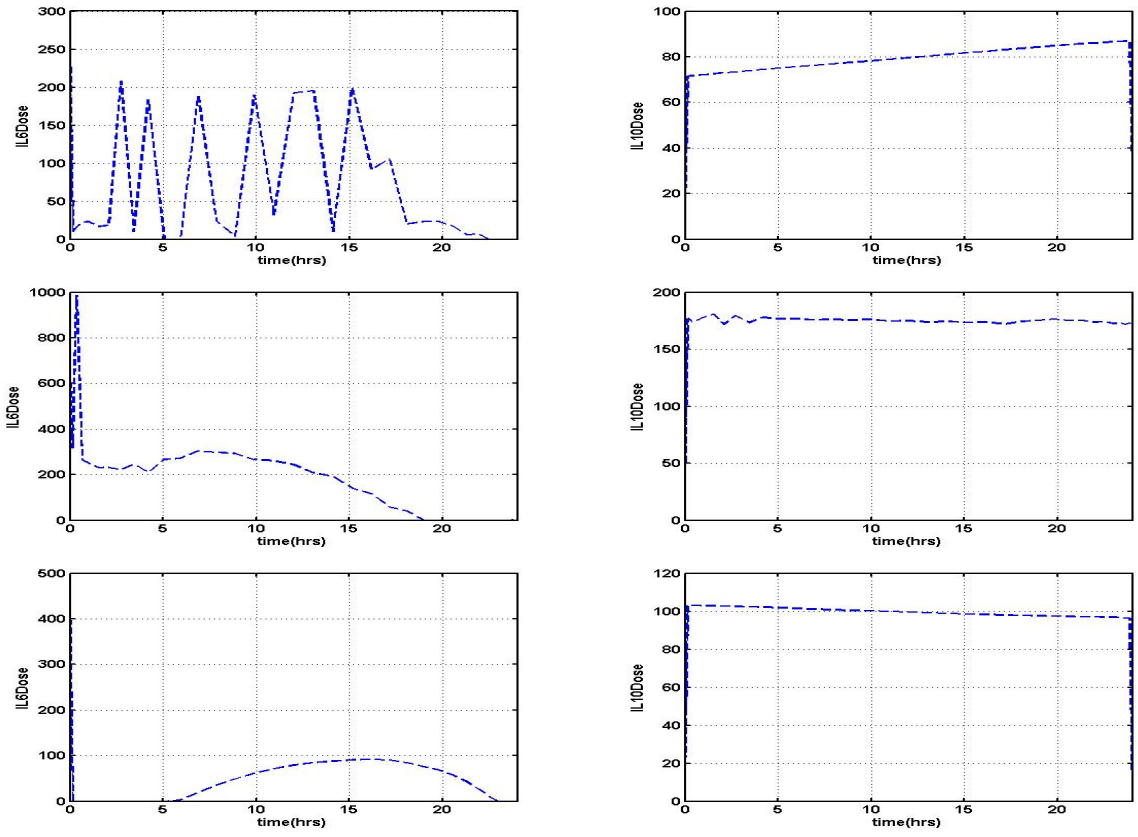

Figure E.2: Model solution under optimal treatment control at $3\,mg/kg$ endotoxin level.

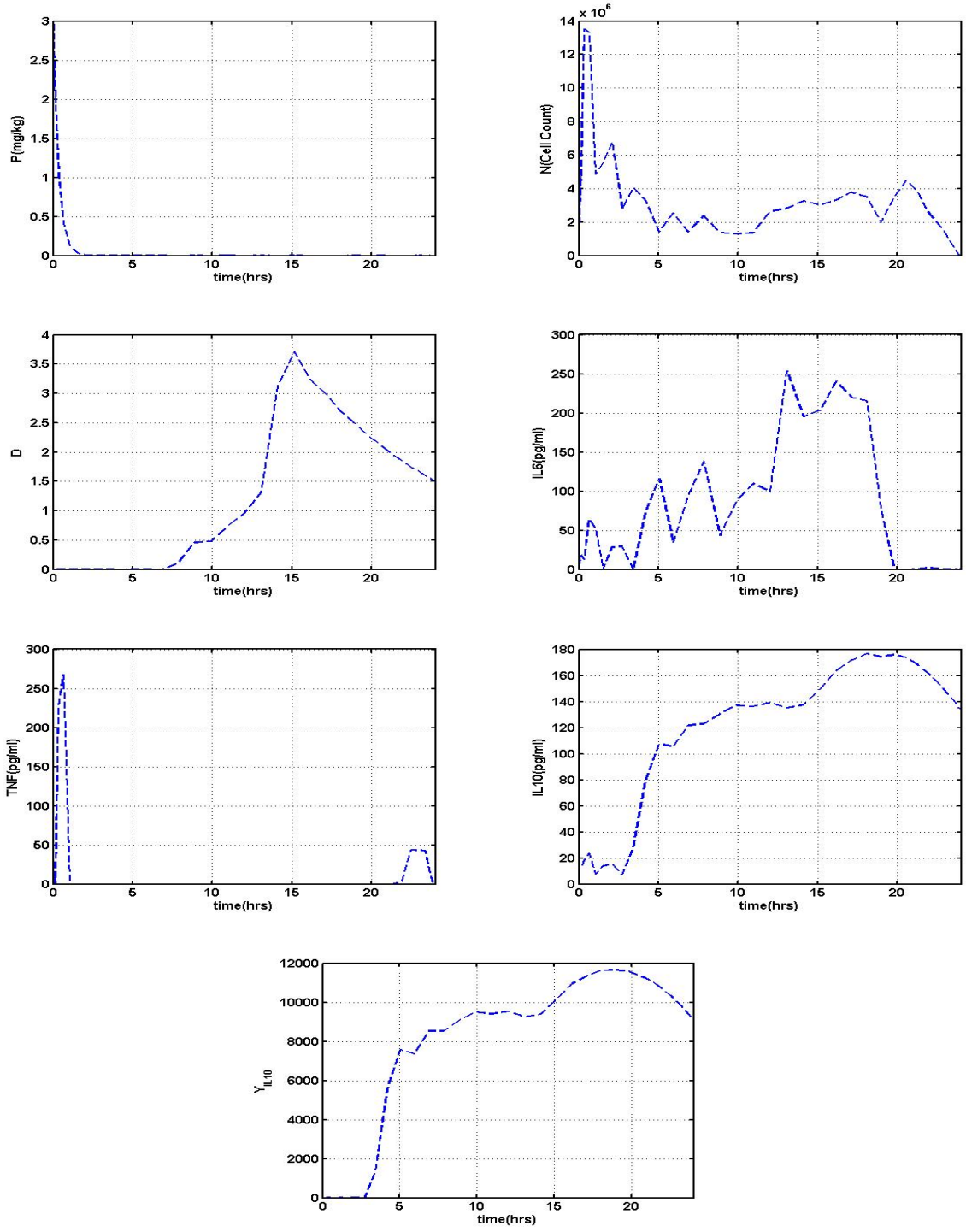

Figure E.3: Model solution under optimal treatment control at $6\,mg/kg$ endotoxin level.

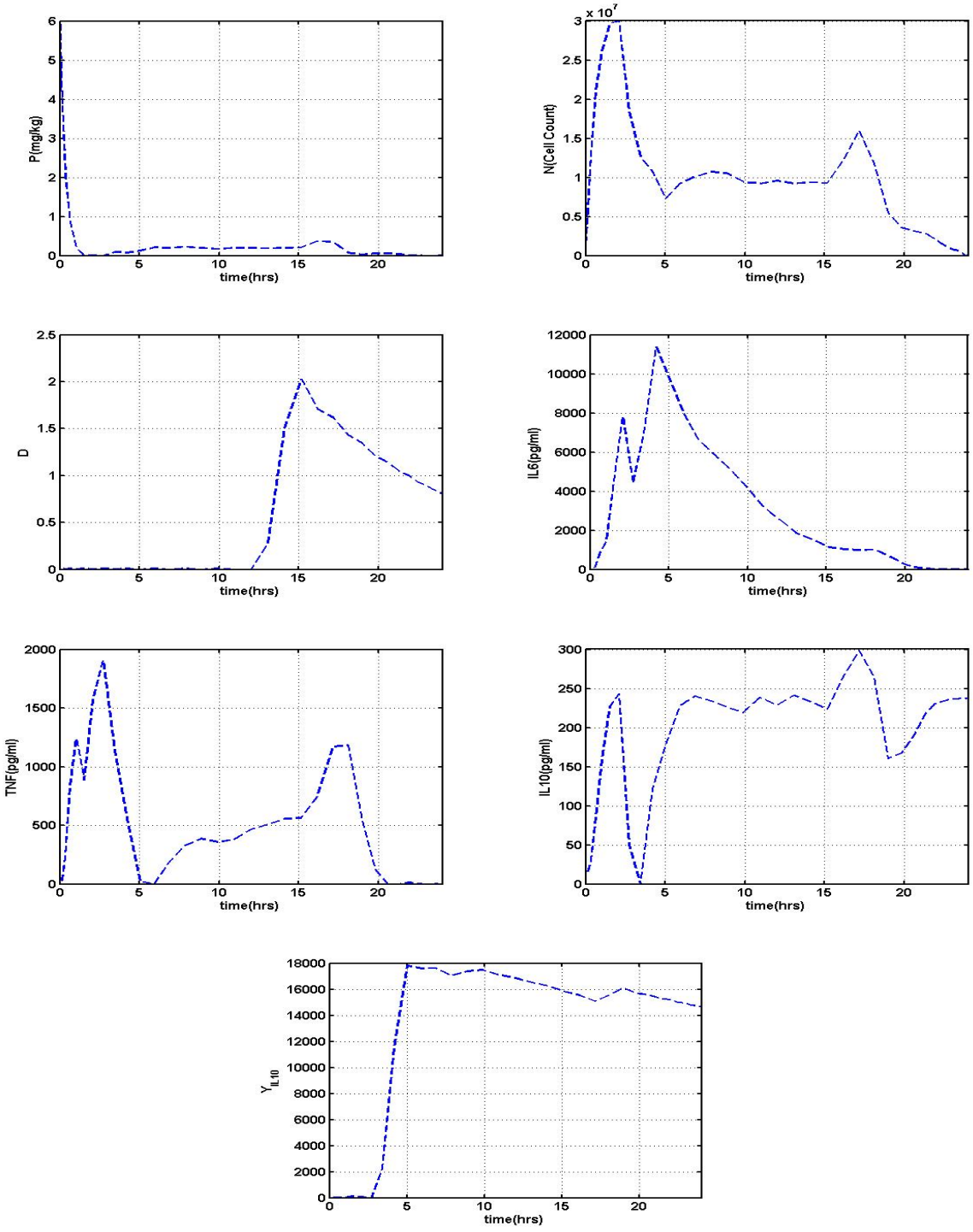

Figure E.4: Model solution under optimal treatment control at $12\,mg/kg$ endotoxin level.

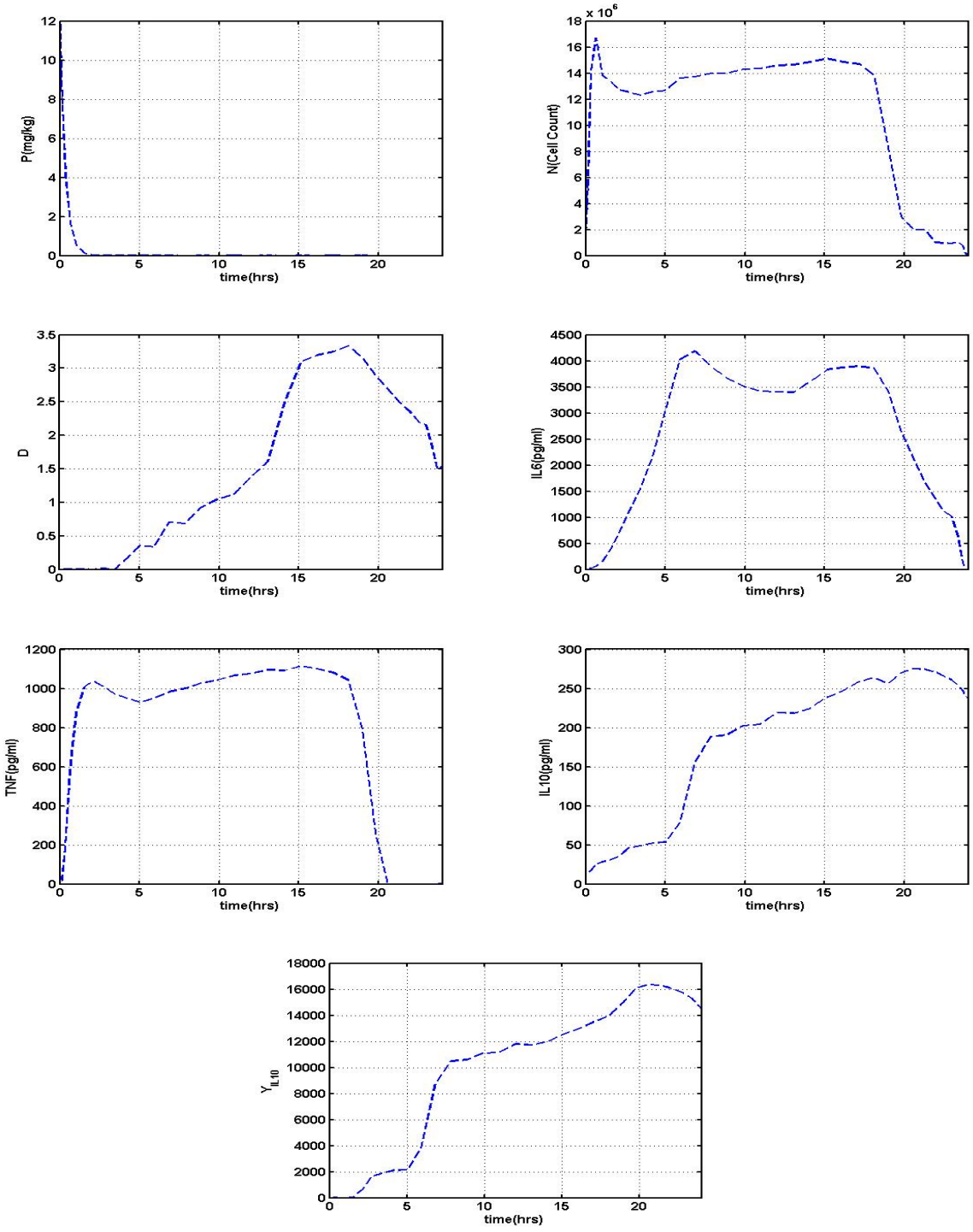

Appendix F

Square-Root Unscented Kalman Filter

The algorithm for Square-Root Unscented Kalman Filter for state estimation is presented here. More information about this algorithm and other UKF algorithms can be found in [141]. First, we define the weights W_i

$$W_0^{(m)} = \frac{\lambda}{L+\lambda}, \tag{F.1}$$

$$W_0^{(c)} = \frac{\lambda}{L+\lambda} + 1 - \alpha^2 + \beta, \tag{F.2}$$

$$W_i^{(m)} = W_i^{(c)} = \frac{1}{2(L+\lambda)}, \quad i = 1, \ldots, 2L, \tag{F.3}$$

$\lambda = \alpha^2(L+\kappa) - L$ is a scaling parameter. The constant α determines the spread of the sigma points around $\bar{\mathbf{x}}$, and it is usually set to a small positive value (e.g, $1 \leq \alpha \leq 10^{-4}$). The constant κ is a secondary scaling parameter, which is usually set to $3 - L$, and β is used to incorporate prior knowledge of the distribution of $\mathbf{x}$ (for Gaussian distributions, $\beta = 2$ is optimal) and L is the dimension of the state space.

Algorithm F.0.2

Initialize with

$$\hat{\mathbf{x}}_0 = \mathbf{E}[\mathbf{x}_0], \qquad \mathbf{S}_0 = chol\{\mathbf{E}[(\mathbf{x}_0 - \hat{\mathbf{x}}_0)(\mathbf{x}_0 - \hat{\mathbf{x}}_0)^T]\}. \tag{F.4}$$

For $k \in \{1, \cdots, \infty\}$.

The sigma-point calculation and time update are given by

$$\mathcal{X}_{k-1} = [\hat{\mathbf{x}}_{k-1} \quad \hat{\mathbf{x}}_{k-1} + \gamma \mathbf{S}_k \quad \hat{\mathbf{x}}_{k-1} - \gamma \mathbf{S}_k], \tag{F.5}$$

$$\mathcal{X}^*_{k|k-1} = \mathbf{F}(\mathcal{X}_{k-1}, \mathbf{u}_{k-1}), \tag{F.6}$$

$$\hat{\mathbf{x}}^-_k = \sum_{i=0}^{2L} W_i^{(m)} \mathcal{X}^*_{i,k|k-1}, \tag{F.7}$$

$$\mathbf{S}^-_k = qr\left\{\left[\sqrt{W_1^{(c)}}(\mathcal{X}^*_{1:2L,k|k-1} - \hat{\mathbf{x}}^-_k) \quad \sqrt{\mathbf{R}^{\mathbf{v}}}\right]\right\}, \tag{F.8}$$

$$\mathbf{S}^-_k = cholupdate\{\mathbf{S}^-_k, \mathcal{X}^*_{0,k|k-1} - \hat{\mathbf{x}}^-_k, W_0^{(c)}\}, \tag{F.9}$$

(augment sigma points)[1]

$$\mathcal{X}_{k|k-1} = [\mathcal{X}^*_{k|k-1} \quad \mathcal{X}^*_{0,k|k-1} + \gamma\sqrt{\mathbf{R}^{\mathbf{v}}} \quad \mathcal{X}^*_{0,k|k-1} - \gamma\sqrt{\mathbf{R}^{\mathbf{v}}}] \tag{F.10}$$

$$\mathcal{Y}_{k|k-1} = \mathbf{H}(\mathcal{X}_{k|k-1}) \tag{F.11}$$

$$\hat{\mathbf{y}}^-_k = \sum_{i=0}^{2L} W_i^{(m)} \mathcal{Y}_{i,k|k-1}, \tag{F.12}$$

and the measurement update equations are

$$\mathbf{S}_{\bar{\mathbf{y}}_k} = qr\left\{\left[\sqrt{W_1^{(c)}}(\mathcal{Y}_{1:2L,k} - \hat{\mathbf{y}}_k) \quad \sqrt{\mathbf{R}^{\mathbf{n}}{}_k}\right]\right\}, \tag{F.13}$$

$$\mathbf{S}_{\bar{\mathbf{y}}_k} = cholupdate\{\mathbf{S}_{\bar{\mathbf{y}}_k}, \mathcal{Y}_{0,k} - \hat{\mathbf{y}}_k, W_0^{(c)}\}, \tag{F.14}$$

$$\mathbf{P}_{\mathbf{x}_k\mathbf{y}_k} = \sum_{i=0}^{2L} W_i^{(c)}(\mathcal{X}_{i,k|k-1} - \hat{\mathbf{x}}^-_k)(\mathcal{Y}_{i,k|k-1} - \hat{\mathbf{y}}^-_k)^T, \tag{F.15}$$

$$\mathcal{K}_k = \frac{(\mathbf{P}_{\mathbf{x}_k\mathbf{y}_k}/\mathbf{S}^T_{\bar{\mathbf{y}}_k})}{\mathbf{S}_{\bar{\mathbf{y}}_k}}, \tag{F.16}$$

$$\hat{\mathbf{x}}_k = \hat{\mathbf{x}}^-_k + \mathcal{K}_k(\mathbf{y}_k - \hat{\mathbf{y}}^-_k),$$

$$\mathbf{U} = \mathcal{K}_k \mathbf{S}_{\bar{\mathbf{y}}_k}, \tag{F.17}$$

$$\mathbf{S}_k = cholupdate\{\mathbf{S}^-_k, \mathbf{U}, -1\}. \tag{F.18}$$

[1] Alternatively, *redraw* a new set of sigma points that incorporate the additive process noise, i.e., $\mathcal{X}_{k|k-1} = [\hat{\mathbf{x}}^-_k \quad \hat{\mathbf{x}}^-_k + \gamma\mathbf{S}^-_k \quad \hat{\mathbf{x}}_k - \gamma\mathbf{S}^-_k]$.